AN ABSTRACT OF THE DISSERTATION OF

Ryan D. Stewart for the degree of Doctor of Philosophy in Water Resources Engineering presented on June 5, 2013.

Title: Characterization of Hydrologic Parameters and Processes in Shrink-swell Clay Soils

Abstract approved:_____
John S. Selker

Vertisols and other *vertic*-intergrade soils are found all over the globe, including many agricultural and urban areas. These soils are characterized by their cyclical shrinking and swelling behaviors, where bulk density and porosity distribution both vary as functions of time and/or soil moisture. In turn, alterations in physical soil parameters become manifest as crack networks, which open during the shrinkage phase and re-seal as the soil swells. As a consequence, when present these soils can significantly impact agriculture and infrastructure, and can act as a dominant control on the local hydrology. Therefore, understanding how water moves through and interacts with these soils is of utmost importance to ensure their proper utilization and management.

This study had three objectives: 1) to identify the role of initial soil moisture on infiltration in a rigid (non-swelling) soil; 2) to quantify variation in the soil's hydraulic properties, using single-ring infiltration measurements taken in a *vertic* soil over a 1.5 year period; and 3) to build on these concepts to examine data from a set of instrumented field plots in a *vertic* soil located in the *Secano Interior* region of Chile.

Significant findings of the study include 1) the development of a new formulation to describe a soil's wetting front potential (a measure of capillary pull) in terms of initial degree of saturation;

2) the creation of a simple correction to approximate the decrease of wetting front potential in wetter soils, thereby improving the accuracy of the traditional Green and Ampt sorptivity model in such conditions; 3) an equation to accurately estimate hydraulic parameters from short-duration infiltration tests, when steady-state conditions have not been realized; 4) a new theoretical model to estimate crack porosity as a function of soil moisture, which was developed based on the soil shrinkage curve; and 5) modification of the traditional two-term Philip infiltration model for use in *vertic* soils.

The field study also showed that crack networks cause highly complex and non-linear wetting of the soil profile, with water simultaneously infiltrating from the soil surface and from the soil-crack interfaces; that cracks can seal at the surface while remaining open and hydraulically active below the surface, which indicates that surface-based monitoring alone may not be sufficient to predict water movement and soil response in *vertic* soils; and that the transition between infiltration and runoff may be strongly correlated with the cumulative amount of net precipitation that had reached the soil surface, so that cumulative amount of precipitation has the potential to be a simple yet accurate metric to predict runoff in *vertic* soils.

These findings offer improved understanding of soil-water interactions in *vertic* soils, and reveal that very simple concepts underlie seemingly complex systems. As a result, the concepts and formulations developed in this study should allow for straightforward integration into other studies and models.

Characterization of Hydrologic Parameters and Processes in Shrink-swell Clay Soils

by
Ryan D. Stewart

A DISSERTATION

submitted to

Oregon State University

in partial fulfillment of
the requirements for the
degree of

Doctor of Philosophy

Presented June 5, 2013
Commencement June 2013

Doctor of Philosophy dissertation of Ryan D. Stewart presented on June 5, 2013.

APPROVED:

Major Professor, representing Water Resources Engineering

Director of the Water Resource Graduate Program

Dean of the Graduate School

I understand that my dissertation will become part of the permanent collection of Oregon State University libraries. My signature below authorizes release of my dissertation to any reader upon request.

Ryan D. Stewart, Author

ACKNOWLEDGEMENTS

I would like to express my sincere gratitude to my major advisor, Dr. John S. Selker, for advising me for the past five years. His enthusiasm was contagious, and he always encouraged me to strive to continually better my experiments, analyses and presentations, so as to create maximum possible impact.

I also offer my sincere gratitude and appreciation to Drs. Majdi Abou Najm and David E. Rupp for working with me and guiding me over the course of this project. From doing field work in the hot Chilean sun to engaging in long discussions over Skype to providing careful comments and edits on manuscripts, they have been a major ingredient to my and the project's success.

I would also like to thank my minor advisor, Dr. Maria Dragila, for giving great feedback and encouragement throughout this process. At the same time I would like to recognize my other committee members, Drs. Richard Cuenca and Todd Scholz for offering their time and expertise. Overall, I feel very fortunate to have been surrounded by such bright, dedicated and caring advisors.

I would like to thank the National Science Foundation for providing the funding which supported this work, under Grant No. 0943682. I offer my sincere gratitude to everyone who was a part of the "Scale and Time Dependent Hydrologic Response of Sites with Expansive Soils" project, including Dr. Hamil Uribe of the Instituto Nacional de Investigaciones Agropecuarias (INIA), and Dr. José Luis Arumí, Dr. Diego Rivera and Mr. Carlos Cea of the Department of Recursos Hídricos at the Universidad de Concepción, Chillán. This research would not have been possible without their cooperation, inspiration, knowledge and assistance. I also would like to recognize

Alejandra Lavados Carrasco, Viviana Gavilan Pino and Abraham Arevalo Neira for helping collect field data and run the experiments in Chile. The second field season would not have been successful without their diligent efforts. Similarly, Brian Dougherty, John Hesseltine, Emeline Perret and Lifang Xie were responsible for conducting significant portions of the laboratory soil testing and analyses. Dr. J. Reed Glassman of Willamette Geological Service provided me with the use of his research equipment and his expertise on mineralogy, both of which proved very helpful.

Additionally, I would like to acknowledge the contributions of the participants of the NSF-funded Undergraduate Chilean Field Hydrology Course for assisting with field installation and data collection: Hayden Ausland, Felipe Bretón, Wiebke Boettche, Sebastián Bonelli, Maria Brown, Liam Kyle Cahill, Daniela Castañeda, Jenna Duffin, Nick Dummer, Alex Fisher, Hector Flores, Zak Grimes, Rachel Gross, Leah Kammel, Chuan Li, Marianela Matta, Claudia Maureira, Mackenzie Osypian, Hazel Owens, Julianne Quinn, William Rhoads, Ghislaine Rossel, and Jennifer Vettel. At the same time, I would like to thank Dr. John W. Lane of the USGS for serving as an instructor for the field course and providing leadership on the geophysical monitoring and analysis.

I wish to recognize my office- and department-mates, including Abraham Mooney, Daniel Moreno, Daniel Bailey, Aida Arik, Tara O'Donnell, Estephania Elorriaga, Chadi Sayde, Laureinne El Khoury, Ari Petrides, Landon Gryczkowski, Joshua Owens, Travis Roth and Jake Sherberg. I will always treasure the many hours we spent in the office (or other places) discussing our findings and life.

Matt and Bonnie Cox merit special thanks for allowing me to poke, prod, dig, flood and instrument their backyard for over two years. Likewise, Sra. Irene Acevedo deserves to be commended for generously allowing us to install and house our equipment and to perform a variety of measurements on her property in Chile.

Finally, I would like to thank my family, including my delightful daughter, Linette, and especially my wonderful wife, Jen, for providing support, understanding and love. I truly appreciate all that you do to encourage me.

CONTRIBUTION OF AUTHORS

John Selker, Majdi Abou Najm and David Rupp were intricately involved in the experimental plan, instrument installation, and data collection. All three were very helpful in reviewing these manuscripts. John W. Lane collected and analyzed the electrical resistivity data. Hamil C. Uribe provided historical, meteorological and flume measurements. José Luis Arumí, Diego Rivera and Carlos Cea of the Universidad de Concepción – Chillán provided site and data management for the Chilean field site.

The students of the Chilean international field hydrology camp – Hayden Ausland, Felipe Bretón, Wiebke Boettche, Sebastián Bonelli, Maria Brown, Liam Kyle Cahill, Daniela Castañeda, Jenna Duffin, Nick Dummer, Alex Fisher, Hector Flores, Zak Grimes, Rachel Gross, Leah Kammel, Chuan Li, Marianela Matta, Claudia Maureira, Mackenzie Osypian, Hazel Owens, Julianne Quinn, William Rhoads, Ghislaine Rossel, and Jennifer Vettel – helped collect and analyze data in 2011.

In addition, Alejandra Lavados Carrasco, Viviana Gavilan Pino and Abraham Arevalo Neira helped collect and analyze data in 2012, and Lifang Xie, Emeline Perret, Brian Dougherty and John Hesseltine helped with the laboratory soil testing and analysis.

TABLE OF CONTENTS

TABLE OF CONTENTS (Continued)

Page

TABLE OF CONTENTS (Continued)

Page

LIST OF FIGURES

LIST OF FIGURES (Continued)

Figure Page

LIST OF FIGURES (Continued)

LIST OF TABLES

LIST OF APPENDICES

LIST OF APPENDIX FIGURES

LIST OF APPENDIX TABLES

1. General introduction

Background and Relevance of the Research

Shrink-swell clay soils, also known as *Vertisols* or *vertic*-intergrades, are found on every continent except Antarctica. In certain regions, including parts of Australia, Africa, the United States and Latin America, more than 25% of the soil can be classified as *vertic*. *Vertic* soils generally contain a high proportion of smectite, with lesser amounts of vermiculite, kaolinite, and other clay-sized particles. Due to their fine texture, these soils have high nutrient concentrations and water-holding capabilities, traits typically indicative of productive agricultural soils. However, these soils also exhibit large variation in bulk density as they wet and dry, which leads to the formation of crack networks which seasonally open and close and the development of topographic features known as *gilgai.* This variation in soil density can make agriculture difficult, due to soil deformation causing physical stress on the plants, water becoming preferentially delivered below the root zone through macropore flow, and poor drainage when the soil cracks seal.

In addition to affecting agricultural productivity, *vertic* soils also can cause significant damage to buried infrastructure such as water mains [*Hudak et al.*, 1998] and surface structures such as roads and building foundations [*Stavridakis*, 2006; *Jones and Jefferson*, 2012]. One estimate suggested that one in four homes in the United States

have been damaged to some degree by shrink-swell clay soils [*Krohn and Slosson*, 1980]. Therefore, understanding the hydrologic response of *vertic* soils is necessary in order to best manage them for both agricultural and infrastructural purposes.

Vertic soils behave differently in many aspects than rigid (non-swelling) soils. For example, the former experience significant changes in physical properties such as bulk density and porosity and pore size distributions, whereas these properties are assumed to be constant in rigid soils. Likewise, the variation in physical properties in swelling soils can cause large variations in hydraulic parameters, including the effective hydraulic conductivity (K_{eff}). As a result, many of the basic concepts developed for rigid soils to describe hydrologic processes such as infiltration, runoff, preferential flow, and soil-water storage cannot be directly used for swelling soils. A plethora of solutions to describe these processes in *vertic* soils have been developed, but generally these methods suffer from two main drawbacks: 1) they are often highly complex, with a multitude of parameters to describe a single process; and 2) they are often focused on small-scale behaviors, such as at the individual crack, clod or ped-scale, without any linkage to how those behaviors would become linked and integrated across a landscape. This argues for the need for simple yet accurate methods to describe hydrologic processes in non-rigid soils, which will allow for integration into large-scale models.

Scope and Objectives

The overall objective of this study was to better understand and quantify the hydrology of shrink-swell clay (*vertic*) soils. This was done by modifying concepts used to describe water movement in non-swelling soils, such as infiltration, to quantify hydrological parameters and processes in swelling soils. This effort was divided into three major sections.

The first section examined the concept of soil sorptivity, which is essentially the capillary pull that a soil exerts on an infiltrating fluid. Sorptivity is an important force which, along with gravity, drives infiltration. However, few studies have measured how sorptivity varies across different soils and at different moisture contents. This section, therefore, had four objectives: 1) to better quantify the wetting front potential of a soil; 2) to assess the influence of soil type and initial soil moisture on wetting front potential and sorptivity; 3) to develop an expression to estimate a soil's hydraulic conductivity from sorptivity measurements; and 4) to use this theoretical framework for describing sorptivity to identify shifts in the hydraulic properties of a *vertic* soil.

The second section focused on infiltration measurements taken in a *vertic* soil to quantify the soil's effective hydraulic conductivity. Whereas most previous studies have found large variations in hydraulic conductivity due to flow down large cracks,

few field-based studies have examined the hydraulic conductivity of the soil matrix. This section of the study therefore had two main goals: 1) to use small, surface-based single-ring infiltration measurements to quantify variation in hydraulic conductivity of the soil matrix as the soil went through cycles of wetting and drying; and 2) to develop a theoretical framework which would describe how the soil matrix hydraulic conductivity was related to the amount of soil moisture.

The third and final section utilized data collected from heavily-instrumented experimental runoff plots. This section had three main objectives: 1) to identify how water moves through an initially dry *vertic* soil; 2) to assess how soil properties and parameters such as soil moisture, crack volume and effective hydraulic conductivity changed as the soil profile wetted up; and 3) to quantify common threshold behaviors between the various plots, so as to allow for runoff prediction without having to track individual crack and soil matrix behaviors.

References

Hudak, P., B. Sadler, and B. Hunter (1998), Analyzing underground water-pipe breaks in residual soils, *Water Engineering and Management, 145*, 15-20.

Jones, L. D., and I. Jefferson (2012), *Expansive soils*, ICE Publishing, Telluride, CO.

Krohn, J. P., and J. E. Slosson (1980), *Assessment of expansive soils in the United States, paper presented at Expansive Soils*, ASCE.

Stavridakis, E. I. (2006), Assessment of anisotropic behavior of swelling soils on ground and construction work, *Expansive Soils: Recent Advances in Characterization And Treatment*, 371-384.

2. The role of initial soil moisture on sorptivity and infiltration

Ryan D. Stewart[1]*, David E. Rupp[2], Majdi R. Abou Najm[3], John S. Selker[1]

[1] *Biological & Ecological Engineering Department, Oregon State University, Corvallis, OR, United States.*

[2] *Oregon Climate Change Research Institute, College of Earth, Ocean and Atmospheric Sciences, Oregon State University, Corvallis, OR, United States.*

[3] *Civil & Environmental Engineering, American University of Beirut. Beirut, Lebanon*

*Corresponding Author (stewarry@onid.orst.edu)

Submitted to Water Resources Research

Submitted on February 14, 2013

Abstract

A soil's capillarity, associated with the parameter sorptivity, is a dominant factor controlling infiltration, particularly at the onset of rainfall or irrigation. Many mathematical models used to estimate infiltration and sorptivity are only valid for dry soils, which often makes them inappropriate for settings of interest. This paper examines how sorptivity and its capillary component (as wetting front potential) change with initial degree of saturation. We propose a simple modification to the classic Green-Ampt model of sorptivity which captures these effects, thereby reducing the model's error when used in wetter soils. This modified model also enables quantification of a soil's saturated hydraulic conductivity from sorptivity measurements, given estimates of the soil's characteristic curve and initial water content. This method is particularly useful in soils of low permeability, where the time required to estimate hydraulic conductivity through steady-state methods can be impractical.

Introduction

Because infiltration affects water availability for vegetation, groundwater recharge, overland flow, and solute transport, it has been the focus of considerable study over the previous century [*Green and Ampt*, 1911; *Philip*, 1957; *Wooding*, 1968; *Brutsaert*, 1977]. Under normal conditions, two main forces, gravity and capillarity,

drive vertical infiltration, whereas capillarity alone drives horizontal infiltration [*Philip*, 1957].

Under constant head conditions, one- and three-dimensional vertical infiltration into a uniform soil can be described as:

$$I = S\sqrt{t} + Ct \quad (1)$$

where I is cumulative infiltration over time t and S is the soil sorptivity. For one-dimensional vertical infiltration C is a scaled form of the soil's saturated hydraulic conductivity (K_s), whereas for three-dimensional infiltration C includes both saturated hydraulic conductivity and sorptivity [*Smiles and Knight*, 1976; *Fuentes et al.*, 1992; *Touma et al.*, 2007].

From Equation 1 we see that sorptivity dominates infiltration at early times ($t << S^2/C^2$), and for very early times the second term may be neglected [*White et al.*, 1992]. Conversely, the second term dominates at late times (i.e., when $t >> S^2/C^2$). In the case of one-dimensional vertical infiltration, gravity dominates as $t \rightarrow \infty$, generally allowing for the estimation of the saturated hydraulic conductivity [*Philip*, 1957]. For three-dimensional flow from a circular source, *Wooding* [1968] estimated K_s from late-time infiltration data by including an approximation of capillary edge effects, based on the source radius and soil characteristics. However, in both one and three dimensions the time required to reach late-time or quasi-steady state conditions may

be impractical, particularly for soils with low hydraulic conductivity, such as fine-textured clays and silts. At the same time, assumptions of homogeneity are typically violated for long infiltration experiments.

In the field we often encounter infiltration which occurs over intermediate or transient timescales (neither exclusively early- nor late-time) and possesses three-dimensional behavior. One such example is infiltration from an axisymmetric single ring source [*Braud et al.*, 2005], which can provide a rapid and low-cost measurement of soil hydraulic properties. However, the interpretation of such infiltration measurements can be difficult because both the S and C terms must be included simultaneously. Various manipulations of Equation 1 have therefore been developed in order to differentiate between sorptivity and saturated hydraulic conductivity for such infiltration conditions [*Smiles and Knight*, 1976; *Smettem et al.*, 1995; *Vandervaere et al.*, 2000], but these methods may be inadequate for estimating small K_s values [*Smettem et al.*, 1995]. As such, it can be argued that in many fine-textured soils, single-ring infiltration measurements, when taken over the course of a typical measurement session (< 10 hours), will more provide a more accurate estimation of S than of K_s.

Though sorptivity is often described as representing the soil's capillary ability to draw or pull water [*Philip*, 1957; *Touma et al.*, 2007], it also is a function of the soil's

hydraulic conductivity. This is evident, e.g., in *Parlange* [1975]'s precise solution for sorptivity (as modified for positive ponded conditions by *Touma et al.* [2007])

$$S^2 = 2K_s(\theta_s - \theta_r)(1-\Theta_0)h_{surf} + (\theta_s - \theta_r)\int_{h_0}^{0}(1+\Theta-2\Theta_0)K(h)dh \tag{2}$$

where Θ is the degree of saturation

$$\Theta = \frac{\theta - \theta_r}{\theta_s - \theta_r} \tag{3}$$

θ_0, θ_s, and θ_r are the initial, saturated, and residual volumetric soil water contents, respectively, $K(h)$ is the hydraulic conductivity as a function of soil matric potential, h_0 is the initial matric potential, and h_{surf} is the depth of ponding at the surface.

Hydraulic conductivity also appears in the simpler, or "traditional" as we will refer to it here, definition of sorptivity provided by the *Green and Ampt* [1911] model:

$$S^2 = \frac{2K_s(\theta_s - \theta_r)(1-\Theta_0)(h_{wf} + h_{surf})}{\varphi} \tag{4}$$

where h_{wf} is the wetting front potential, which is also referred to as the effective capillary drive [*Morel-Seytoux et al.*, 1996], capillary pull, or macroscopic capillary length [*White and Sully*, 1987]. The correction factor φ accounts for deviations from a rectangular wetting front and/or viscous damping effects. For example, $\varphi = 1$ for a

Green and Ampt [1911] solution, 1.1 for the *White and Sully* [1987] solution, and 1.1-1.7 for the *Morel-Seytoux and Khanji* [1974] solution.

Because hydraulic conductivity is embedded in sorptivity, certain measurements of the latter can be used to infer the former. One such approach is to utilize field-based sorptivity measurements in conjunction with the traditional sorptivity model (Equation (4)) to quantify K_s. To do so, however, requires estimates of both the initial soil moisture and the wetting front potential. This can be readily accomplished in dry soils (when $\Theta_0 \approx 0$), as solutions exist to quantify wetting front potential [*Rawls et al.*, 1992; *Morel-Seytoux et al.*, 1996] in such conditions. For instance, *Morel-Seytoux et al.* [1996] approximated the wetting front potential of a dry soil as

$$h_{wf} = \left(\frac{1}{\alpha}\right)\left(\frac{0.046m + 2.07m^2 + 19.5m^3}{1 + 4.7m + 16m^2}\right) \tag{5}$$

where α and m are parameters of the water retention curve, for $\alpha > 0$ and $0 < m < 1$.

However, h_{wf} is recognized to change with the initial moisture state of the soil [*Green and Ampt*, 1911], and the aforementioned solutions for estimating wetting front potential do not include corrections for this variation. In a different approach, *Bouwer* [1964] and *Neuman* [1976] described h_{wf} as a function of soil matric potential, h. At early infiltration times, h_{wf} can be calculated by

$$h_{wf} = \frac{1}{2}\int_0^{h_0}\left(1+\frac{\theta-\theta_0}{\theta_s-\theta_0}\right)K_r(h)dh \tag{6}$$

where $K_r(h)$ is the relative hydraulic conductivity function $K(h)/K_s$. While it is possible to put Equation (6) in terms of Θ_0 by using a characteristic curve relationship [*Brooks and Corey*, 1964; *Van Genuchten*, 1980], the resulting equations will in general be highly complex with many terms.

Instead, in this paper, we propose an alternative formulation of wetting front potential as a function of initial degree of saturation. This allows for a modification to the traditional (Green and Ampt) sorptivity model so that it better approximates sorptivity throughout the soil moisture range. This modified expression can then be used to interpret single ring infiltration measurements, so as to quantify the magnitude and variability in time and space of a soil's saturated hydraulic conductivity, even in wet soils.

Theory

The *Parlange* [1975] expression for sorptivity in terms of soil diffusivity (D) and degree of saturation (Θ) is:

$$S^2 = (\theta_s-\theta_r)^2\int_{\Theta_0}^{\Theta_f}\left(\Theta_f+\Theta-2\Theta_0\right)D(\Theta)d\Theta \tag{7}$$

where, in addition to previously defined terms, θ_f is the final volumetric soil water content. Of the several diffusivity expressions applicable to actual soils, we focus on the *Van Genuchten* [1980] equation based on the *Mualem* [1976] model, due to its widespread usage and broad utility:

$$D(\Theta) = \frac{(1-m)K_s}{\alpha m(\theta_s - \theta_r)} \Theta^{1/2-1/m} \left[\left(1-\Theta^{1/m}\right)^{-m} + \left(1-\Theta^{1/m}\right)^{m} - 2 \right] \quad (8)$$

It should be noted that using the *Mualem* [1976] model allows for estimation of the parameter *m* using the more commonly referenced parameter *n* through the relationship $m = 1 - 1/n$.

Next, by combining Equations (7) and (8), sorptivity can be expressed for a soil with any initial water content as

$$S^2 = K_s(\theta_s - \theta_r) \frac{(1-m)}{\alpha m} \int_{\Theta_0}^{\Theta_f} \left(\Theta_f + \Theta - 2\Theta_0\right) \Theta^{1/2-1/m} \left[\left(1-\Theta^{1/m}\right)^{-m} + \left(1-\Theta^{1/m}\right)^{m} - 2 \right] d\Theta \quad (9)$$

For positive (ponded) pressure head [*Haverkamp et al.*, 1999], (9) can be modified as

$$S^2 = K_s(\theta_s - \theta_r)2h_{surf}(1-\Theta_0)$$

$$+ K_s(\theta_s - \theta_r)\left\{\frac{(1-m)}{\alpha m}\int_{\Theta_0}^{1}(1+\Theta-2\Theta_0)\Theta^{1/2-1/m}\left[\left(1-\Theta^{1/m}\right)^{-m}+\left(1-\Theta^{1/m}\right)^{m}-2\right]d\Theta\right\}$$

(10)

Equations (9) and (10) allow for accurate quantification of sorptivity throughout the soil moisture range. Finally, we can express the wetting front potential as a function of initial degree of saturation by equating Equation (10) with Equation (4) and then solving for h_{wf} :

$$h_{wf} = h_{surf}(\varphi - 1) +$$

$$\left(\frac{(1-m)\varphi}{2\alpha m(1-\Theta_0)}\int_{\Theta_0}^{1}(1+\Theta-2\Theta_0)\Theta^{1/2-1/m}\left[\left(1-\Theta^{1/m}\right)^{-m}+\left(1-\Theta^{1/m}\right)^{m}-2\right]d\Theta\right) \quad (11)$$

Results and Discussion

Equations (10) and (11) were integrated numerically to get sorptivity and wetting front potential, respectively, over the range $0 \leq \Theta_0 < 1$. The depth of ponding h_{surf} was assumed to be 0, which is a typical assumption for a single-ring infiltration test of short duration. Seven soils were analyzed, with their properties listed in Table 1.

Sorptivity and wetting front potential behave differently as functions of initial degree of saturation (Figure 1). The shape of the h_{wf} vs. Θ_0 curves show considerable dependence on soil texture (with a maximum difference across soil textures of more than 30% on the scale of 0 to 1), whereas the scaled S^2 vs. Θ_0 curves are tightly constrained throughout the range of initial soil moisture for all soil types (with a maximum difference across soil textures of less than 3% on the same scale of 0 to 1). The similarity between S^2 vs. Θ_0 curves also stands in contrast to the relationship between sorptivity and soil matric potential, h, where the curves for the various soils are generally unique in both shape and magnitude (Figure 2). Thus, we believe for our application it is preferable to describe sorptivity using Θ rather than h.

Additionally, it can be seen in Figure 1 that at the dry end of the curve the traditional sorptivity model in Equation (4) accurately captures the variation in sorptivity due to different initial water contents. In soils with high initial water contents, however, the traditional model overestimates the value of sorptivity compared to the more accurate Equations (7), (9) and (10). This is due to a decrease in wetting front potential at higher soil moistures. Soils with moderately broad pore size distributions ($0.2 < m < 0.7$) differ more from the traditional model than those with narrow or very broad pore size distributions, which we discuss in the next section.

To approximate the change in wetting front potential caused by increased initial degree of saturation, and to thereby counter the overestimation of sorptivity in

Equation (4), we suggest multiplying the Θ_0 term of Equation (4) by a correction factor a :

$$S^2 = \frac{2K_s(\theta_s - \theta_r)(1 - a\Theta_0)(h_{wf} + h_{surf})}{\varphi} \tag{12}$$

When, for example, a = 1.025, sorptivity from Equation (12) differs from Equation (9) by less than 2% (over the range 0 to 1) for all soils with an initial degree of moisture between $0 < \Theta_0 < 0.9$. In contrast, the traditional model (Equation (4)) can differ from Equation (12) by up to 4% (over the range 0 and 1) within that same moisture range.

The Nature of Wetting Front Potential

As discussed above, wetting front potential diminishes with increasing initial degree of saturation, with different rates of decrease between soil types. Nonetheless, as can be seen in Figure 1 and Table 2, the scaled wetting front potential is nearly constant for all soil types over the range $0 < \Theta_0 < 0.5$. As such, the *Morel-Seytoux et al.* [1996] approximation (Equation (5)) provides a suitable estimate of wetting front potential for this range. Beyond $\Theta_0 = 0.5$, however, soils with moderate pore size distributions ($0.2 < m < 0.8$) begin to experience a pronounced drop in wetting front potential (Figure 3), with the largest effect occurring at $m = 0.47$.

It can be noted that soils with a uniform pore size distribution ($m = 1$) have a constant wetting front potential throughout the entire moisture range, and thus will behave as Green and Ampt soils. However, because most real soils have pore size distributions in the range $0.2 < m < 0.7$, the assumption of constant wetting front potential is not valid, and Equations (9), (10) or (12) provide better estimates of soil sorptivity.

Further, the pore size distribution term (m) has a strong influence on the magnitude of the wetting front potential. Traditionally, h_{wf} has been considered to be a capillary term, which would suggest that finer soils, having smaller pore sizes, will have greater wetting front potentials [*Swartzendruber et al.*, 1954; *Selker et al.*, 1999]. However, as can be seen in Figure 4 (where wetting front potential isolines are plotted as functions of van Genuchten parameters α and m), increasing the pore size distribution (decreasing m) reduces the wetting front potential. This is particularly notable for $m < 0.3$, and is the reason that Columbia Silt soil can have both α and h_{wf} which are smaller than those of Grenoble Sand soil. The Haines model [*Haines*, 1930] of soil filling and draining – where soil is idealized to be made up of a connected network of pore necks and pore bodies – may provide at least a partial physical explanation of this phenomenon. In the Haines model, capillarity will be controlled by the radii of the bodies of the largest connected pores, since the wetting front will not advance until those pore bodies have filled. Conversely, hydraulic conductivity will be governed by the necks of the smallest connected pores [*Hunt and*

Gee, 2002]. Thus, for many soils, both wetting front potentials and sorptivity will be smaller than predicted by traditional formulations such as the Laplace and Poiseuille equations [*Washburn*, 1921; *Swartzendruber et al.*, 1954; *Selker et al.*, 1999].

Application – Determining Saturated Hydraulic Conductivity from Sorptivity

As discussed previously, hydraulic conductivity is embedded within sorptivity. Thus, sorptivity measurements can be used to quantify hydraulic conductivity. This can be achieved by combining equations (5) and (12) and then solving for saturated hydraulic conductivity

$$K_s = \left(\frac{S^2 \alpha \varphi}{(\theta_s - \theta_r)(1 - a\Theta_0)} \right) \left(\frac{1 + 4.7m + 16m^2}{0.092m + 4.14m^2 + 39m^3} \right) \tag{13}$$

Equation (13) allows for early-time infiltration data, such as can be obtained with single-ring tests, to be used to directly estimate K_s. This was verified through numerical simulations of one-dimensional horizontal infiltration for five of the soils listed in Table 1, at five different initial water contents (Θ_0 = 0, 0.1, 0.3, 0.6 and 0.9) using the HYDRUS-1D model [*Simunek et al.*, 2005]. The model domain was 5 m in length, with a node spacing of 0.01 m. The origin boundary condition was set as $\theta = \theta_s$ and the far boundary was set as no flux. For early times, when the water content of the far boundary varied by less than 1%, sorptivity was calculated from the water

flux, i, through the origin by using $S = 2i(t^{0.5})$. φ was assumed to be 1 and a was assumed to be 1.025.

Equation (13) was able to predict the K_s values for all five soils under all five initial degrees of saturation (Table 3). The error was minimal for the dry soils, ranging from 0.6 – 4.6% for Θ_0 = 0.1 and 0.3. For the wettest soils (Θ_0 = 0.9), the error increased (ranging from 8.1 – 17%), but nevertheless represents a valid approach to estimate saturated hydraulic conductivity. Using a soil specific value of φ could also be used to account for deviations in the wetting front shape between soils and improve estimates of K_s. It should be noted that for the Hygiene Sandstone soil at Θ_0 = 0.9, Equation (12) overestimated K_s by nearly a factor of two, due to the divergence of the analytical sorptivity solution (Equation (9)) and the HYDRUS-1D numerical solution. This can also be seen in Figure 5, which shows sorptivity values predicted by both Equation (9) and HYDRUS-1D.

Even though Equation (13) requires sorptivity and initial degree of saturation to be measured, as well as knowledge of soil parameters θ_s, θ_r, α and m, this nonetheless represents a reduction of the amount of needed data compared to other suggested methods. For example, the Beerkan Method [*Braud et al.*, 2005] requires estimates of the initial and final volumetric water contents, bulk density, and the final depth of wetting for each infiltration test.

Further, K_s has been shown to exhibit significantly greater spatial variability than α, m, θ_r, or θ_s, with θ_s and m possessing the least spatial variability [*Mallants et al.*, 1996]. This signifies that for any single location, the denominator of Equation (13) can be constrained using relatively few soil samples compared to the number of infiltration tests. This in turn makes it possible to use simple infiltration tests (such as the single ring infiltrometer) to quantify the spatial distribution of K_s in a single soil type.

At the same time, if the soil parameters assumed to be constant (α, m, θ_r, and θ_s) have already been estimated or measured, it is possible to forego soil sampling completely by using a simple qualitative estimation of initial moisture content, such as the system proposed by *Klocke and Fischbach* [1984]. This system allows for the division of the S-Θ_0 curve into five regions: 1) dry (0-25% available water content); 2) slightly moist (25-50% available water content); 3) moist (50-75% available water content); 4) wet (75-100% available water content); and 5) very wet, where the soil is above field capacity, and water may be draining via gravity. An example is shown in Figure 6, where field capacity is estimated to occur at $\Theta_0 = 0.9$, a value which corresponds to the degree of saturation of the Columbia Silt and Guelph Loam soils at a soil water potential of $h = 0.33$ m. In this example, by identifying the proper available moisture region (using the *sandy clay loam, loam and silt loam soils* section of *Klocke and*

Fischbach [1984]) and then using the suggested Θ_0 value in Figure 6, the scaled sorptivity value (S/S_{max}) should be within 15% (over the range 0 to 1).

Application – Sorptivity Isolines

Another application of Equations (9), (10) and/or (12) is to generate sorptivity isolines. This can help identify deviations in soil properties under different moisture contents, such as the hydraulic conductivity of a swelling soil.

To demonstrate, results of a set of single-ring infiltration experiments from a site near Corvallis, Oregon, are shown (Figure 7). The experiments took place monthly for a period of 16 months. Infiltration measurements were taken at 12 points within a 2 x 3 m grid, located in an open field characterized by a vertic Waldo silty clay soil. Up to 1 L of water (with a minimum of 0.4 L) was added to each 0.09 m diameter ring in 0.1 L increments, and the time between pours was recorded. Sorptivity was estimated using the early-time approximation for the first 0.4 L, where $S = I(t^{-0.5})$ [*White et al.*, 1992], and is presented as a mean and standard deviation of all 12 points on a single date. Mean initial degree of saturation was determined from six soil cores taken within the grid on each sampling date, and was calculated for each sample by dividing the moisture ratio, ϑ, by the void ratio, e.

$$\Theta_0 = \frac{\vartheta}{e} = \left(\frac{V_w/V_s}{V_v/V_s}\right) = \frac{V_w}{V_v} = \left(\frac{(m_0 - m_{dry})/\rho_w}{V_0 - (m_{dry}/\rho_s)}\right) \qquad (14)$$

where V_w is the volume of water, V_s is the volume of solids, V_v is the volume of voids, m_0 is the mass of the sample, m_{dry} is the mass of the sample after drying for 24 hours at 105 °C, ρ_w is the density of water, V_0 is the original volume of the sample, and ρ_s is the density of the solids (assumed to be equal to 2.67 g cm^{-3}).

In Figure 7, the arrows indicate chronological progression. It can be seen that the initial measurements were taken in relatively dry soils, and that as the soils wet up the apparent saturated hydraulic conductivity decreases, to approximately 25% of the original. At the same time, the variability of sorptivity is seen to increase as the initial degree of saturation increases, likely due to the loss of macro-porosity as the soil hydrates and swells.

As the soil re-dries hysteresis is observed, with the effective saturated hydraulic conductivity increasing by a factor of four compared to the original value, even with similar initial degrees of saturation. This is likely due to new cracks opening within the single-ring sampling areas. While more information about the soil parameters would be needed to utilize Equation (13), the isolines generated by Equations (9), (10), or (12) are useful for easily identifying qualitative shifts in soil properties, and in this example demonstrate that the effective saturated hydraulic conductivity of a cracking soil is neither constant nor unique as the soils wets and dries.

Summary and Conclusions

Sorptivity of a soil can be calculated by use of a diffusivity function, such as the *Parlange* [1975] formulation, or by use of a combination of conductivity and capillarity terms, such as the *Green and Ampt* [1911] sorptivity model. By equating these two approaches, we explore the capillarity (as wetting front potential) term in greater detail, as well as the effects of changes in both initial water content and soil parameters. It is seen that the relationship between sorptivity and initial degree of saturation can be predicted nearly independent of soil type, which allows for calculation of sorptivity even in wet soils. This relationship also allows for a minor correction to the traditional (i.e. Green-Ampt) model of sorptivity, which approximates the decrease of wetting front potential at higher degrees of saturation, and thereby improves the model's ability to predict sorptivity when soils are wet.

A useful result of this study is the ability to quantify saturated hydraulic conductivity from simple single ring infiltration tests, requiring only an estimate of the initial degree of saturation and basic soil parameters. This represents a simplification of standard methods for interpreting such infiltration tests. At the same time, the solution is valid even for wet soils (provided a satisfactory measurement of the soil sorptivity can be made in such conditions). This in turn can be useful for monitoring changes in soil properties during wetting, drying, sealing and other processes, or in predicting rainfall-runoff relationships for wet soils.

Finally, the findings presented in this paper are particularly useful for fine-textured soils, such as silts and clays. Fine-textured soils tend to retain more moisture, which means it is difficult to encounter the initially dry conditions required by many methods. At the same time, due to the restrictive nature of such soils, it is impossible to attain steady-state flow conditions during reasonable amounts of time. This in turn signifies that sorptivity is the principle parameter that can be utilized to interpret infiltration results or to predict water movement. The ability to describe sorptivity of a soil under any initial moisture content, therefore, is a significant and useful advance.

Acknowledgement

This work has been supported under National Science Foundation award 0943682.

References

Bouwer, H. (1964), Unsaturated flow in ground-water hydraulics, *Journal of the Hydraulics Division, Proceedings of the American Society of Civil Engineers*, *90*(HY5), 121-144.

Braud, I., D. De Condappa, J. M. Soria, R. Haverkamp, R. Angulo-Jaramillo, S. Galle, and M. Vauclin (2005), Use of scaled forms of the infiltration equation for the estimation of unsaturated soil hydraulic properties (the Beerkan method), *European Journal of Soil Science*, *56*(3), 361-374.

Brooks, R. H., and A. T. Corey (1964), Hydraulic properties of porous media, *Hydrology Papers*, Colorado State University.

Brutsaert, W. (1977), Vertical infiltration in dry soil, *Water Resources Research*, *13*(2), 363-368.

Fuentes, C., R. Haverkamp, and J. Y. Parlange (1992), Parameter constraints on closed-form soilwater relationships, *Journal of Hydrology*, *134*(1), 117-142.

Green, W. H., and G. Ampt (1911), Studies on soil physics, *Journal of Agricultural Science*, *4*(1), 1-24.

Haines, W. B. (1930), Studies in the physical properties of soil. V. The hysteresis effect in capillary properties, and the modes of moisture distribution associated therewith, *Journal of Agricultural Science*, *20*(01), 97-116.

Haverkamp, R., F. Bouraoui, C. Zammit, and R. Angulo-Jaramillo (1999), Soil properties and moisture movement in the unsaturated zone, *Handbook of Groundwater Engineering*.

Hunt, A. G., and G. W. Gee (2002), Application of critical path analysis to fractal porous media: comparison with examples from the Hanford site, *Advances in Water Resources*, *25*(2), 129-146.

Klocke, N. L., and P. Fischbach (1984), G84-690 Estimating Soil Moisture by Appearance and Feel, *Historical Materials from University of Nebraska-Lincoln Extension*, *Paper 1201*.

Mallants, D., B. P. Mohanty, D. Jacques, and J. Feyen (1996), Spatial variability of hydraulic properties in a multi-layered soil profile, *Soil Science*, *161*(3), 167.

Morel-Seytoux, H. J., and J. Khanji (1974), Derivation of an Equation of Infiltration, *Water Resources Research*, *10*(4), 795-800.

Morel-Seytoux, H. J., P. D. Meyer, M. Nachabe, J. Touma, M. T. van Genuchten, and R. J. Lenhard (1996), Parameter equivalence for the Brooks-Corey and van Genuchten soil characteristics: Preserving the effective capillary drive, *Water Resources Research*, *32*(5), 1251-1258.

Mualem, Y. (1976), A new model for predicting the hydraulic conductivity of unsaturated porous media, *Water Resources Research*, *12*(3), 513-522.

Neuman, S. P. (1976), Wetting front pressure head in the infiltration model of Green and Ampt, *Water Resources Research*, *12*(3), 564-566.

Parlange, J. Y. (1975), On solving the flow equation in unsaturated soils by optimization: Horizontal infiltration, *Soil Science Society of America Journal*, *39*(3), 415-418.

Philip, J. R. (1957), The theory of infiltration: 4. Sorptivity and algebraic infiltration equations, *Soil Science*, *84*(3), 257.

Rawls, W. J., L. R. Ahuja, D. L. Brakensiek, A. Shirmohammadi, and D. Maidment (1992), *Infiltration and soil water movement*, McGraw-Hill Inc.

Selker, J. S., C. K. Keller, and J. T. McCord (1999), *Vadose zone processes*, 339 p. pp., Lewis Publishers, Boca Raton, Fla.

Šimůnek, J., M. T. Van Genuchten, and M. Sejna (2005), The HYDRUS-1D software package for simulating the one-dimensional movement of water, heat, and multiple solutes in variably-saturated media, *University of California, Riverside, Research reports*, *240*.

Smettem, K., P. Ross, R. Haverkamp, and J. Parlange (1995), Three-Dimensional Analysis of Infiltration from the Disk Infiltrometer: 3. Parameter Estimation Using a Double-Disk Tension Infiltrometer, *Water Resources Research, 31*(10), 2491-2495.

Smiles, D., and J. Knight (1976), A note on the use of the Philip infiltration equation, *Soil Research, 14*(1), 103-108.

Swartzendruber, D., M. F. De Boodt, and D. Kirkham (1954), Capillary Intake Rate of Water and Soil Structure, *Soil Science Society of America Journal, 18*(1), 1-7.

Touma, J., M. Voltz, and J. Albergel (2007), Determining soil saturated hydraulic conductivity and sorptivity from single ring infiltration tests, *European Journal of Soil Science, 58*(1), 229-238.

van Genuchten, M. T. (1980), A closed-form equation for predicting the hydraulic conductivity of unsaturated soils, *Soil Science Society of America Journal, 44*(5), 892-898.

Vandervaere, J. P., M. Vauclin, and D. E. Elrick (2000), Transient Flow from Tension Infiltrometers I. The Two-Parameter Equation, *Soil Science Society of America Journal, 64*(4), 1263-1272.

Washburn, E. W. (1921), The Dynamics of Capillary Flow, *Physical Review, 17*(3), 273-283.

White, I., and M. Sully (1987), Macroscopic and microscopic capillary length and time scales from field infiltration, *Water Resources Research, 23*(8), 1514-1522.

White, I., M. J. Sully, and K. M. Perroux (1992), Measurement of surface-soil hydraulic properties: Disk permeameters, tension infiltrometers, and other techniques, in *Advances in measurement of soil physical properties: Bringing theory into practice*, 69-103.

Wooding, R. (1968), Steady infiltration from a shallow circular pond, *Water Resources Research, 4*(6), 1259-1273.

Figures

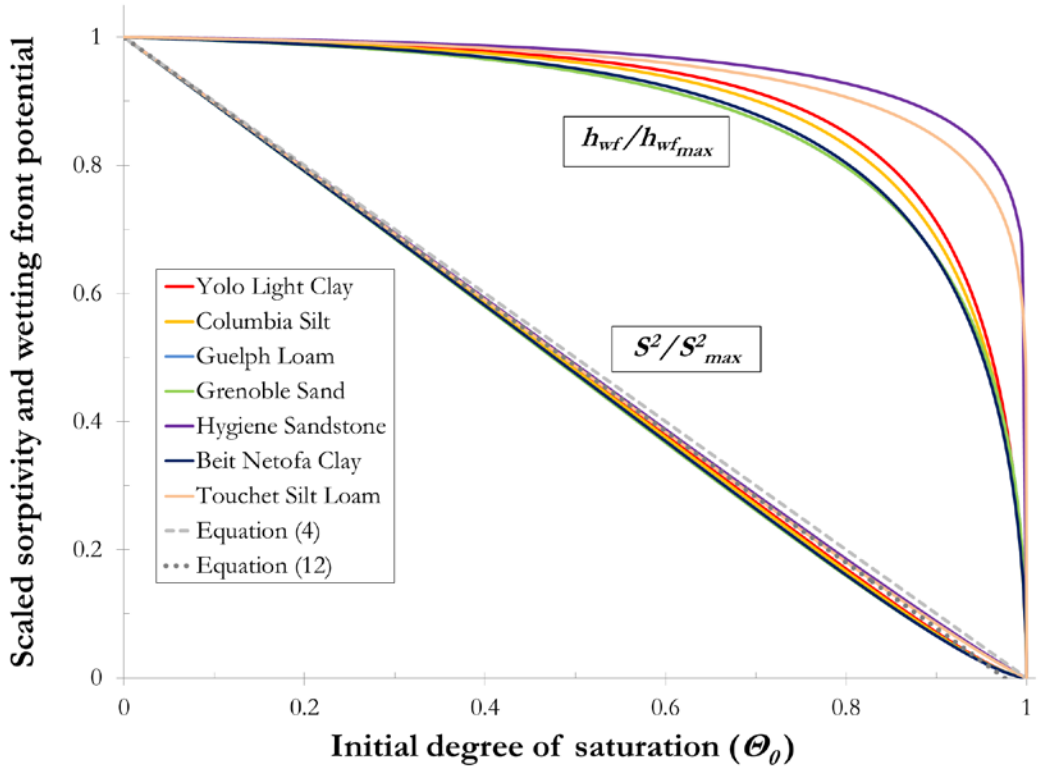

Figure 1 – Scaled sorptivity (S^2/S^2_{max}) and scaled wetting front potential ($h_{wf}/h_{wf,max}$) as functions of initial degree of saturation for the seven soils of Table 1. Values were calculated using Equations (10) and (11), respectively. Scaled forms of the traditional sorptivity model (Equation (4)) and modified sorptivity model (Equation (12)) are also shown.

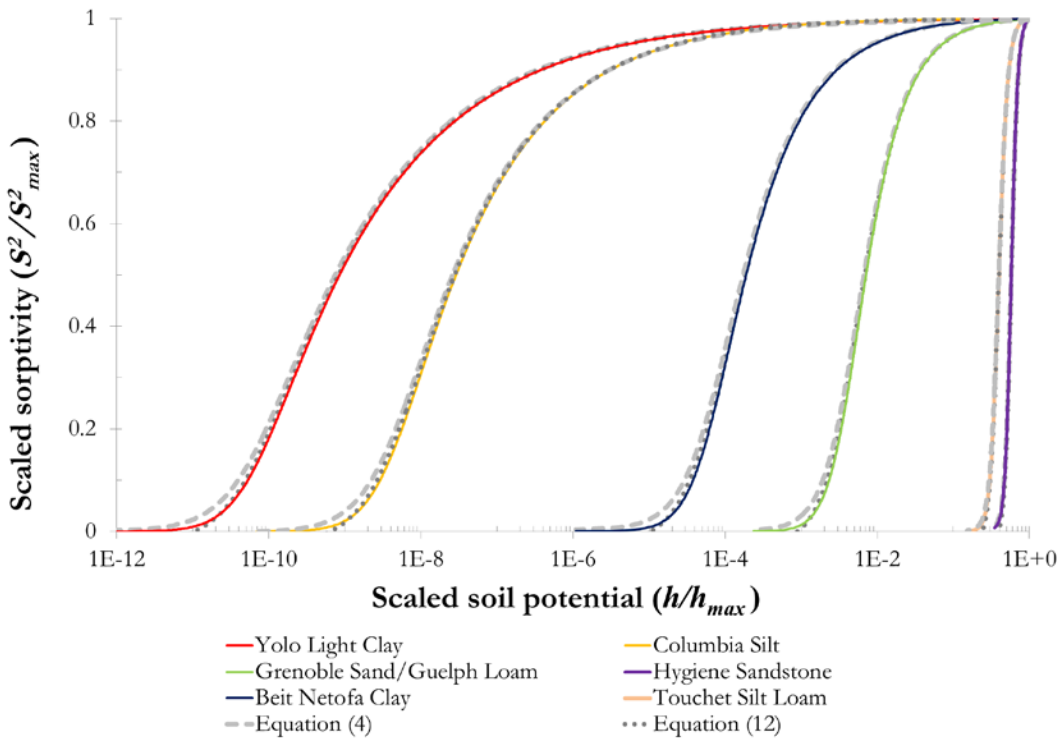

Figure 2 – Scaled sorptivity as a function of scaled soil potential for the seven theoretical soils. The scaled forms of Equations (4) (traditional sorptivity model) and Equation (12) (modified sorptivity model) are also shown for each soil type. It should be noted that the Grenoble Sand and Guelph Loam have nearly identical scaled shapes, and therefore are represented as a single curve.

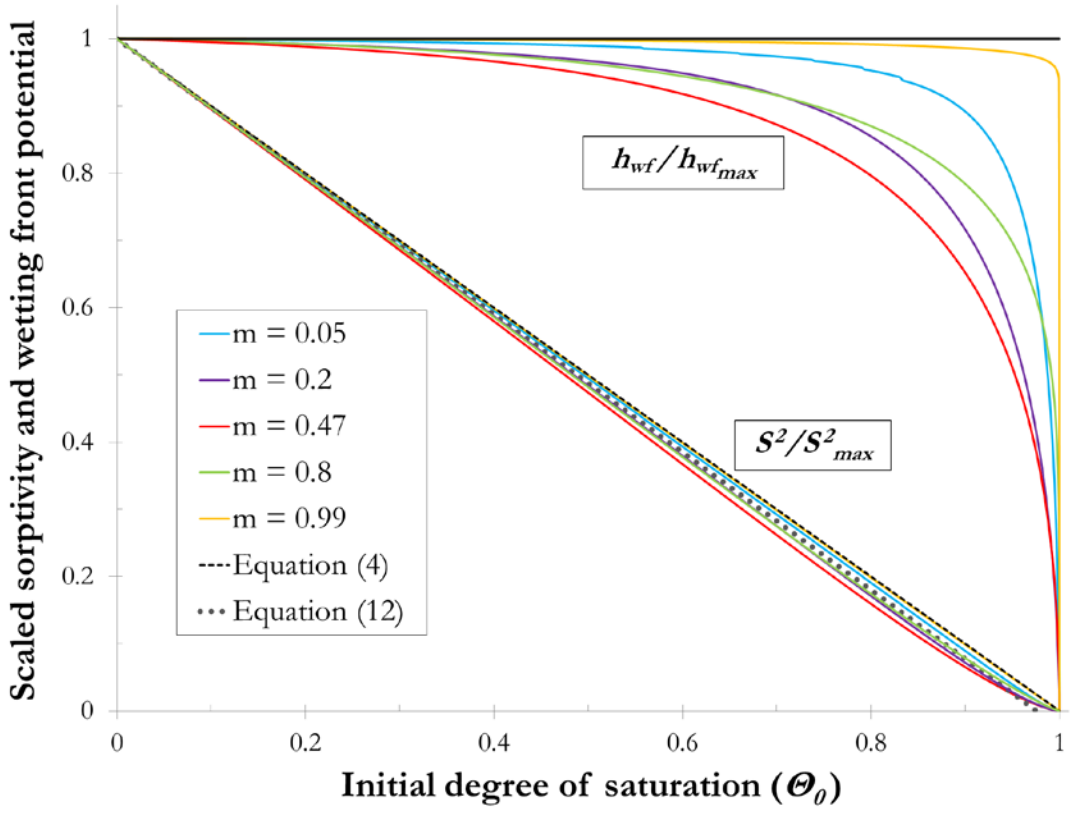

Figure 3 – The effect of pore size distribution (m) on wetting front potential and sorptivity. Equations (4) and (12) give, respectively, the traditional and modified sorptivity models.

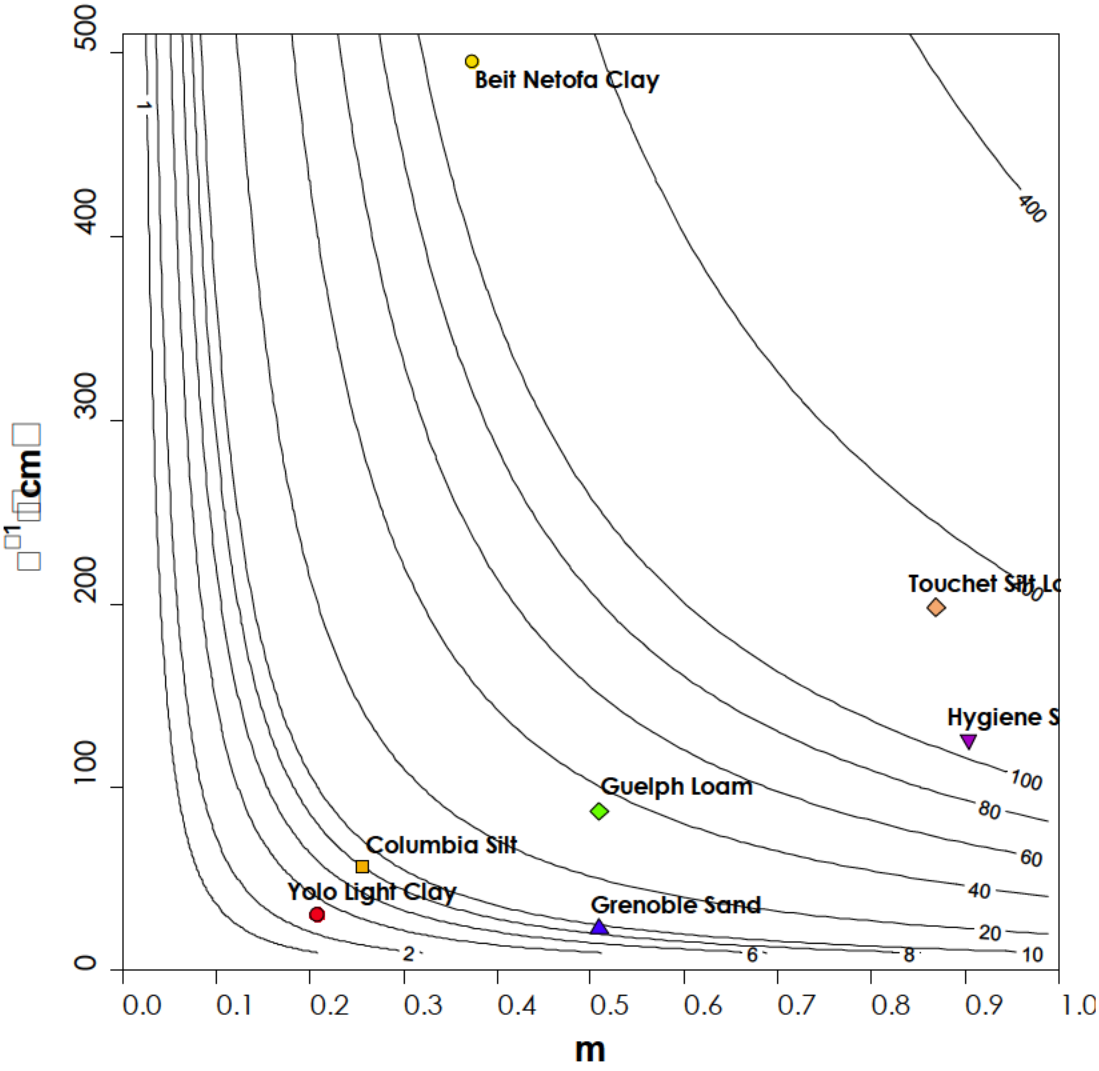

Figure 4 – Wetting front potential isolines (in cm) for initially dry soils as a function of van Genuchten parameters α and m. The seven soils of Table 1 are plotted for reference.

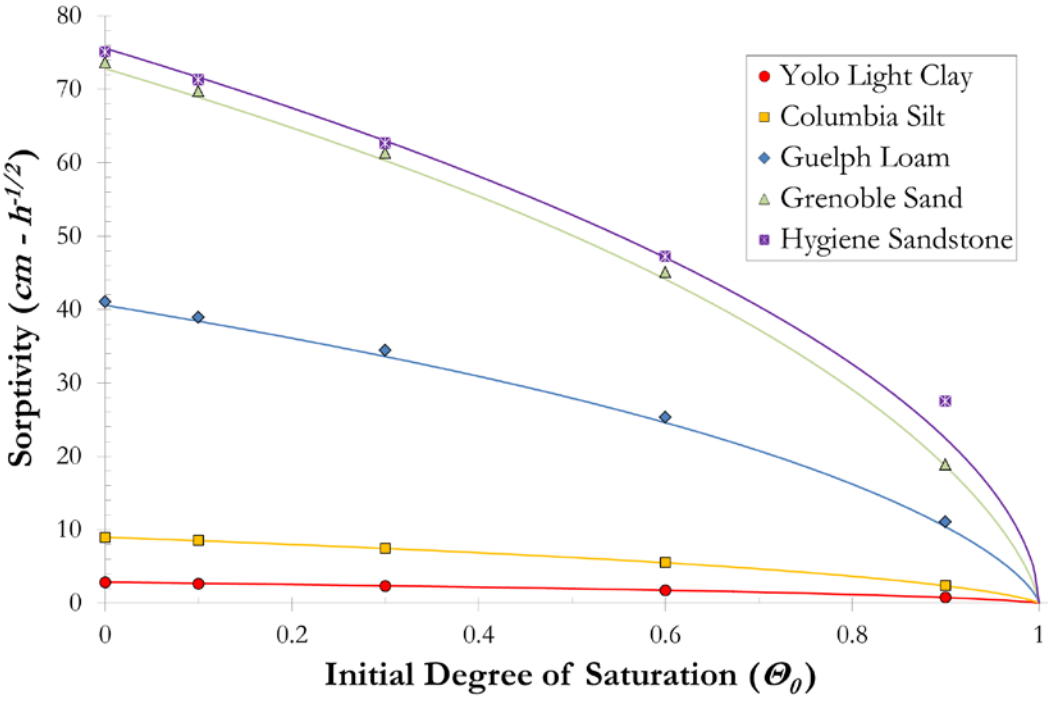

Figure 5 – Sorptivity versus initial degree of saturation for five of the theoretical soils. The lines are calculated using Equation (9), while the points are based on HYDRUS-1D simulations.

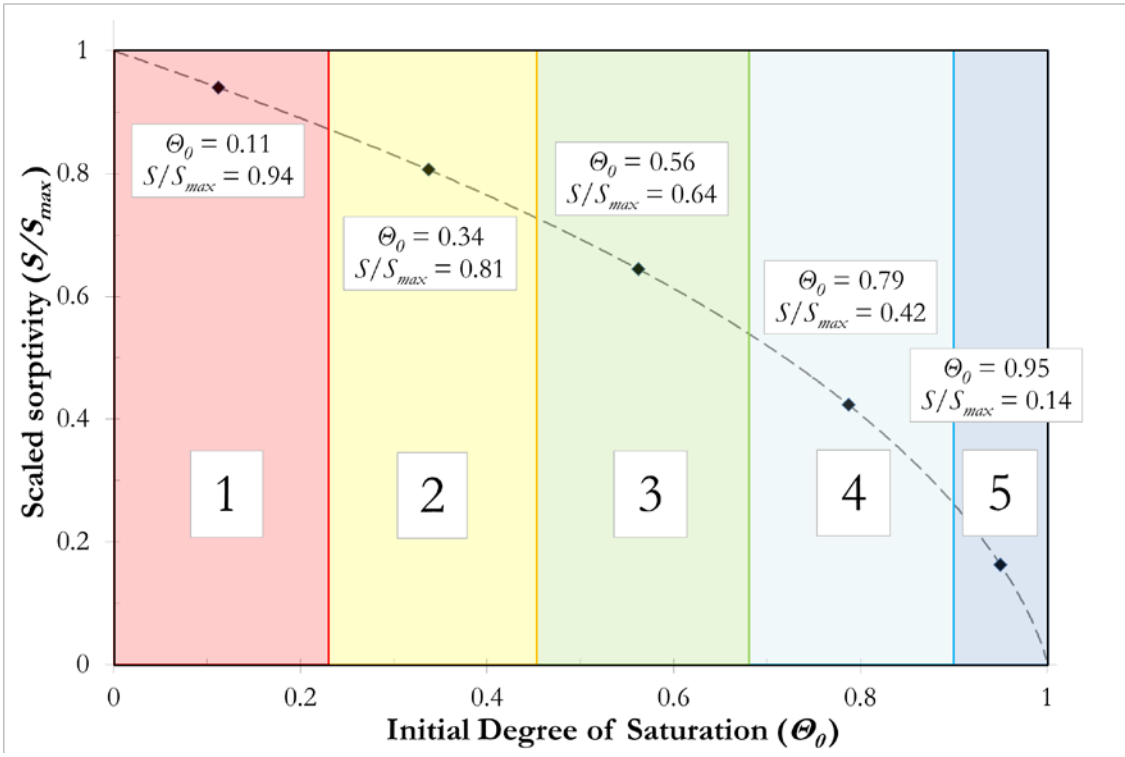

Figure 6 – Division of the S-Θ_0 curve into five qualitative regions, based on easily observed soil conditions. Region 1 corresponds to dry soils (0-25% available water content), Region 2 to slightly moist soils (25-50% available water content), Region 3 to moist soils (50-75% available water content), 4 to wet soils (75-100% available water content), and 5 to very wet soils (above field capacity).

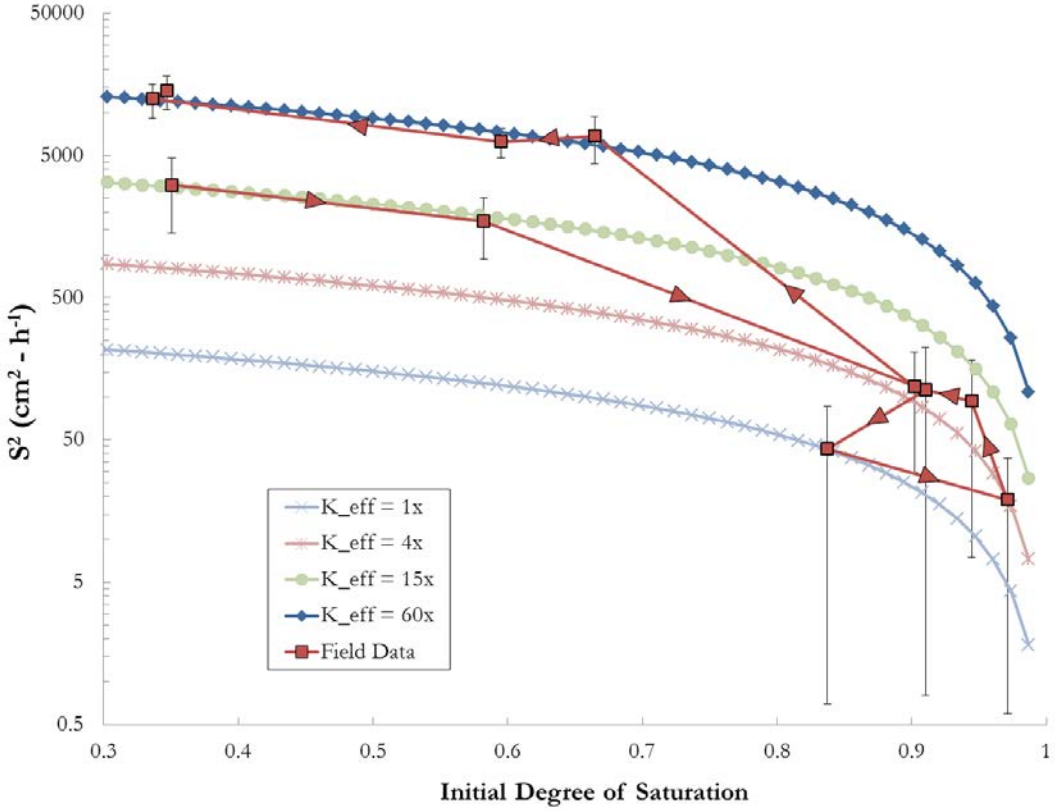

Figure 7 – Sorptivity isolines based on the relationship between sorptivity and initial degree of saturation (using Equation (10) and assuming $h_{surf} = 0$). The isolines represent the expected sorptivity of a soil with a constant saturated hydraulic conductivity. The field data come from a soil with vertic (shrink-swell) properties, which has varying effective hydraulic conductivity (K_{eff}) as macropores open and close. Sorptivity was estimated using the early-time approximation of *White et al.* [1992].

Tables

Table 1 – Parameters of the seven theoretical soils used for comparison (from *Fuentes et al.* [1992]).

Soil	θ_r	θ_s	α (cm^{-1})	m	n	K_s ($cm\ h^{-1}$)
Grenoble Sand	0	0.312	0.04318	0.5096	2.039	15.37
Guelph Loam	0.2183	0.52	0.0115	0.5089	2.036	1.3167
Columbia Silt	0	0.401	0.0176	0.256	1.344	0.21
Yolo Light Clay	0	0.495	0.0324	0.208	1.263	0.0443
Beit Netofa Clay	0.2859	0.4460	0.00202	0.3725	1.594	0.0034
Touchet Silt Loam G.E.3	0.1903	0.4690	0.00505	0.8690	7.634	12.625
Hygiene Sandstone	0.1531	0.2500	0.00793	0.9035	10.363	4.5

Table 2 – Wetting Front Potential (in cm) of seven theoretical soils at five different degrees of initial saturation. The column M-S uses the approximation of *Morel-Seytoux et al.* [1996] (Equation (5)) for initially dry soils.

Soil	$\Theta_0 = 0.0$	$\Theta_0 = 0.1$	$\Theta_0 = 0.3$	$\Theta_0 = 0.6$	$\Theta_0 = 0.9$	M-S
Grenoble Sand	9.22	9.18	9.03	8.46	6.10	9.64
Guelph Loam	34.57	34.39	33.85	31.75	23.03	36.11
Columbia Silt	7.98	7.95	7.85	7.49	5.51	8.29
Yolo Light Clay	3.08	3.07	3.04	2.92	2.20	3.18
Beit Netofa Clay	125.1	124.4	122.7	115.4	80.3	130.7
Touchet Silt Loam G.E.3	162.4	161.9	160.6	156.0	137.5	166.1
Hygiene Sandstone	109.1	108.9	108.2	105.5	95.5	111.0

Table 3 – Saturated Hydraulic Conductivities (K_s) used as input parameters, versus those calculated by Equation (13), for four different initial degrees of saturation. Units are in cm h^{-1}. Absolute error ranged from approximately 2% for dry soils to 17% for infiltration into wet sand. The solution poorly estimated the hydraulic conductivity for Hygiene Sandstone at $\Theta_0 = 0.9$, because of divergence in the sorptivity as calculated by HYDRUS-1D and by Equation (9).

Material	K_s Actual	K_s Calculated – Equation (13)			
		$\Theta_0 = 0.1$	$\Theta_0 = 0.3$	$\Theta_0 = 0.6$	$\Theta_0 = 0.9$
Grenoble Sand	15.4	15.0	15.1	14.6	12.8
Guelph Loam	1.32	1.29	1.31	1.27	1.21
Columbia Silt	0.210	0.203	0.201	0.200	0.180
Yolo Light Clay	0.0443	0.0439	0.0423	0.0414	0.0388
Hygiene Sandstone	4.5	4.4	4.4	4.5	7.5

3. Is the only constant change? Improved infiltration parameters for shrink-swell clay soils

Ryan D. Stewart[1]*, David E. Rupp[2], Majdi R. Abou Najm[3], John S. Selker[1]

[1] *Biological & Ecological Engineering Department, Oregon State University, Corvallis, OR, United States.*

[2] *Oregon Climate Change Research Institute, College of Earth, Ocean and Atmospheric Sciences, Oregon State University, Corvallis, OR, United States.*

[3] *Civil & Environmental Engineering, American University of Beirut. Beirut, Lebanon*

*Corresponding Author (stewarry@onid.orst.edu)

To be submitted for publication

Abstract

Shrink-swell clay soils are recognized to possess physical properties, such as saturated hydraulic conductivity and bulk density, which significantly vary with moisture content. This has made modeling infiltration in these soils challenging. Most approaches either try to capture the effects of large cracks while assuming the properties of the soil matrix itself do not vary, or else utilize complex physical models, including alternate coordinate systems, to intricately describe changes in the soil matrix due to long-time swelling. Neither approach, however, is an accurate reflection of actual field conditions. We use single-ring infiltration data collected monthly over a period of 1.5 years to examine how hydraulic properties within the soil matrix vary. It was determined that the use of initial soil moisture (Θ_0) as an additional parameter greatly increased the ability of infiltration models developed for non-swelling (rigid) soils to describe infiltration in a swelling medium, reducing the root mean square error (RMSE) by a factor of five. At the same time, a new soil "constant", A_0, was proposed as a replacement for effective hydraulic conductivity.

Introduction

Clay soils with shrink-swell properties – generally classified as *Vertisols* or *vertic* intergrades – are found all over the world, including many agricultural regions. *Vertic* soils are known to experience significant variation in their physical properties on seasonal and shorter timescales, as they dry out and then become re-wetted [*Messing*

and Jarvis, 1990; *Chertkov and Ravina*, 2001; *Peng and Horn*, 2007]. The mechanisms by which these soils interact with and are altered by water have been the subject of considerable study.

For example, it has been shown that the surface elevation of a swelling soil may increase during the course of an infiltration experiment [*Smiles*, 1974; *Gérard-Marchant et al.*, 1997]. During infiltration tests of long duration, this increased surface elevation will change the system's overall potential and overburden pressure [*Philip*, 1969; *Smiles*, 1974; *Talsma and Lelij*, 1976; *McIntyre et al.*, 1982a; *Giraldez and Sposito*, 1985]. However, there is reason to believe that material swelling is not a significant factor during short- or transient-time infiltration tests performed on structured soils. First, it has been found that swelling proceeds slowly [*Talsma and Lelij*, 1976; *McIntyre et al.*, 1982b], over time-scales of hours to days. Second, it has been shown that the total amount of elevation increase is relatively small compared to the time of testing. For example, *Gérard-Marchant et al.* [1997] had two samples which increased in height only 0.3 and 0.55 cm over infiltration tests lasting up to two days. Likewise, *Smiles* [1974] presents data which shows a quasi-linear relationship between time of swelling and increase in sample height, with a total increase of 2 cm over a period of approximately 100 hours. These relatively minor increases suggest that for purposes of rapid infiltration tests from shallowly-installed single ring infiltrometers, it may be valid to ignore the change in elevation. This opens up the

possibility of using infiltration equations developed for non-swelling soils to describe transient infiltration in swelling soils.

Using non-swelling soil concepts to describe infiltration in swelling soils requires a few special considerations, the most important of which is how to treat physical properties such as effective hydraulic conductivity (K_{eff}). For example, a handful of laboratory and field measurement have found that the effective hydraulic conductivity of a *vertic* soil decreases as the soil becomes wetter and the cracks decrease in size [*Bouma et al.*, 1979; *Leeds-Harrison et al.*, 1986; *Messing and Jarvis*, 1990], though this effect was considered to be primarily based on the contributions of large (> 1 cm) cracks which formed throughout the soil profile. This has led to the development of infiltration models which describe flow into cracks using modifications to the kinematic wave equation [*Greco*, 2002; *Römkens and Prasad*, 2006], the Richards' equation [*Novák et al.*, 2000] or the Green-Ampt model [*Davidson*, 1984].

There has been less study and consensus on how (and if) the hydraulic conductivity of the soil matrix itself varies at different water contents. Some formulations make the simple assumption that the properties of the soil matrix are essentially constant in time and can therefore be described with the Darcy-Buckingham and Richards equations [*Kutílek*, 1996; *Novák et al.*, 2002]. Other studies have assumed that the permeability of a swelling soil matrix will increase as the soil swells and the space

between clay particles increases [*Tavenas et al.*, 1983; *Su,* 2010]. Similarly, it has been theorized that small, inter-aggregate (capillary) cracks within the soil matrix can provide significant contribution to both vertical and horizontal hydraulic conductivity under wet conditions [*Chertkov and Ravina,* 2000; 2001; *Chertkov,* 2002], an effect that will diminish as soil dries and the cracks dewater. *Das Gupta et al.* [2006] showed that field-saturated hydraulic conductivity (K_{fs}) increased as the soils became wetter, though the correlation was weak. On the other hand, *Jabro* [1996] used a Guelph permeameter to estimate K_{fs} in an expansive silt loam, and found that K_{fs} increased as the soils became drier.

Altogether, there appears to exist a significant disconnect about how the matrix properties of an aggregated *vertic* soils vary with moisture. This study, based on repeated infiltration tests conducted in the matrix (non-macropore) portion of a shrink-swell soil, therefore had two main objectives. The first was to use standard infiltration models to identify shifts in the hydraulic properties of the soil matrix at soil moisture contents, specifically to quantify variations in effective hydraulic conductivity. The second goal was then to use that information to develop a suitable expression to which describes how water moves through the matrix of *vertic* soils under any moisture content.

Theory

For purposes of this discussion we will consider soil to have three porosity domains: 1) the *inter*-particle domain, which includes the pores between individual soil particles [*Abou Najm et al.*, 2010]; 2) the *inter*-aggregate domain, which includes *intra*- and *inter*-pedal pores [*Kutílek*, 1996], capillary cracks [*Chertkov and Ravina*, 2001], and *intra*-matrix macropores [*Abou Najm et al.*, 2010]; and 3) the *inter*-block domain, which includes visible macropores such as large shrinkage cracks, as well as any decrease in surface elevation of the soil due to subsidence (Figure 1). For purposes of this discussion, Domain 1 will be referred to as the *inter*-particle porosity (V_{ip}), Domain 2 will be referred to as the *inter*-aggregate (micro) cracks (V_{ia}), and Domain 3 will be referred to as the *inter*-block cracks (V_{ib}). Domains 1 and 2 form what is considered to be the soil matrix, whereas Domains 2 and 3 collectively form what can be referred to as the structural porosity of the soil.

Void ratio (e), moisture ratio (ϑ) and degree of saturation (Θ) for a soil sample may be calculated by

$$e = \frac{V_p}{V_s} \tag{1}$$

$$\vartheta = \frac{V_w}{V_s} \tag{2}$$

$$\Theta = \frac{\vartheta}{e} = \left(\frac{V_w / V_s}{V_p / V_s} \right) = \frac{V_w}{V_p} = \left(\frac{(m_0 - m_{dry}) / \rho_w}{V_0 - (m_{dry} / \rho_s)} \right) \quad (3)$$

where V_w is the volume of water, V_s is the volume of solids, V_p is the volume of pores (voids), m_0 is the mass of the sample, m_{dry} is the mass of the sample after drying for 24 hours at 105 °C, ρ_w is the density of water, V_0 is the original volume of the sample, and ρ_s is the density of the solids (assumed to be equal to 2.7 g cm^{-3}).

Many different soil shrinkage curve models have been developed to describe the relationship between e and ϑ for the *inter*-particle domain, with varying number of terms and parameters [*Giráldez et al.*, 1983; *McGarry and Malafant*, 1987; *Braudeau*, 1988; *Tariq and Durnford*, 1993]. Most of these models have a sigmoid shape which includes three, four or five distinct shrinkage phases. Though these models generally describe e as a function of ϑ , it is also possible to use the relationship between Θ_0, e and ϑ (Equation (3)), to plot e against Θ (Figure 2).

The relative void ratio (e/e_{max}) can be then approximated using a simple one-term model:

$$\frac{e}{e_{\max}} = \frac{\xi \Theta^n}{1 + \xi \Theta^n} \quad (4)$$

where ξ and n are shape parameters and emax is the maximum void ratio, when $\Theta = 0$ (Figure 2).

Now let us take a representative soil element of fixed volume. If the individual solid particles do not significantly change in volume, it stands to reason that total porosity of the representative soil volume will be unchanged [*Kutílek*, 1996]. Therefore, as the *inter*-particle porosity decreases according to the soil shrinkage curve, the *inter*-aggregate and *inter*-block (structural) porosities will necessarily increase [*Novák*, 1976]. That is to say, if we take a constant representative soil volume, as the *intra*-aggregate void ratio decreases, the structural porosity (Φ) will increase. This relative structural porosity (Φ / Φ_{max}) will therefore have an inverse sigmoidal shape, which can be approximated using the following equation:

$$\frac{\phi}{\phi_{\max}} = \frac{1}{1 + \xi \Theta^{n}} \tag{5}$$

where Φ_{max} is the maximum structural porosity, when $\Theta = 0$ (Figure 2).

We now make a series of basic assumptions. First, we suppose that the structural porosity will be distributed among multiple scales. Some of the porosity will be manifest in *inter*-block shrinkage cracks, but some of the porosity will occur as micro-cracks within the soil matrix, around and between individual aggregates. Because these *inter*-aggregate cracks will likely be far more permeable than the actual

aggregates, we can assume that the hydraulic properties of the soil matrix will be greatly affected by the size of these micro-cracks. Contrary to *Chertkov and Ravina* [2001], we assume that in a structured soil the size of the micro (capillary) cracks will increase with decreasing soil moisture.

Next, we assume that the distribution of porosity between the *inter*-particle and structural domains is reversible and independent of the process direction, which therefore ignores any hysteretic effects. We also assume that both the *inter*-block and *inter*-aggregate porosities can be well-described using Equation (5), and they may be differentiated by use of distinct values of Φ_{max} (Figure 3). Several studies have concluded that the geometries of soil cracks can be described over multiple scales using fractal concepts [*Peyton et al.,* 1994; *Preston et al.,* 1997], giving validity to this conjecture.

Further, if the *inter*-aggregate cracks are indeed analogous to the easily observed *inter*-block cracks, then we can assume that their widths are much smaller than their other dimensions. As such, it can be stated that changes in micro-crack porosity will be proportional to changes in crack width, i.e.

$$w \propto \frac{1}{1+\xi\Theta^{n}} \tag{6}$$

Finally, if we assume that water moving through these micro-cracks will demonstrate Newtonian behavior (i.e. will behave as bulk, rather than adsorbed water), then the flow can be modeled using the Plane-Poiseuille equation for flow between parallel plates and the mean velocity ($\bar{u}$) can be related to the crack width by

$$\bar{u} = -\frac{w^2}{12\mu}\nabla P \tag{7}$$

where μ is the fluid viscosity and ∇P is the pressure gradient driving the flow. For flow between parallel plates (slits), the hydraulic conductivity can then be found by [*Tuller and Or*, 2001]

$$K_s = \frac{\rho g w^2}{12\mu} \tag{8}$$

We make three assumptions here: 1) for short time periods, such as during short duration infiltration tests, soil swelling can be ignored and the geometry of the slits will be constant; 2) air is able to escape in advance of the wetting front, so as to not create pressure equilibriums; and 3) behind the wetting front the slits are filled with water, so that we can equate K_{eff} with K_s. With these assumptions, Equations (6) and (8) can be combined to describe how K_{eff} varies with degree of saturation

$$K_{eff} \propto \left(\frac{1}{1+\xi\Theta^n}\right)^2 \tag{9}$$

In the classic Philip model for one-dimensional vertical infiltration [*Philip*, 1957], infiltration (I) can be expressed as an equivalent water depth by

$$I = S\sqrt{t} + At \tag{10}$$

where S is the soil sorptivity and A is a term to describe the flow's resistance to gravity. A is typically considered to be directly related to K_{eff}. For real soils values of $0.3 < A/K_{eff} < 0.4$ have been found to provide realistic results [*Philip*, 1990]. This in turn implies that the parameter A, like K_{eff}, should be constant for a given soil. In a *vertic* soil, however, the influence of *inter*-aggregate cracks should cause these parameters to significantly vary. Therefore, we propose that for describing infiltration in shrink-swell clay soils the second term, A, in the two-term Philip model be replaced with the following expression

$$A = A_0\left(\frac{1}{1+\xi\Theta^n}\right)^2 \tag{11}$$

where A_0 becomes a soil constant which is proportional to the effective hydraulic conductivity of the dry soil.

Finally, we turn to the sorptivity of the soil. When water is infiltrating from a source of low constant head ($h \approx 0$), the sorptivity of a rigid (non-swelling) soil varies with initial degree of saturation (Θ_0) by (Stewart *et al.*, in review)

$$S = S_0\sqrt{(1-a\Theta_0)} \tag{12a}$$

$$S_0 = \sqrt{2K_{eff}h_{wf}(\theta_s - \theta_r)} \tag{12b}$$

where S_0 is the dry soil sorptivity, h_{wf} is the wetting front potential, θ_s and θ_r are the saturated and residual water contents, respectively, and a is a constant used to approximate the decrease in wetting front potential at higher moisture contents. In a swelling soil, it would be expected that sorptivity will vary as the soil aggregates swell and shrink. However, because subsequent analysis showed that trying to account for swelling offered no appreciable improvement in this particular soil, Equation (12) was retained for the sake of both simplicity and brevity. The alternative expression for sorptivity is presented as an appendix which follows the main portion of the paper.

Finally, substituting Equations (11) and (12) into (10), vertical infiltration into a swelling soil can be described as

$$I(\Theta_0) = S_0\sqrt{(1-a\Theta_0)t} + A_0\left(\frac{1}{1+\xi\Theta_0{}^n}\right)^2 t \tag{13}$$

Methods

Sampling protocol

Over an 18-month period (September 2011 – March 2013), single ring infiltration tests were conducted on a 2 x 3 m field plot located near Corvallis, Oregon. Twelve shallowly-installed rings of 9.6 cm diameter were used for the tests; slightly-positive ($h \geq 0$) constant head conditions were used. The soil was classified as a Waldo silty loam, though its strong *vertic* properties suggested that the soil may be better described as an inclusion of Witham silty clay loam from an adjacent mapping unit [*Knezevich*, 1975]. Hydrometer measurements showed the soil to have sand, silt and clay percentages of 5%, 37%, and 58%, respectively.

The infiltration tests were conducted monthly, with the exception of January 2012, when flooding of the field site made infiltration measurements impossible. The rings were left in the same place for the first year; however, as the soil re-dried in the summer of 2012, the soil within the rings became degraded, including a notable decrease in relative surface elevation and the presence of large cracks inside the ring. For this reason, it was determined that tests taken in the period June – September 2012 would not be included in the subsequent analysis, as the observed infiltration rates were indicative of macropore flow through large *inter*-block cracks rather than flow through the soil matrix. Beginning in October 2012, the rings were randomly repositioned within the grid to ensure that new soil was being sampled each month.

For each infiltration test, water was added to the ring in 0.1 L increments, up to 1 L total. Water was added to the ring once the water level had fallen enough to expose approximately 50% of the soil surface, and the time of each pour was recorded. An example infiltration data set, collected on May 8, 2012, is shown in Figure 4.

As part of each infiltration test, soil samples were collected from two depths – 8 cm and 12 cm – at three random locations within the plot. The soil samples were 5.4 cm in diameter and 3 cm in length, for a total volume of 68.7 cm^3, and were used to determine bulk density and gravimetric water content, and could be used to determine void ratio, moisture ratio and degree of saturation using Equations (1) – (3).

In addition, six of the collected samples were measured for their water retention curves, using a positive pressure system over the range 0 – 500 kPa. The retention curves were then fit using the *Van Genuchten* [1980] model, with mean values of α = 3.85 x 10^{-3} and m = 2.2 x 10^{-1}. These values translated to an equivalent wetting front potential (in dry soil conditions) of 50 cm [*Morel-Seytoux et al.,* 1996].

Data Analysis

The infiltration test data were analyzed using the two-term Philip infiltration model (Equation 10), rewritten in the general form suggested by *Smiles and Knight* [1976]

$$I = C_1 t^{1/2} + C_2 t \qquad (14)$$

where C_1 and C_2 are constants which describe the capillary (sorptivity) and gravity forces, respectively. If Equation (14) is divided by √t, i.e.

$$\frac{I}{t^{1/2}} = C_1 + C_2 t^{1/2} \tag{15}$$

then C_1 and C_2 can be determined as the intercept and slope of a line fit to infiltration data.

As an assessment of how non-swelling soil infiltration concepts would describe the effective hydraulic conductivity, K_{eff}, of a swelling soil, both infiltration terms (C_1 and C_2) were independently used to estimate K_{eff}. In the case of the former, C_1 was assumed to be equal to the soil sorptivity, S, and Equation (12) was rearranged to produce

$$K_{eff\ i} = \frac{C_{1_i}{}^2}{2h_{wf}(\theta_s - \theta_r)(1 - a\Theta_{0_i})} \tag{16a}$$

In the case of the latter, C_2 was assumed to be related to K_{eff} by a proportionality constant [*Philip*, 1990], which we will call P, so that

$$K_{eff\ i} = \frac{C_{2_i}}{P} \tag{16b}$$

A value of $P = 0.55$ was selected, as it was found to best approximate three-dimensional flow effects (please refer to the electronic supplement for more detail). Other values assumed during analysis were $h_{wf} = 50$ cm, $(\theta_s - \theta_r) = 0.4$, and $a = 1$.

Crack porosity shape parameters

Using Equation (4) to describe the soil shrinkage curve in terms of e and Θ, it was determined that values of $\xi = 11$ and $n = 7$ provided the best fit to laboratory-measured soil shrinkage data for a Witham silty clay soil [*Stewart et al.*, 2012] (as seen in Figure 1). The inverse curve shape (Equation 5) also matches well with observed increase of crack porosity with decreasing volumetric water content shown for a Slovakian Vertisol [*Novák*, 1976] when using those same values for ξ and n.

Error assessment

To compare between different infiltration models (i.e. between Equation (10) and Equation (13)), a single-value Root Mean Square Error (RMSE) estimator was used.

Each infiltration test had up to $n = 10$ values of measured elapsed time, t, which corresponded to the time at which 0.1 L (1.4 cm) of water, added incrementally at each time t_{i-1}, had completely infiltrated in the single-ring infiltrometer. Here j indexes the elapsed time measurement: $j = 1, 2, \ldots n$. For test k, the actual infiltration I (in cm) at t_j can be given by

$$I_{j,k} = 1.4j \tag{17}$$

and the predicted infiltration $\hat{I}$ at that same time can be expressed as

$$\hat{I}_{j,k} = C_1\sqrt{t_{j,k}} + C_2 t_{j,k} \tag{18}$$

where constants C_1 and C_2 will differ between models and tests.

The single value RMSE over all m tests was calculated by

$$RMSE = \sqrt{\frac{\sum_{k=1}^{m}\sum_{j=1}^{n}\left(\frac{\hat{I}_{j,k} - I_{j,k}}{I_{j,k}}\right)^2}{mn}} \tag{19}$$

Results and Discussion

Infiltration parameters

203 individual infiltration tests were conducted over the 1.5 year duration of the experiment, and were then analyzed for coefficients C_1 and C_2 using Equation (15) (Figure 5). Due to visible macropores forming within the rings during the summer of 2012, the measurements for June, July, August, and September of that year were not included in subsequent analyses (these measurements are shown shaded in gray in Figure 5). 48 individual measurements were thus removed, leaving 155 in total. Of those 155, an additional 10 provided negative estimates for C_1, and were also excluded from subsequent analysis.

For the remaining 145 valid measurements, C_2 (the gravity term) was generally of the same order of magnitude or larger than C_1^2 (the sorptivity term squared) (Figure 6). Thus, at all but the very earliest times gravity appears to be a significant factor driving flow in *vertic* soils. This appears to be true even in wet conditions, and stands in contrast to previous work which estimated that the effect of gravity will be limited and that the first infiltration term will dominate for long periods [*Smiles*, 1974]. However, that specific conclusion was based on the hydraulic conductivity of a continuous (non-cracked) soil matrix of very low permeability, and is likely not indicative of structured soils found in field settings.

Next, Equation (16) was used to assess variations in effective hydraulic conductivity, as captured by both infiltration terms. Interestingly, the K_{eff} calculated from C_1 did not show any significant trend over the range of initial soil moisture (Figure 7a), with an r^2 value of 0.01. This is in contrast to K_{eff} calculated from C_2, which strongly decreased over the range of soil moisture ($r^2 = 0.4$), changing almost two orders of magnitude from dry to wet conditions (Figure 7b). Moreover, the K_{eff} derived from C_2 reached a value at the wet end which was similar to the overall mean value of K_{eff} found from C_1 (5 cm-hr^{-1}). This suggests that the first and second infiltration terms may truly be capturing different scales and/or processes, that the pores controlling capillarity may be more stable in size and/or geometry than those affected by gravity,

and that as the soil swells the *inter*-particle matrix pores, rather than the *inter*-aggregate micro-cracks, become increasingly important to infiltration.

It should be noted here that all of the infiltration measurements were performed under a slight positive head, which likely allowed water to flow through any structural porosity, including the micro-cracks. It is not clear if the observed inverse relationship between K_{eff} and soil moisture would still be seen if a tension infiltrometer had instead been used, though measurements taken by *Das Gupta et al.* [2006] showed drier soils having higher hydraulic conductivity under tension values < -10 cm.

Evaluation of A_0 parameter

Individual and mean A_0 values were determined from the C_2 values of the Philip two-term model by

$$A_{0i} = C_{2_i}(1+\xi(\Theta_{0_i})^n)^2 \qquad \overline{A_0} = \frac{1}{n}\sum_{i=0}^{n} C_{2_i}(1+\xi(\Theta_{0_i})^n)^2 \tag{20}$$

using values of $\xi = 11$ and $n = 7$ (as previously discussed in the *Crack porosity shape parameters* section) . It should be noted that the arithmetic mean was utilized based on the assumption that the heterogeneity of the media was much greater in the direction parallel to flow (vertical) than in the direction perpendicular to flow (horizontal).

The A_0 parameter showed significant variability (Figure 8), even for measurements repeated monthly in fixed locations, yet the overall and individual trend lines did not show significant bias and could therefore be considered essentially constant. Thus, for swelling soils A_0 may be considered to be a more appropriate descriptive parameter than K_{eff}.

Comparison of models

Next, the mean value of $\overline{A_0}$ (Equation 20) was used to compare the standard (non-swelling soil) infiltration model (Equation (10)) with the adjusted infiltration model (Equation (13)). For the non-swelling model, A was assumed to be constant and equal to the mean calculated C_2 value, while S was assumed to vary only with initial degree of saturation according to Equation (12), with the constant a = 1.025.

The results show that Equation (13), due to incorporation of the moisture-dependent crack porosity term, substantially improved the ability to model short-time infiltration into swelling soils, with a fivefold reduction in RMSE (Figure 9). Further, the median values for Equation (13) followed the theoretical 1:1 line compared to a notable over-prediction of infiltration depth by Equation (10). Altogether, Equation (13) was deemed to have provided a suitable correction for the effect of micro-scale cracks on the effective hydraulic conductivity.

Use in other vertic soils

Infiltration data collected from a *vertic* soil located in South-central Chile were also used for purposes of comparison (a detailed description of the site, procedures, and analysis are found in Chapter 4). The soil's near-surface (0-20 cm) percentages of sand, silt and clay were measured as 44%, 31%, and 25%, respectively, which provides a distinctly different texture from the main soil discussed in this paper. Using values of ξ =7 and n = 6, A_0 appears to be a constant (though once again noisy) parameter throughout range of initial soil moisture (Figure 10). Thus, it appears that Equation (11) can be used to satisfactorily describe the infiltration behavior of different types of aggregated *vertic* soils.

Summary

Field infiltration data from a shrink-swell (*vertic*) soil were analyzed using the two-term, one-dimensional vertical Philip infiltration model. This model showed that the effective hydraulic conductivity (K_{eff}) experienced a sharp decrease with increasing soil moisture. This was likely due to changes in the size and structure of microscopic capillary cracks found throughout the soil matrix.

By using a simple one-term approximation to describe the soil shrinkage curve (as measured from collected soil samples), we were able to describe changes in capillary crack porosity as a function of degree of saturation (Θ). This capillary crack porosity

term was then used to modify the hydraulic conductivity of a swelling soil, so as to approximate how it varied with water content. This led to the proposal of a new soil constant, A_0, which could be substituted for effective hydraulic conductivity. A_0 , combined with the expression for relative crack porosity, was seen to significantly improve the ability of the standard Philip two-term model to describe infiltration into a swelling soil at all water contents, reducing RMSE by a factor of five.

Overall, A_0 and relative crack porosity represent simple descriptive parameters which, when combined, provide an accurate way to account for changes in the structure and hydraulic properties of an aggregated *vertic* soil. Unlike competing solutions, which utilize complex formulations involving large parameter sets, translation into material coordinates, transformation of variables, and/or complicated integrals and partial differential equations, these parameters can be directly substituted into basic infiltration solutions developed for non-swelling soils. This in turn should allow for their straightforward incorporation into large-scale hydrologic models and other practical applications.

Appendix – Sorptivity as a function of micro-crack porosity

Sorptivity, as expressed by Equation (12), includes both an effective hydraulic conductivity term (K_{eff}) and a term for wetting front potential (h_{wf}). Both of these parameters are expected to vary as the soil aggregates swell and shrink. While changes in K_{eff} have has already been described using Equation (9), to estimate the

changes in h_{wf} we begin with the Laplace equation, which, while not exactly equivalent to wetting front potential, in this instance allows for a suitable approximation for the capillary rise (h_c) as a function of separation width between parallel plates

$$h_c = \frac{2\sigma \cos\gamma}{w} \tag{3.A1}$$

where σ is the surface tension of the fluid and γ is the contact angle between the fluid and the surface. Using the crack porosity function of Equation (6), h_{wf} can now be proportionally related to the capillary crack porosity by

$$h_{wf} \propto 2\sigma \cos\gamma (1 + \xi \Theta_0{}^n) \tag{3.A2}$$

We now define B_0 as the dry soil capillarity, and consider it to be the product of K_{eff} and h_{wf} under initially dry conditions ($\Theta_0 = 0$). As such, B_0 has units of $L^2\ t^{-1}$. We can then combine Equations (9), (12) and (3.A2) to express sorptivity for a swelling soil as

$$S = \sqrt{2B_0(\theta_s - \theta_r)\frac{(1 - a\Theta_0)}{(1 + \xi \Theta_0{}^n)}} \tag{3.A3}$$

When equation (3.A3) is used within the two-term Philip model, i.e.,

$$I(\Theta_0) = \left(2B_0(\theta_s - \theta_r)\frac{(1 - a\Theta_0)}{(1 + \xi{\Theta_0}^n)}t \right)^{1/2} + A_0\left(\frac{1}{1 + \xi{\Theta_0}^n} \right)^2 t \qquad (3.A4)$$

it may offer a slight improvement to the estimate of soil sorptivity compared to Equation (12) (Figure 3.A1a), though the overall RMSE values were nearly identical.

When used in conjunction with a one-term early time approximation model [*White et al.*, 1992], i.e.,

$$I = S\sqrt{t} = \left(2B_0(\theta_s - \theta_r)\frac{(1 - a\Theta_0)}{(1 + \xi{\Theta_0}^n)}t \right)^{1/2} \qquad (3.A5)$$

Equation (3.A3) offers a better visual description of sorptivity (Figure 3.A1b), though again overall RMSE values were unchanged.

References

Abou Najm, M. R., J. D. Jabro, W. M. Iversen, R. H. Mohtar, and R. G. Evans (2010), New method for the characterization of three-dimensional preferential flow paths in the field, *Water Resources Research, 46*(2).

Bouma, J., A. Jongerius, and D. Schoonderbeek (1979), Calculation of saturated hydraulic conductivity of some pedal clay soils using micromorphometric data, *Soil Science Society of America Journal*, *43*(2), 261-264.

Braudeau, E. (1988), Essai de caractérisation quantitative de l'état structural d'un sol basé sur l'étude de la courbe de retrait, *CR Académie des Sciences, Série 2*, 307, 1933-1936.

Chertkov, V. Y. (2002), The Horizontal Hydraulic Conductivity of Vertical Interaggregate Capillary Cracks in Clay Soils, in *Physical Methods in Agriculture*, edited, pp. 39-50, Springer.

Chertkov, V. Y. (2012), Physical modeling of the soil swelling curve vs. the shrinkage curve, *Advances in Water Resources*.

Chertkov, V. Y., and I. Ravina (2000), Shrinking-swelling phenomenon of clay soils attributed to capillary-crack network, *Theory and Applied Fracture Mechanics*, *34*(1), 61-71.

Chertkov, V. Y., and I. Ravina (2001), Effect of interaggregate capillary cracks on the hydraulic conductivity of swelling clay soils, *Water Resources Research*, *37*(5), 1245-1256.

Davidson, M. R. (1984), A Green-Ampt Model of infiltration in a cracked soil, *Water Resources Research*, *20*(11), 1685-1690.

Das Gupta, S., B. P. Mohanty, and J. M. Köhne (2006), Soil hydraulic conductivities and their spatial and temporal variations in a vertisol, *Soil Science Society of America Journal*, *70*(6), 1872-1881.

Gérard-Marchant, P., R. Angulo-Jaramillo, R. Haverkamp, M. Vauclin, P. Groenevelt, and D. Elrick (1997), Estimating the hydraulic conductivity of slowly permeable and swelling materials from single-ring experiments, *Water Resources Research*, *33*(6), 1375-1382.

Giraldez, J. V., and G. Sposito (1985), Infiltration in swelling soils, *Water Resources Research*, *21*(1), 33-44.

Giráldez, J. V., G. Sposito, and C. Delgado (1983), A general soil volume change equation: I. The two-parameter model, *Soil Science Society of America Journal*, *47*(3), 419-422.

Greco, R. (2002), Preferential flow in macroporous swelling soil with internal catchment: model development and applications, *Journal of Hydrology*, *269*(3), 150-168.

Jabro, J. D. (1996), Variability of field-saturated hydraulic conductivity in a Hagerstown soil as affected by initial water content, *Soil Science, 161*(11), 735-739.

Knezevich, C. A. (1975), Soil Survey of Benton County Area, Oregon, US Soil Conservation Service.

Kutílek, M. (1996), Water relations and water management of vertisols, *Developments in Soil Science, 24*, 201-230.

Leeds-Harrison, P., C. Shipway, N. Jarvis, and E. Youngs (1986), The influence of soil macroporosity on water retention, transmission and drainage in a clay soil, *Soil Use and Management, 2*(2), 47-50.

McGarry, D., and K. W. J. Malafant (1987), The analysis of volume change in unconfined units of soil, *Soil Science Society of America Journal*, *51*(2), 290-297.

McIntyre, D., J. Loveday, and C. Watson (1982a), Field studies of water and salt movement in an irrigated swelling clay soil. I. Infiltration during ponding, *Soil Research*, *20*(2), 81-90.

McIntyre, D., C. Watson, and J. Loveday (1982b), Swelling of a clay soil profile under ponding, *Soil Research*, *20*(2), 71-79.

Messing, I., and N. J. Jarvis (1990), Seasonal variation in field-saturated hydraulic conductivity in two swelling clay soils in Sweden, *Journal of Soil Science, 41*(2), 229-237.

Morel-Seytoux, H. J., P. D. Meyer, M. Nachabe, J. Touma, M. T. van Genuchten, and R. J. Lenhard (1996), Parameter equivalence for the Brooks-Corey and van Genuchten soil characteristics: Preserving the effective capillary drive, *Water Resources Research*, *32*(5), 1251-1258.

Novák, V. (1976), Cracks in swelling soil and the calculation of their characteristics, *Water in Heavy Soils, Proc. II, ICID and ISSS, Bratislava*, 21-41.

Novák, V., J. Šimůnek, and M. T. Van Genuchten (2000), Infiltration of water into soil with cracks, *Journal of Irrigation and Drainage Engineering*, *126*(1), 41-47.

Novák, V., J. Šimůnek, and M. T. Van Genuchten (2002), Infiltration into a swelling, cracked clay soil, *Journal of Hydrology and Hydromechanics*, *50*(1), 3-19.

Peng, X., and R. Horn (2007), Anisotropic shrinkage and swelling of some organic and inorganic soils, *European Journal of Soil Science*, *58*(1), 98-107.

Peyton, R. L., C. J. Gantzer, S. H. Anderson, B. A. Haeffner, and P. Pfeifer (1994), Fractal dimension to describe soil macropore structure using X ray computed tomography, *Water Resources Research*, *30*(3), 691-700.

Philip, J. R. (1957), The theory of infiltration: 4. Sorptivity and algebraic infiltration equations, *Soil Science*, *84*(3), 257.

Philip, J. R. (1969), Moisture equilibrium in the vertical in swelling soils. I. Basic theory, *Soil Research*, *7*(2), 99-120.

Philip, J. R. (1990), Inverse Solution for One-Dimensional Infiltration, and the Ratio a/K1, *Water Resources Research*, *26*(9), 2023-2027.

Preston, S., B. Griffiths, and I. Young (1997), An investigation into sources of soil crack heterogeneity using fractal geometry, *European Journal of Soil Science*, *48*(1), 31-37.

Römkens, M. J. M., and S. N. Prasad (2006), Rain Infiltration into swelling/shrinking/cracking soils, *Agricultural Water Management*, *86*(1-2), 196-205.

Smiles, D. E. (1974), Infiltration Into A Swelling Material, *Soil Science*, *117*(3), 140-147.

Smiles, D. E., and J. H. Knight (1976), A note on the use of the Philip infiltration equation, *Soil Research*, *14*(1), 103-108.

Stewart, R. D., M. R. Abou Najm, D. E. Rupp, and J. S. Selker (2012), An Image-Based Method for Determining Bulk Density and the Soil Shrinkage Curve, *Soil Science Society of America Journal*, *76*(4), 1217-1221.

Su, N. (2010), Theory of infiltration: Infiltration into swelling soils in a material coordinate, *Journal of Hydrology*, *395*(1-2), 103-108.

Talsma, T., and A. Lelij (1976), Infiltration and water movement in an in situ swelling soil during prolonged ponding, *Soil Research*, *14*(3), 337-349.

Tariq, A.-u.-R., and D. S. Durnford (1993), Analytical volume change model for swelling clay soils, *Soil Science Society of America Journal*, *57*(5), 1183-1187.

Tavenas, F., P. Jean, P. Leblond, and S. Leroueil (1983), The permeability of natural soft clays. Part II: Permeability characteristics, *Canadian Geotechnical Journal*, *20*(4), 645-660.

Tuller, M., and D. Or (2001), Hydraulic conductivity of variably saturated porous media: Film and corner flow in angular pore space, *Water Resources Research*, *37*(5), 1257-1276.

van Genuchten, M. T. (1980), A closed-form equation for predicting the hydraulic conductivity of unsaturated soils, *Soil Science Society of America Journal*, *44*(5), 892-898.

White, I., M. J. Sully, and K. M. Perroux (1992), Measurement of surface-soil hydraulic properties: Disk permeameters, tension infiltrometers, and other techniques, in *Advances in measurement of soil physical properties: Bringing theory into practice*, 69-103.

Figures

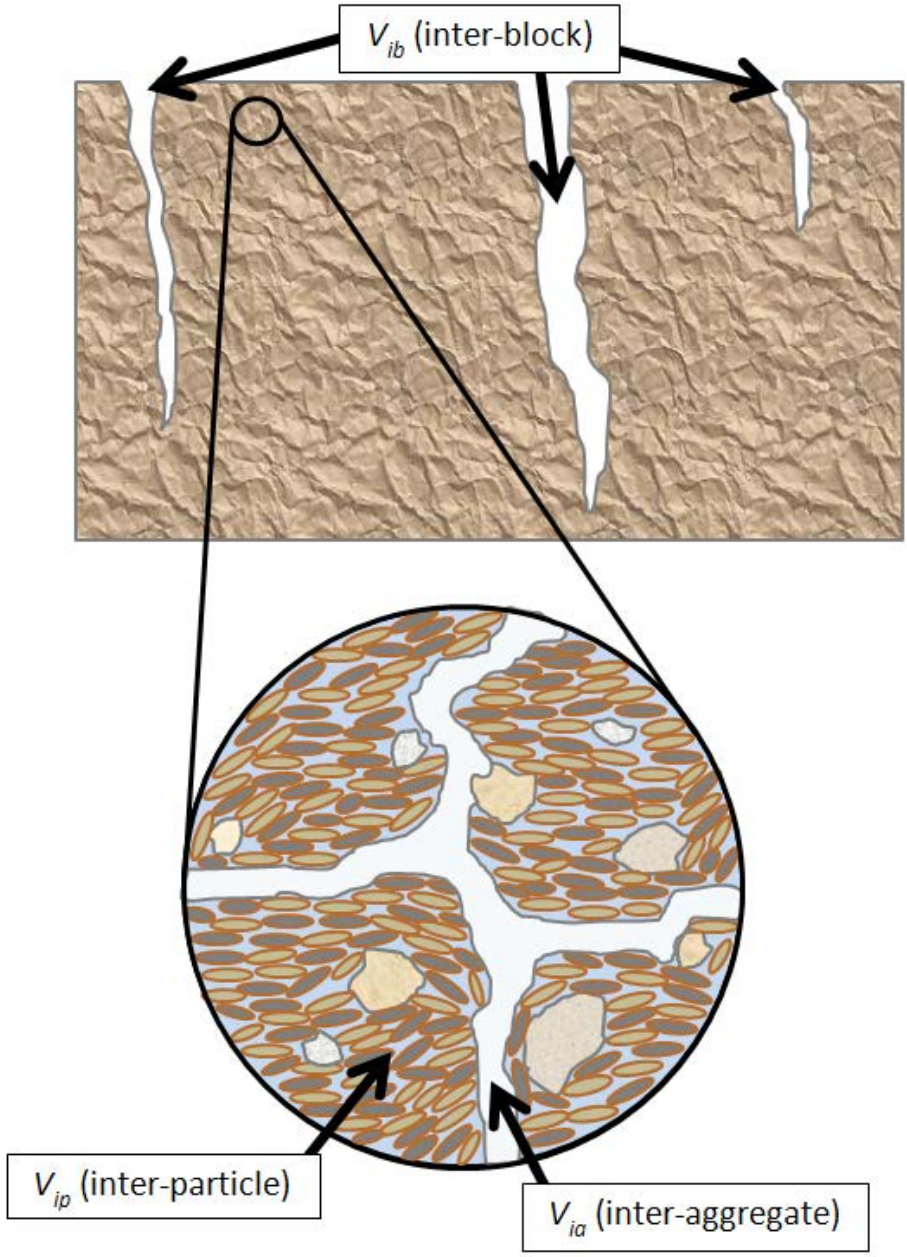

Figure 1 – Division of porosity into three domains: 1) large shrinkage cracks (V_{ib}); 2) micro cracks between individual aggregates (V_{ia}); and 3) inter-particle porosity within the soil aggregates (V_{ip}). Figure adapted from *Abou Najm et al.* [2010].

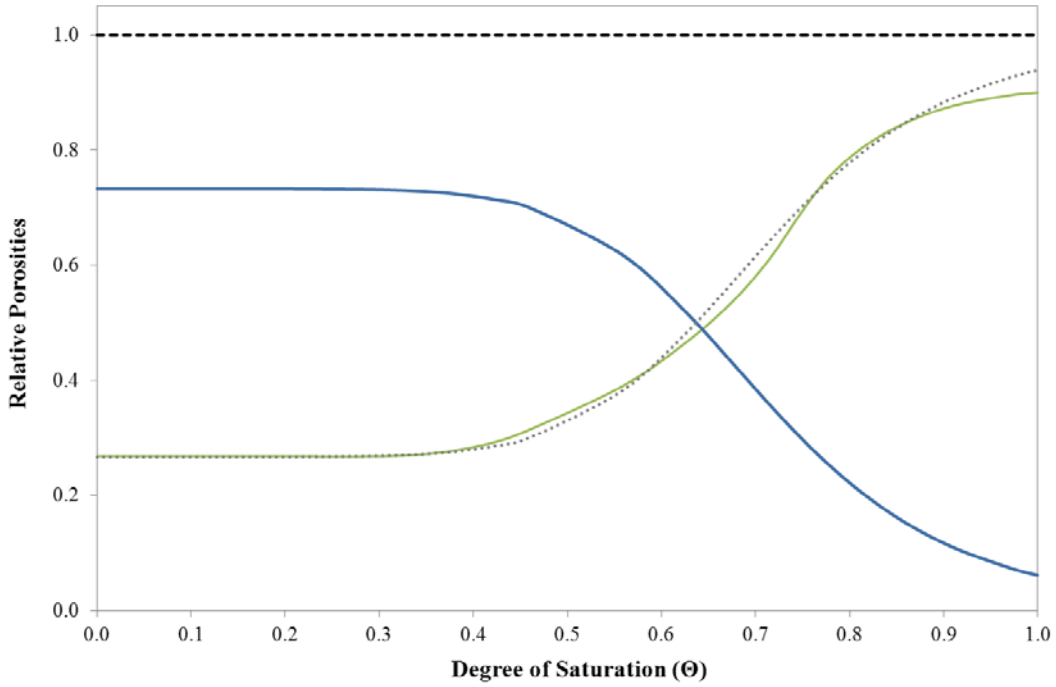

Figure 2 – Measured Soil Shrinkage Curve for a Witham silty clay soil in green (data from *Stewart et al.*, [2012]), and the proposed capillary crack porosity term (Equation (4)) in blue. The dotted gray line shows Equation (3).

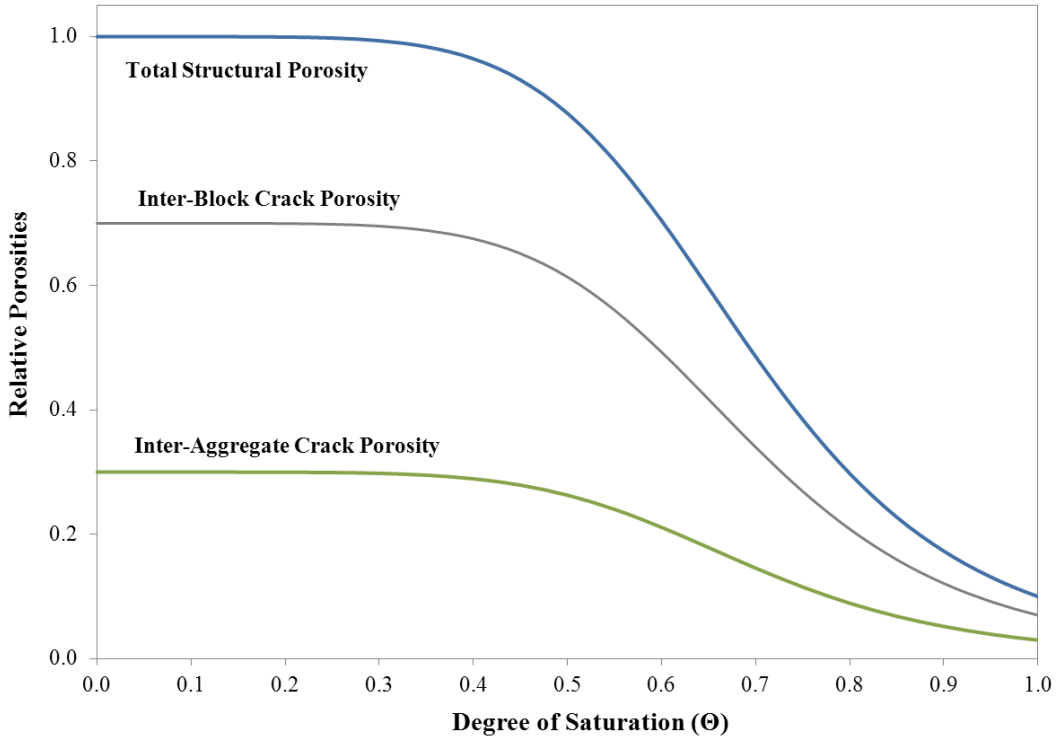

Figure 3 – Theoretical division of the total structural porosity into inter-block (visible) and inter-aggregate (microscopic) crack porosities. All curves are based on Equation (4), and assume that soil cracks are self-similar at multiple scales.

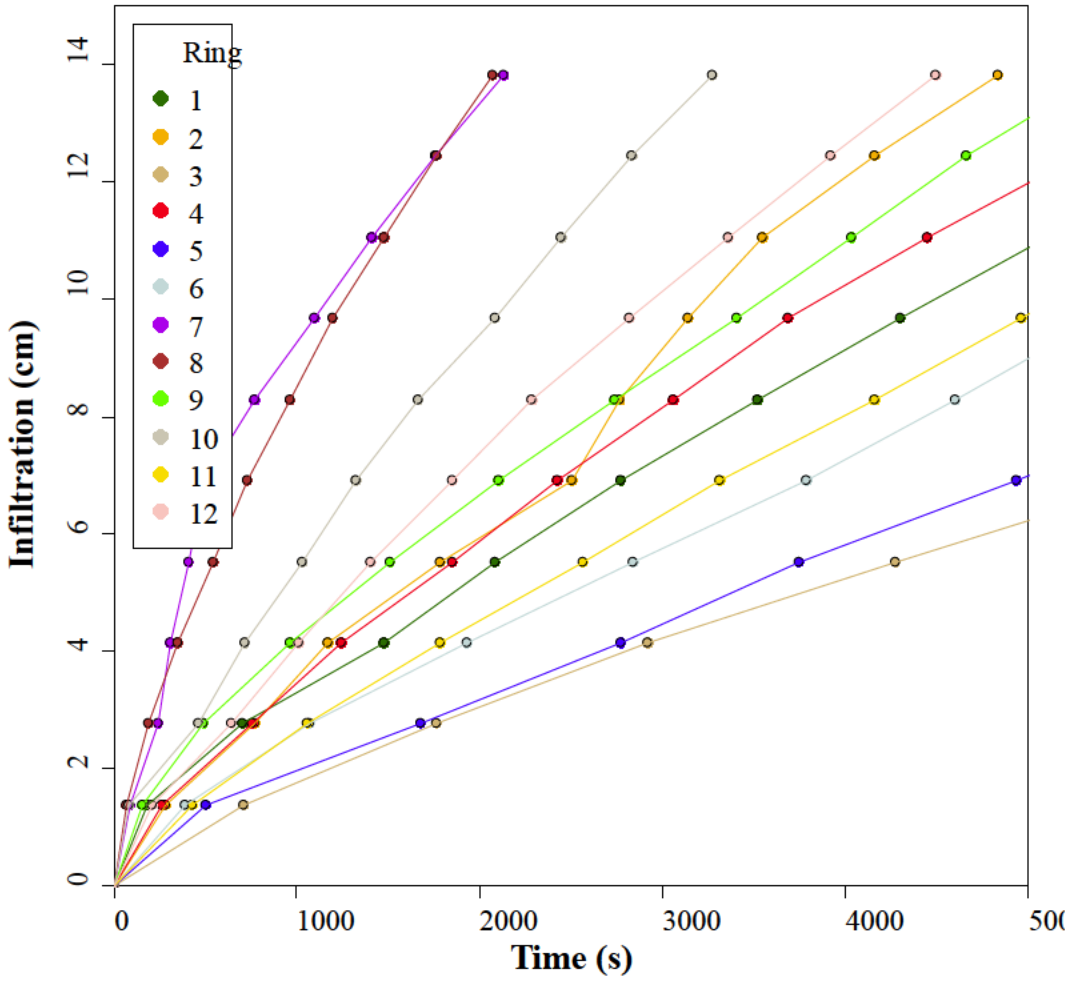

Figure 4 – Results of an infiltration test, showing data that were collected on May 8, 2012.

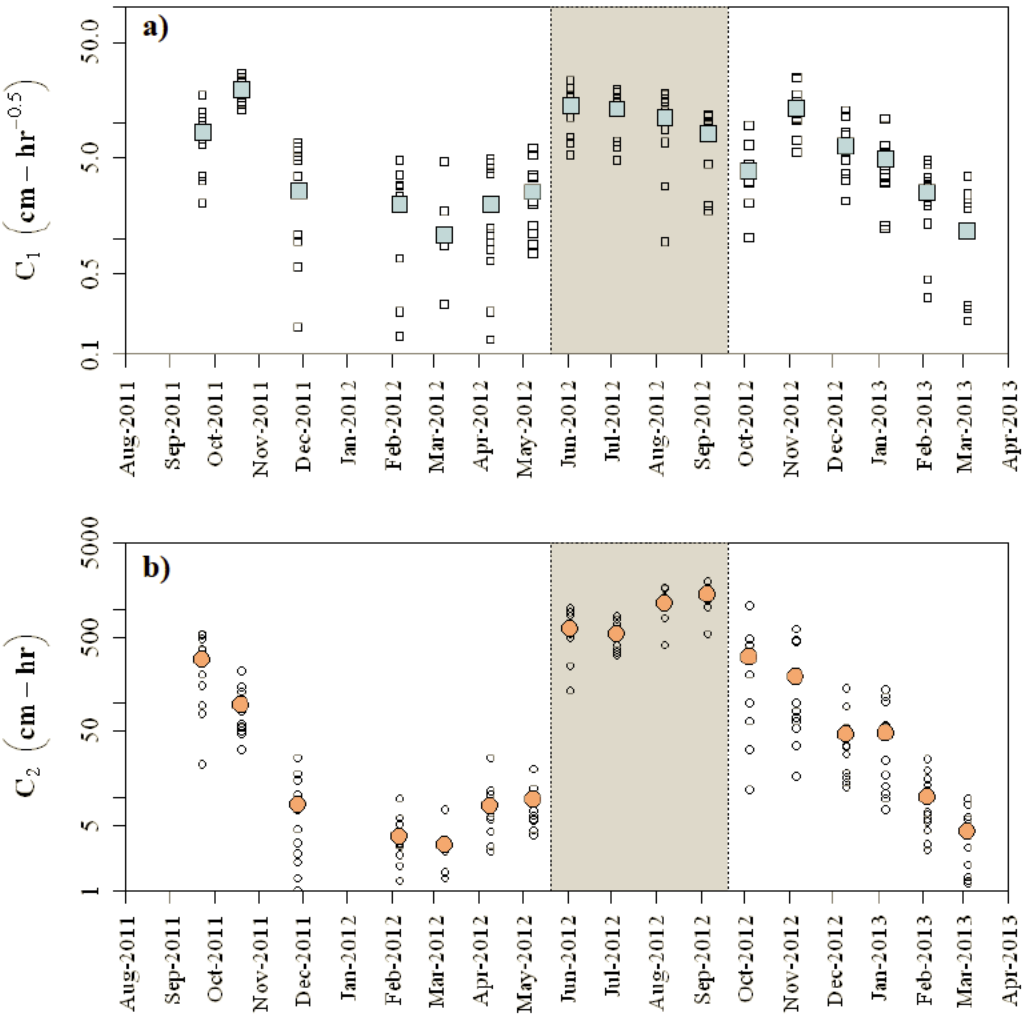

Figure 5 – Calculated values for a) the C_1 term in Equation (15), and b) the C_2 term in Equation (15). The gray shaded box indicates summertime measurements on degraded soil which were excluded from subsequent analyses.

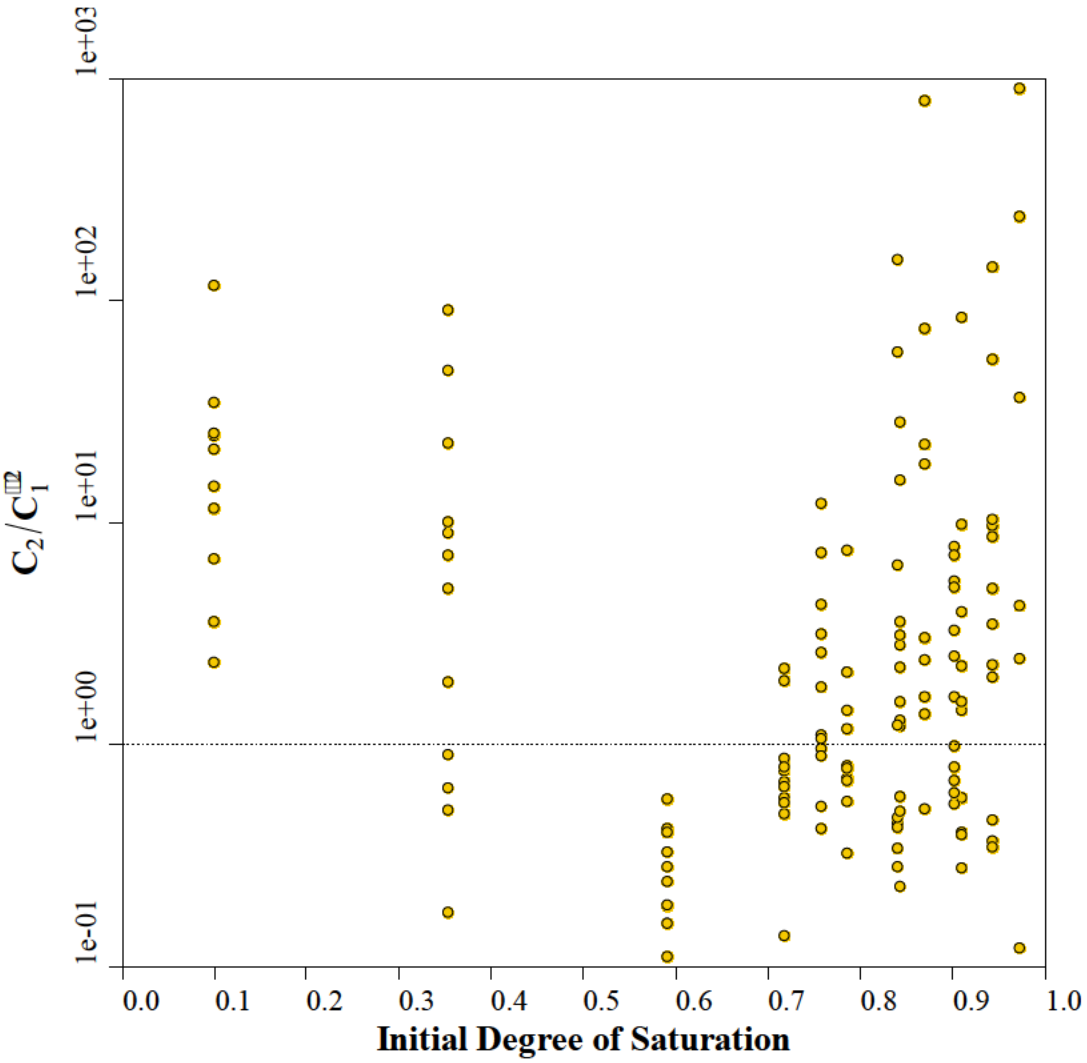

Figure 6 – The ratio of the second (gravity) infiltration term over the first (capillarity) infiltration term squared.

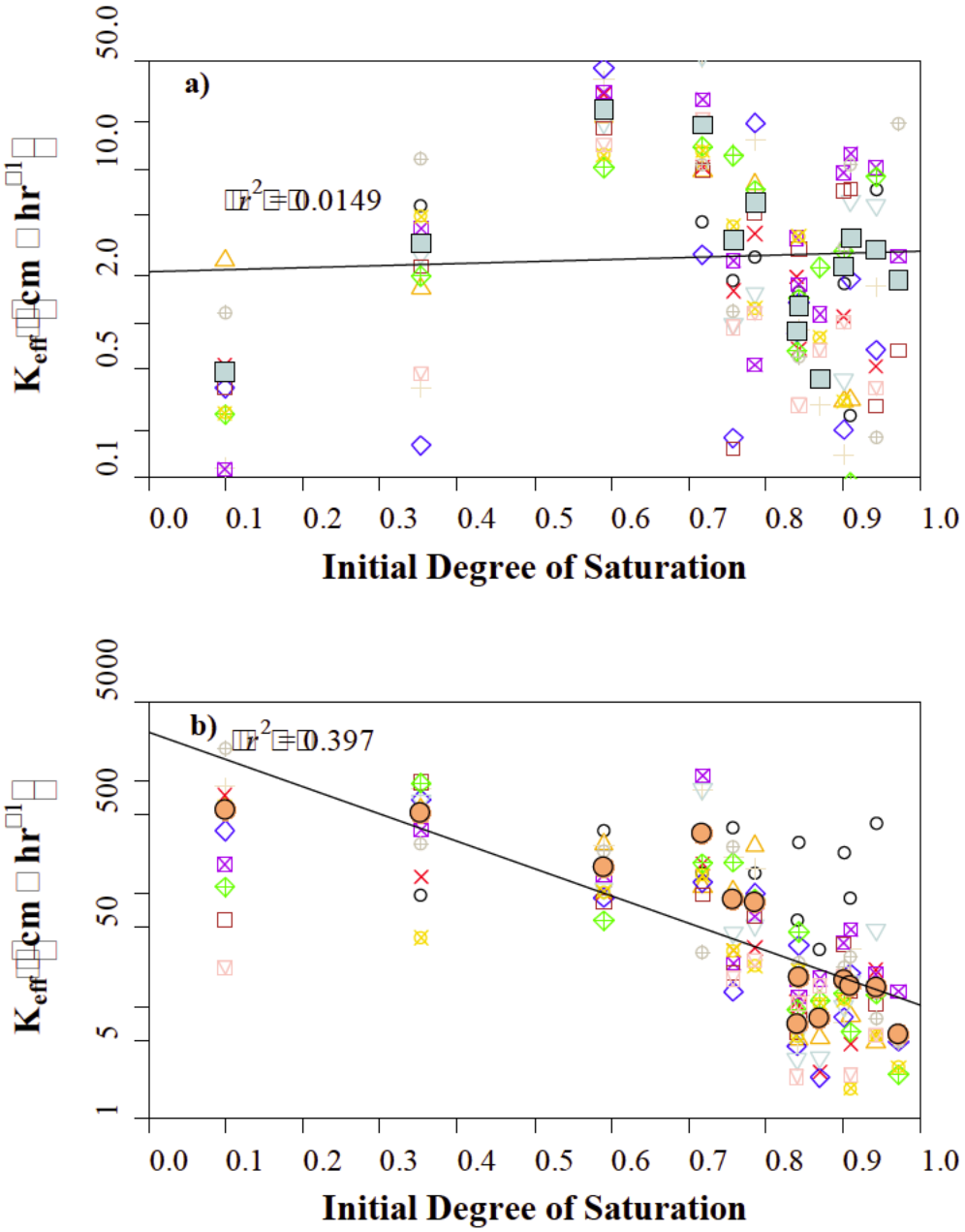

Figure 7 – Comparison of K_{eff} calculated from the PI model based on a) the first term, C_1, using Equation (10), and b) the second term, C_2, assuming $K_{eff} = C_2/0.55$.

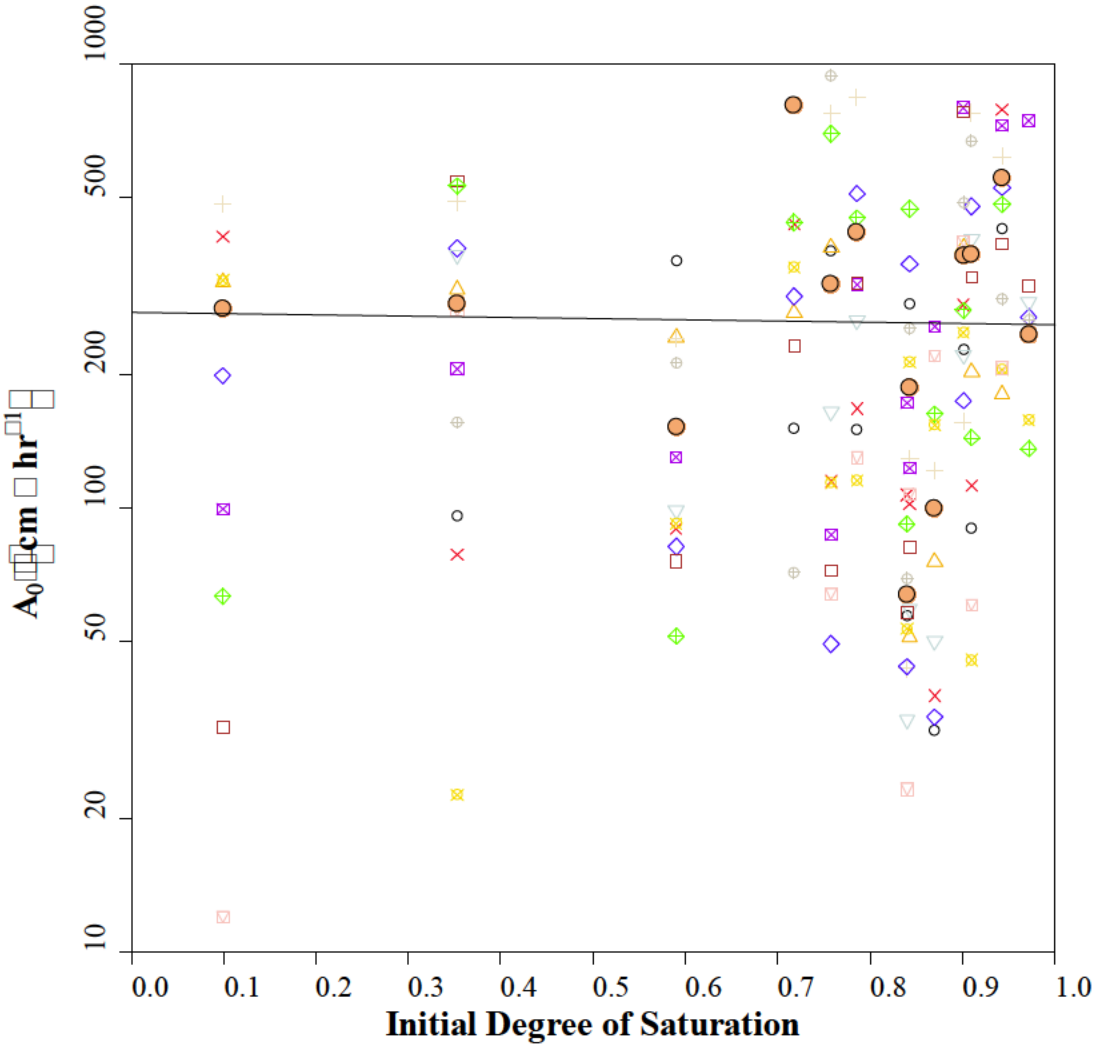

Figure 8 –Proposed soil parameter A_0 plotted against initial degree of saturation (Θ_0). A_0 was calculated by Equation (11) using values of ξ =11 and n = 7.

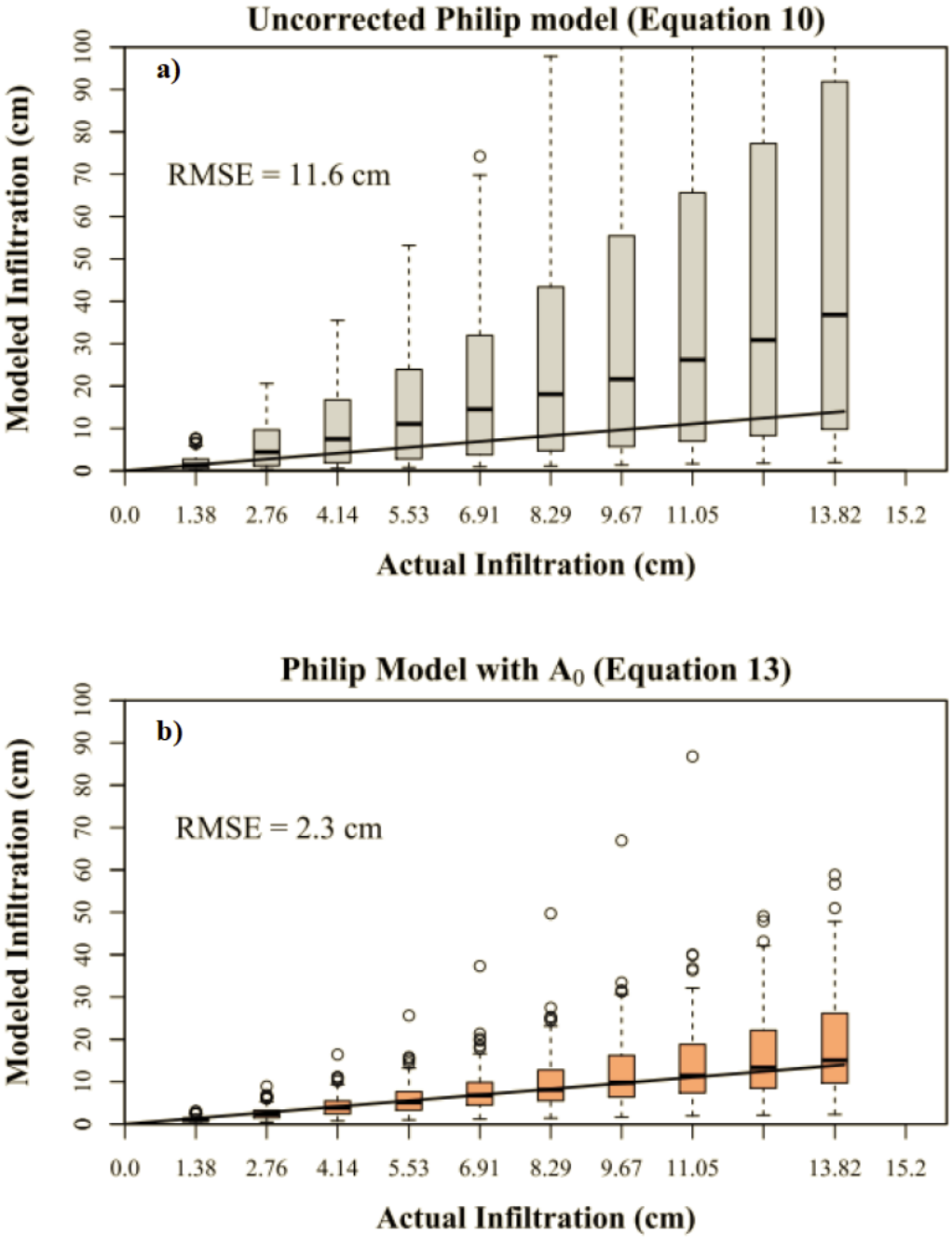

Figure 9 – Comparison of modeled to measured infiltration data assuming a) Equation (10) and b) Equation (13). RMSE was calculated using Equation (19).

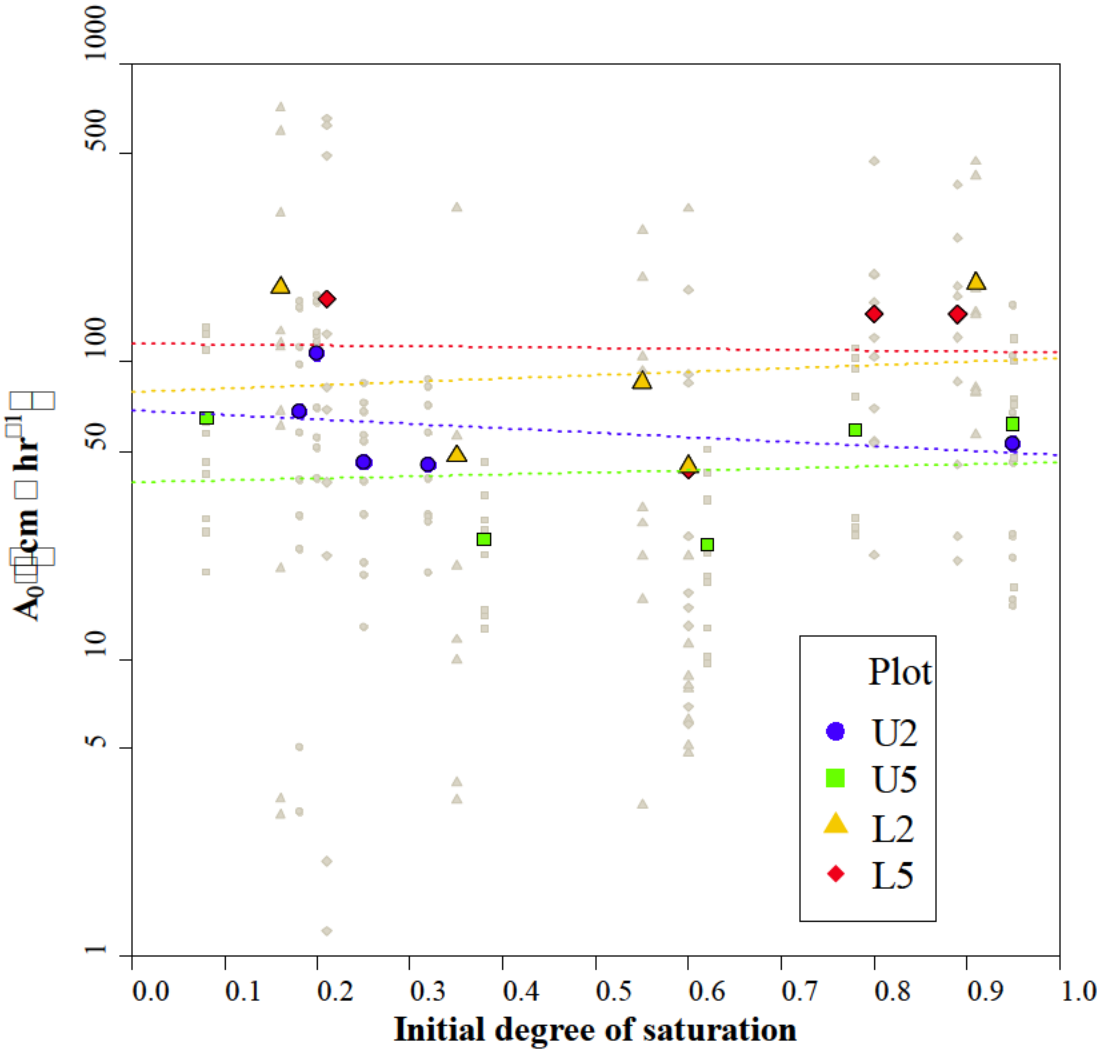

Figure 10 – Effective hydraulic conductivity (A_0) as a function of initial degree of saturation for the infiltration data from Chapter 4. A_0 was calculated by Equation (11) using values of ξ =7 and n = 6.

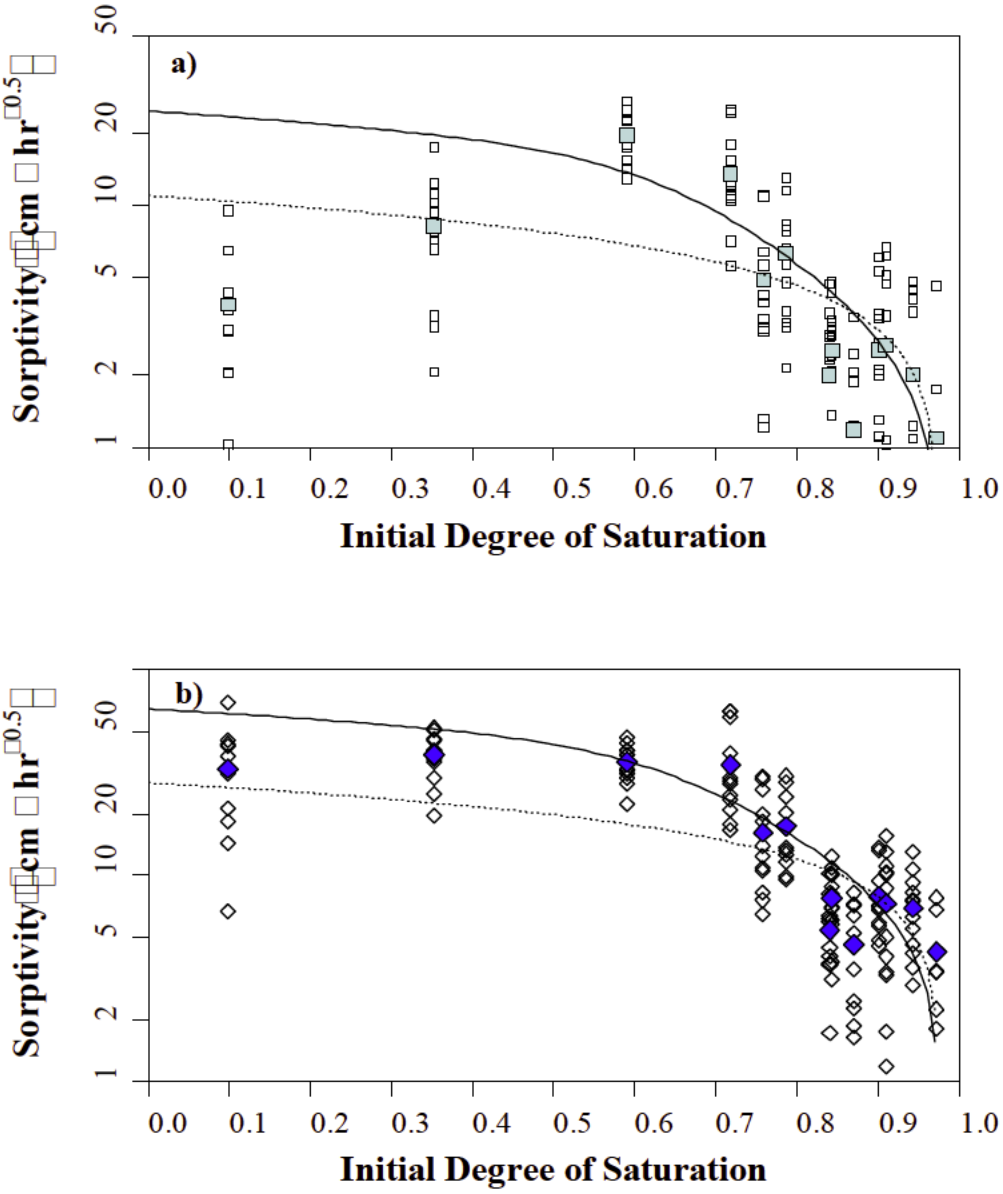

Figure 3.A1 – Comparison of sorptivity as calculated by a) the two-term infiltration model (Equation 14) and b) the early-time approximation model (Equation 3.A5). The dotted lines show expected sorptivity using the traditional expression (Equation 12) and the solid lines show expected sorptivity using the expression for aggregated *vertic* soils (Equation 3.A3).

4. Hillslope runoff thresholds with shrink-swell clay soils

Ryan D. Stewart*[1], Majdi R. Abou Najm[2], David E. Rupp[3], John W. Lane[4], Hamil C. Uribe[5], José Luis Arumí[6], John S. Selker[1]

[1] *Biological & Ecological Engineering Department, Oregon State University, Corvallis, OR, United States.*

[2] *Civil & Environmental Engineering, American University of Beirut. Beirut, Lebanon*

[3] *Oregon Climate Change Research Institute, Oregon State University, Corvallis, OR, United States.*

[4] *U.S. Geological Survey, Office of Groundwater, Branch of Geophysics, Connecticut, USA*

[5] *Instituto Nacional de Investigaciones Agropecuarias, Quilamapu, Chile*

[6] *Departamento de Recursos Hidricos, Universidad de Concepción, Chillán, Chile*

*Corresponding Author (stewarry@onid.orst.edu)

To be submitted for publication

Abstract

Irrigation experiments performed on instrumented field plots were used to assess the impact of dynamic soil crack networks on infiltration and runoff. During applications of intensity similar to a large storm, buried soil moisture probes showed that water could be preferentially delivered to various depths within the soil profile. However, runoff was not observed until soil water content of the entire profile reached field capacity and the surface cracks sealed beyond 60%. When the surface cracks were fully sealed, electrical resistivity measurements suggested that subsurface crack connectivity persisted and actively contributed to water redistribution and lateral transport. Likewise, single-ring infiltrometer measurements taken before and after irrigations indicated that infiltration remained a large component of the water budget at high soil moistures, despite apparent surface sealing. Overall, though the wetting and sealing of the soil profile showed considerable complexity, an emergent property at the plot scale was clearly observed: all of the plots demonstrated a strikingly similar threshold runoff response to the cumulative amount of precipitation.

Introduction

Shrink-swell clay soils are found all over the globe, with up to 350 million ha (more than 2% of the world's ice-free land) being classified as either *Vertisols* or *vertic* intergrades [*Ahmad*, 1996]. *Vertic* soils are characterized by crack networks which form throughout the profile as the soil dries. When open, these crack networks exert

significant influence on hydrologic processes. For example, cracks can act as preferential flowpaths, channeling water and solutes around the soil matrix [*Blake et al.*, 1973; *Bouma and Dekker*, 1978; *Messing and Jarvis*, 1990; *Bronswijk et al.*, 1995; *Greve et al.*, 2010] and increasing overall rates of infiltration [*Jarvis*, 1991; *Heppell et al.*, 2000; *Novák et al.*, 2000; *Sanders et al.*, 2012] and evaporation [*Weisbrod et al.*, 2009].

The presence, volume, and connectivity of crack networks can determine when a soil will experience ponding and/or overland flow (runoff) at its surface [*Wells et al.*, 2003]. At a minimum, runoff should not occur until the cumulative volume of rainfall has exceeded the total crack volume [*Kutílek*, 1996]. However, total crack volume can be a difficult parameter to measure or estimate, especially because it is generally assumed that crack volume will vary depending, among other factors, on the moisture content of the soil [*Jarvis and Leeds-Harrison*, 1987; *Morari and Knisel*, 1997; *Novák et al.*, 2002; *Abou Najm et al.*, 2010].

Much of the research related to *vertic* soils has been focused on the shrinkage phase, when cracks are forming and increasing in volume. For example, numerous models have been developed to describe the soil shrinkage curve [*Giráldez et al.*, 1983; *McGarry and Malafant*, 1987; *Tariq and Durnford*, 1993; *Boivin et al.*, 2006] and to predict crack formation and propagation [*Chertkov*, 2002; *Vogel et al.*, 2005]. The corresponding swelling phase of *vertic* soils, on the other hand, has received

much less attention. Only a limited number of studies have looked at the soil swelling curve [*Peng and Horn*, 2007; *Chertkov*, 2012]. Likewise, few studies have looked at how cracks physically seal during the swelling phase. Instead, it is commonly assumed either that cracks seal from the bottom up [*Bouma and Loveday*, 1988; *van Dam*, 2000; *Novák et al.*, 2002], or that the volume change in discrete crack layers is directly related to the amount of water that is adsorbed [*Greco*, 2002; *Arnold et al.*, 2005]. Some studies have called into question the assumption of the former [*Favre et al.*, 1997; *Römkens and Prasad*, 2006; *Greve et al.*, 2012], finding that cracks may seal initially at the soil surface. The latter assumption does not appear to have been independently verified or refuted, due primarily to a scarcity of observational data relating subsurface crack volume and soil moisture.

If cracks do initially seal at the soil surface, the utility of surface-based crack measurements [*Zein el Abedine and Robinson*, 1971; *Ringrose-Voase and Sanidad*, 1996; *Návar et al.*, 2002; *Wells et al.*, 2003; *Arnold et al.*, 2005; *Kishné et al.*, 2009; *Abou Najm et al.*, 2010] may be limited. Instead, techniques which primarily monitor subsurface crack dynamics, such as Electrical Resistivity Tomography (ERT) [*Samouëlian et al.*, 2003; *Samouëlian et al.*, 2004; *Amidu and Dunbar*, 2007; *Krzeminska et al.*, 2009; *Sentenac and Zielinski*, 2009; *Greve et al.*, 2010; 2012] or physically installing subsurface monitoring instruments into representative cracks

[*Stewart et al.*, 2012] may prove more informative about the rate and degree to which cracks close.

To date, however, a reliable description of the relationship between moisture content and crack dimensions both at and below the soil surface does not exit. Moreover, there has not yet been successful integration between measurements of soil moisture and crack closure and measurements of hydrologic processes such as infiltration and overland flow. This present study, therefore, had three main objectives. First, we wanted to observe and quantify how water moves through an initially dry *vertic* soil under irrigation at rates and amounts similar to a heavy storm. Second, we sought to monitor soil properties and parameters such as soil moisture, effective hydraulic conductivity, crack volumes and crack surface areas as the soil profile went from dry conditions to saturation. Finally, we attempted to identify threshold points associated with the beginning of runoff and then later associated with overland flow becoming the dominant hydrologic response.

Materials and Methods

Site Location and Instrumentation

The study took place between May 2010 and September 2012, in the *Secano Interior* region of South-Central Chile, which is located on the leeward (eastern) side of the Chilean coast range., The climate of the *Secano Interior* is semi-arid with annual

mean precipitation of 0.7 m; the majority of precipitation occurs in the months of May-August (based on a government-maintained weather station located in San Agustin de Punual (36°23' 47.53" S , 72° 25' 45.25"W), located 7 km from the study area).

The field site was located near the commune of Ninhue (36°25’04”S, 72°31’05”W) (Figure 1), on a hillside of moderate slope. The site was covered by native pasture with a few scattered pines and acacia trees. By January (i.e. mid-summer) of each year, the plant available water became depleted, causing the grasses to senesce. Thus, transpiration by the grasses was assumed to be insignificant during mid and late summer. The site’s soils were granitic, with a depth to saprolite varying from approximately 0.6 m at the upper slope to approximately 0.8 cm at the mid-slope. Hydrometer and x-ray diffraction analyses were performed on samples taken at various depths from the surface down to 0.85 m. Percentages of sand, silt and clay, as well as the mineralogy of the clay fraction, are summarized in Table 1.

Two sets of nine 3.5 x 11 m instrumented runoff plots were located on the hillside. The upper set (Plots U1-U9) was located on the shoulder of the hill, at an average slope of 12°. The lower set (Plots L1-L9) was located near the mid-slope, at an average slope of 18.5°. Each set of plots was further divided into three groups of three plots each, with an intragroup spacing of 1 m between plots and an intergroup spacing of 1.5 m between plot triplets. Along the perimeter of each plot, except for the

downhill edges, a 0.3 m tall plastic divider was embedded into the soil to a depth of 0.15 m. At the downhill edge of each plot a covered concrete floor and channel collected all overland flow. Once in the channel, the flow was directed to a single 4 m x 0.09 m PVC pipe, which emptied into a runoff measurement system described below.

Runoff collection

In 2011, all runoff was collected and measured in twin 0.2 m^3 metal drums. The water from the runoff plots drained into the first barrel. This barrel was in turn connected to a secondary barrel via a narrow chute near the top, with the chute accepting the water from one of ten equal-sized slots, so that when the water level reached the chute approximately 10% of the incoming water was transported to the second barrel. 90% of the water was spilled into a 6 m long drain pipe which took the overflow downhill from the site. Each barrel system was located 3 m downhill from the irrigation plots in a 1 m deep pit with a cement slab and wooden slats to support the sides (Figure 2). The drums were periodically emptied using either a hand pump or a bucket.

In 2012, the runoff monitoring system in Plots L2-L5 and Plots U2-U4 and U6 was improved because of shortcomings from the two-drum system. In the improved system (the “leaky bucket” system) runoff was directed into a vertical 0.1 m pipe capped at the bottom end. The 0.1 m pipe was perforated with holes of increasing diameter with height. After passing through a screen to filter debris, the runoff filled

the pipe and would drain from the holes. Water level within the pipe was measured using HOBO U20-002 pressure transducer (Onset Corporation), set at 15-second recording intervals. Based on the hole configuration and the water level within the pipe, pipe discharge rate Q was inferred using Torricelli's law:

$$Q = \sum_{i=1}^{n} c_i A_i \sqrt{2gH_i} \quad (1)$$

where H is the height of water (relative to hole i), g is the gravitational constant, A is the cross-sectional area of hole i, and c is a correction term which accounts for roughness of hole i (with $c = 1$ representing a perfectly smooth hole), and n is the number of holes below the water level. A laboratory calibration found c to equal 0.65. Runoff rate was then calculated as Q plus the rate of change in water stored in the pipe.

Soil moisture

To measure soil moisture, the center of each plot was instrumented with Decagon Devices 5TM capacitance probes at depths of 0.15, 0.30, 0.60 and 0.85 m. Decagon Devices EM50 data loggers were used to record the data. Soil moisture readings began on May 25, 2010. Measurement frequency was generally every 15 minutes, increasing to every minute during the periods of active experimentation. Occasional data gaps exist for individual probes due to cables being inadvertently stepped on and temporarily unplugged, animal interference, and/or batteries losing contact with the

data logger. In addition, four of the individual probes inexplicably ceased operating during the experiment.

To correct for temperature effects on the 5TM soil moisture probe readings, a first-order correction was applied to the 0.15 and 0.30 m probes, as recommended by *Campbell* [2001].

Surface-connected cracks

Finally, representative surface-connected cracks were chosen within the plots for monitoring. Monitoring consisted of two approaches: 1) large cracks within three of the plots were instrumented with the *crackometer* instrument [*Stewart et al.*, 2012], which consists of a 1 L intravenous therapy (IV) bag placed within the crack which is then filled with water from a connected standpipe, enabling measurement of relative volume change; and 2) medium-to-large sized cracks from within five plots were marked by 0.5 x 0.5 m frames and then imaged from above at various times during the experiments. Images were collected from a height of 0.6 m using a Pentax K-x digital SLR and a 28mm lens. The surface area of cracks was quantified by converting the image to black and white, representing the crack and soil, respectively, and then counting the number of black pixels. Minor color and contrast adjustments were made on some images in an attempt to eliminate artifacts such as shadows, cables, and vegetation. An example photo is included as part of the electronic supplement.

Irrigation Experimental Setup

An irrigation system was used to provide controlled water application to the plots. The system was constructed from 0.032 m PVC pipe, laid out in a 12 x 12 m square. This allowed for the simulator to be placed around a group of three runoff plots. The two sides of the simulator parallel to the slope direction each had four sprinkler heads, with one at each corner and two spaced equally in between. Each sprinkler head could be adjusted for length of travel as well as angle and intensity of the water stream. This allowed for on-the-fly adjustments of individual sprinkler heads in an attempt to create uniform coverage.

The rainfall simulator was used for two-week periods in January of both 2011 and 2012, when the antecedent dry conditions had created large crack networks throughout the soil plots. Water for the irrigation system was extracted from the *Río Lonquén* (36° 27' 29.891" S, -72° 21' 5.461" W; approximately 18 km from the site by road) by a water truck, and was pumped either directly from the truck or from a temporary storage tank constructed adjacent to the plots. Each irrigation event was therefore equal to the capacity of the water truck, or approximately 10 m^3 of water. This corresponded to a rainfall rate of between 0.3 and 0.8 mm-min^{-1} (20 – 50 mm-hr^{-1}) or a per event depth of irrigation which ranged from 20 to 60 mm.

Due to the configuration of the irrigation system, plots were grouped into four sets of three plots (L1-L3, L4-L6, U1-U3, and U4-U6). The four sets were then assigned

different experimental treatments, where the number of irrigations per day and the number of days between irrigations were varied (irrigation schedules for both years are shown in Table 2). Plots L1-L3 were irrigated with the long-time, high-rate treatment, in which two truckloads were applied on Days 1, 7, and 14, and in between the plots were covered with 0.2 mm plastic to inhibit evaporation. Plots L4-L6 were irrigated with the short-time, high-rate treatment, in which four truckloads of water were applied over Days 8 and 9, with a fifth truckload applied on Day 13. Plots U1-U3 were irrigated with a mixed-time, low-rate treatment, in which one truckload was applied at Days 7 and 14, and three loads were applied on Day 16. Plots U4-U6 were irrigated with a long-time, low-rate treatment, in which one truckload was applied on Days 7, 8, 14, 15, and 16, and in-between irrigations the plots were covered with 0.2 mm plastic. Differences in the experimental treatments were analyzed by comparing the cumulative amount of runoff after 23 cm of simulated rainfall had been applied.

During irrigation events, water application was recorded within the individual plots with an array of catch cans located within the plots. Each plot had 11 catch cans, placed in a regular pattern. Intra-plot uniformity was analyzed using the Distribution Uniformity (DU) coefficient, which can be described as [*Warrick*, 1983]:

$$DU = 1 - \frac{Average\ of\ the\ lowest\ quartile\ of\ depth\ of\ water\ infiltrated}{Average\ depth\ of\ water\ infiltrated} \qquad (2)$$

In order to derive rainfall-runoff relationships, per-event amounts of precipitation were calculated based on the mean amount of water collected in the catch cans for each plot.

Monitoring of Soil Properties

In 2012, single ring infiltration (SRI) tests were performed in Plots L2, L5, U2 and U5 at various points throughout the rainfall infiltration experiment. Each test consisted of 9 - 13 single rings of 0.096 m diameter, shallowly installed in a 2 x 2 m grid. Care was taken to ensure that rings were installed in locations without visible shrinkage cracks, so that infiltration would occur through the soil peds rather than through large macropores. Along with each single ring test, soil cores (volume = 6.87 x 10^{-3} m^3) from each of these plots were collected for quantification of gravimetric water content and bulk density.

Infiltration (I) as an equivalent water depth was modeled using the Philip's equation for one-dimensional vertical infiltration [*Philip*, 1957]

$$I = S\sqrt{t} + At \tag{10}$$

where S is the soil sorptivity and A is term to describe the flow's resistance to gravity. For purposes of this study, effective hydraulic conductivity (K_{eff}) was assumed to be equal to A/0.55 [Stewart, Chapter 3].

Additionally, during the 2011 experiment several other infiltration methods were used on the site while it was in dry conditions ($\Theta_0 < 0.3$). Those methods included Guelph Permeameter (GP) measurements taken at 0.25 m depth, and Double Ring Infiltrometer (DRI) and Mini-disk Tension Permeameter (MTP) measurements taken at the soil surface. The GP (Soilmoisture, Inc. Guelph 2800K1) was installed, operated and analyzed using Equations (19) and (22) from *Verbist et al.* [2013]. The DRI consisted of an outer ring of 0.60 m and an inner ring of 0.30 m, installed to a depth of approximately 0.1 m. Measurements were analyzed using Equation (3.28) from *Selker et al.* [1999]. The MTP (Decagon Devices, Inc.) was operated and analyzed according to manufacturer's recommendations. The applied tension for the MTP was approximately -0.01 m, and the soil was assumed to be a clay loam.

Geophysical monitoring

During the irrigation experiments, it was observed that water seeped through the walls of the collection barrel pit at many of the experimental plots, often beginning in conjunction with the initiation of surface runoff. Because the entirety of the surface runoff was being conveyed into the barrels, the source of this seepage water must have been lateral subsurface flow.

Based on this observation, a concurrent experiment using an electrical resistance was conducted during the 2011 irrigations to determine at what point during water application these subsurface lateral pathways became active and how long they

persisted. A four-electrode Wenner array with a spacing of 2 m was installed approximately 3 m downslope of the lower edge of the irrigation plot, with the array oriented perpendicular to the hillslope and expected direction of flow (Figure 3). Resistivity was measured using a Sting R1 earth resistivity meter (AGI instruments).

Two separate monitoring events were conducted. In the first event (which corresponded to Year 1, Irrigations 1-4 in Plot L2), the soil was initially dry. In the second monitoring event (which corresponded to Year 1, Irrigation 6 in Plot L5), the soil was already wetted from previous simulated rainfall applications so as to simulate wet and presumably swelled soil conditions. These two monitoring events are indicated on the irrigation schedule of Table 2.

Results

Distribution of applied water

The cumulative amounts of applied water and the distribution uniformity (DU) coefficients varied greatly between plots (Table 3), but in general both were highest for the plots furthest to the northeast (i.e. L1, L4, U1, and U3) and lowest for the plots furthest to the southwest of each group (i.e. L3, L6, U3, U6). This pattern was mostly the result of the prevailing wind pattern from the southwest to the northeast during the experiments (despite measures taken to shield the fields from wind by installing 2 m

high, 20m long plastic tarp wind breaks on the up-wind side of plots). Visual assessments of uniformity patterns are included as an electronic supplement.

Soil moisture

The soil moisture response to the irrigation shows several interesting characteristics (Figure 4). For one, the water does not appear to progress through the soil profile as a classical wetting front. For example, while some of the profiles appear to wet from the top down, others clearly show the opposite behavior. Adjacent plots U2 and U3 show this contrast most vividly. In the former, the soil wets in order from top to bottom. In the latter, however, the soil moisture first increases at the 0.85 m depth, then at the 0.60 m depth, while the upper probes in the profile do not show any significant increase in moisture until after the lower depths have reached their maximum values. Further, looking at Plot L2, it can be seen that the 0.60 m probe responds to the increase in moisture before any other probe, followed soon thereafter by the 0.15 m probe. Those two probes then respond in unison, showing an increase in volumetric water content of more than 10% over the first two irrigation events, whereas the 0.30 and 0.85 m probes do not show any change over that same period. In the third irrigation event, the 0.30 m probe increases in soil moisture, while the 0.85 m probe does not respond until the fourth irrigation.

These data indicate the ability of shrinkage cracks to preferentially provide moisture to various depths and locations within the soil profile. This in turn suggests that the

wetting of *vertic* soils is a three-dimensional process, with infiltration occurring at ped-crack interface in addition to wetting from the top (and possibly the bottom) of the profile. The amount, rate and depth of wetting showed significant heterogeneity, beyond that predicted by three-dimensional crack-based wetting models (e.g. *Hoogmoed and Bouma* [1980]). While strongly heterogeneous wetting would seem to argue for inclusion of a soil moisture distribution term into models which predict infiltration, and by extension runoff, rates based on moisture content of the soil profile [*Smith and Goodrich*, 2000; *Chen and Young*, 2006; *Brocca et al.*, 2008], studies on non-cracking soils indicate that initial soil moisture distribution is a relatively unimportant term when considering runoff generation at medium- and large-scales [*Goodrich et al.*, 1994; *Morbidelli et al.*, 2012].

When runoff ratio (runoff divided by rainfall) is plotted as a function of soil moisture, the system shows a near-binary threshold (Figure 5), which may best be described as "hockey-shaped" [*Ali et al.*, 2013]. While the shape of this threshold was similar to those observed for rigid (non-swelling) soils [*James and Roulet*, 2009; *Penna et al.*, 2011], it stands in contrast to the "sigmoid" shaped threshold seen by *Zehe et al.* [2007] for a cracking clay soil. However, in the latter study runoff ratio was determined using integrated stream measurements and soil moisture was estimated using modeled data; thus, its results are not considered to be directly comparable.

When looking at the responses of individual soil moisture probes, the shallowly installed (0.15 m) readings showed the most variability, whereas the deeper sensors showed that runoff ratio could range from 0 (no runoff) to 0.95 (near complete runoff) while the apparent volumetric soil moisture shifted by less than 2%. In the plots which wetted from the top down (such as U2 and L5), the sensors at lower depths suggested there may have been a slight positive correlation between increasing soil moisture and runoff ratio, whereas the plots which wetted non-sequentially (such as L2 and U3) did not show any such correlation.

The capacitance sensors used in this study were small, with a limited sampling volume (~ 3 x 10^{-4} m^3). Therefore, the observed near-binary runoff response may have been caused by the limited ability of these small-scale capacitance sensors to measure soil moisture in *vertic* soils [*Dinka and Lascano,* 2012]. It is possible that larger sensors such as TDR [*te Brake et al.*, 2012] or alternate methods such as neutron attention measurements (which can measure volumes of ~1 – 4 m^3) [*Evett et al.*, 2009] would be able to measure both outer and inner ped soil moisture and thereby reveal the true effect of soil moisture on runoff.

Crack volumes and dynamics

The *crackometer* data suggest that the amount of crack closure may be temporally decoupled from point measurements of soil moisture made within the soil peds (Figure 6). For example, the data from *crackometer* U3-1 shows the soil profile

approaching field capacity water content before the monitored crack begins to seal. *Crackometer* L4-4 shows the opposite response, in that the crack is nearly sealed before the lower soil profile even begins to wet. *Crackometer* L1-4 shows an intermediate behavior.

Imaging analysis suggests that the surface cracks have a more uniform response to changes in soil moisture (Figure 7). In the initial stages of wetting, soil moisture (at 0.15 m depth) increases of around 10% caused the surface cracks to close to less than 40% of their original surface area. Further crack closure then required more significant increases in soil moisture, with no real variation in soil moisture observed during the final 20% of sealing. *Crackometer* U3-1 (also shown in Figure 7) has a nearly opposite response, in that much of the 0.15 m depth soil moisture increase occurs before the crack begins to seal. This suggests that cracks may behave differently at the surface compared to the subsurface, and that surface-based crack measurements may not be sufficient to predict subsurface crack behavior.

Relative crack closure, as measured by both the surface crack imaging and the installed *crackometer* instruments, was compared to runoff ratio (Figure 8). As with soil moisture, the surface cracks show a more uniform response than the responses measured by the *crackometer* instruments. In the case of the former, no runoff is observed until the surface cracks are more than 80% closed, and the runoff ratio increases as the surface cracks fully seal. The *crackometer* measurements, however,

show runoff beginning when the cracks have only closed 60-70%, and that the runoff ratio can fluctuate significantly with no corresponding variation in the apparent crack volume. However, both the surface imaging and the *crackometer* data show a general trend of increasing runoff with decreasing crack size.

Contrary to most modeling approaches for *vertic* soils (and similar to the observational results of *Wells et al.* [2003]), these data suggest that runoff can occur before the cracks have fully sealed. The relationship appears to be relatively consistent across plots and in response to different rainfall intensities. This indicates that it may be possible to develop a simple modeling term to realistically relate runoff to near-surface crack volumes.

Comparison of experimental treatments

The four experimental treatments showed that 0.23 m of rainfall gave rise to 0.01 to 0.05 m of cumulative runoff (Figure 9). Plots L1-L3 and U4-U6 showed very different responses from one another. Since the 0.23 m rainfall level of application was reached for most plots during the fifth irrigation, it is worthwhile to examine differences between treatments with regard to the fifth irrigation. For example, plots L1-L3 had a one week gap between irrigations 4 and 5, whereas for Plots U4-U6 those same irrigations were conducted on consecutive days. Conversely, Plots U1-U3 received irrigations 4 and 5 with less than an hour between them, yet produced less cumulative runoff than Plots U4-U6. This suggests that time-dependent soil swelling

effects may be most pronounced on a time-scale of around one day: at early times, the soil is still swelling, while at times longer than one day water redistribution may become an important factor. The crack swelling and soil moisture data would seem to support this conclusion, as crack volumes and soil moisture were both seen to vary during the inter-irrigation periods (Figure 10). However, due to the limited number of replicates and the high variability of irrigation amounts, when comparing the amount of runoff generated by each treatment, no statistically significant differences were observed using the Student t-test (p-value > 0.09). Therefore, in the future a greater number of replicates and better controlled irrigation uniformity would be needed to truly assess any time- or rate-dependent swelling impacts on runoff generation.

Cumulative Rainfall and Runoff

When the cumulative amounts of per plot simulated rainfall are plotted (based on 2012 data), an interesting trend emerges (Figure 11). All of the plots, regardless of rainfall intensity and time between irrigations, demonstrated no measureable runoff for the first 0.12 m of rainfall. Thereafter, in the narrow band between 0.12 and 0.17 m of cumulative precipitation, all plots began to produce runoff.

Once runoff began, there appears to have been a transition period in which the runoff response varied significantly between plots. As discussed in the previous section, time between irrigation events could be a factor which affects how much runoff is produced in *vertic* soils. However, this effect may be transient, as after the transition

period (which corresponded to 0.05 – 0.1 m additional rainfall) most of the plots again showed a similar runoff response. This agrees with previous observations that hydrologic predictability is poorest in the vicinity of a non-linear threshold and improves as the system moves away from the threshold [*Blöschl and Zehe*, 2005].

As a final note, Plot L1 received significantly more rainfall than the other plots, and its runoff ratio approached unity (full runoff) after a cumulative amount of rainfall of approximately 0.33 m. This suggests the possibility of a second runoff threshold, when the subsurface pathways have become fully sealed. The possible existence of two distinct thresholds can be seen when plotting runoff ratio as a function of cumulative rainfall, which takes on a basic sigmoidal shape (Figure 12). 0.33 m of rainfall represents approximately one-half of the area's mean annual rainfall, so it seems probable that this secondary threshold should be exceeded in at least some of the years.

Infiltration results

Effective hydraulic conductivity (K_{eff}) was plotted as a function of initial degree of saturation for Plots L2, L5, U2 and U5 (Figure 13), based on the single ring infiltrometer (SRI) measurements. The colored points in Figure 13 were calculated based on the arithmetic mean, which was considered to better represent the influence of small cracks on vertical flow [Stewart, Chapter 3]. It should be noted that the mean and standard variation for the very wettest point of Plot L2 were an order of

magnitude larger than the other points, so that point was neither plotted nor included in the determination of the line of best fit.

In dry conditions, the effective hydraulic conductivity of the soil was 1-2 orders of magnitude greater than the rate of simulated rainfall (0.02 - 0.05 m-hr^{-1}). This suggests that when the soil is dry the conceptual model of water ponding on the soil matrix and running into large shrinkage cracks [*Bouma and Loveday*, 1988] should not occur. Instead, Case #1 in *Greco* [2002], where division of water between the soil matrix and the cracks is governed primarily by the horizontal surface area of each, may best describe the early-time infiltration.

In wet conditions, the effective hydraulic conductivity decreased to a level that was of the same order of magnitude as the irrigation rate. This indicates that the observed runoff may have been caused by a combination of the soil profile's decreased infiltration capacity, increased moisture content, and surface sealing of cracks.

When compared to the other infiltration methods (Table 4), the SRI had the largest variability and the highest mean value, likely due to small sample area of each individual measurement. The DRI had the next highest mean value, about one order of magnitude smaller than the SRI. The GP had a similar arithmetic mean to the DRI, but its geometric mean was much smaller, due to one of the measurements being directly affected by a concealed crack. The MTP had consistent measurements which were 1-2 orders of magnitude smaller than those of the other surface-based tests,

possibly because under tension the contribution of macropores and cracks to flow was limited. Altogether, these trends were consistent with those of [*Verbist et al.*, 2013] for a non-swelling Chilean soil, and indicate the strong influence that near-surface cracks and macropores have on the effective hydraulic conductivity of a dry *vertic* soil.

Geophysical Monitoring

It was observed that the apparent electric conductivity (σ) of the soil downhill of the irrigations plots increased with time, corresponding to the periods of irrigation (Figure 14). The change in apparent electric conductivity was calculated as

$$\Delta\sigma = (\Omega_i - \Omega_0)^{-1} \quad (6)$$

where Ω_i is the apparent resistivity measured through time and Ω_0 is the initial apparent resistivity.

In the first monitoring event, no surface runoff was generated during the first two irrigations (Figure 14a). This means that all the water infiltrated into the soil matrix and into preferential flow paths. Interestingly, increases in the monitoring array apparent conductivity were observed during the first and second irrigations, long before any surface runoff occurred. This suggests that crack networks can move water laterally through the shallow subsurface, acting as the “concealed surface runoff” pathways predicted by Horton over 70 years ago [*Beven and Germann*, 1982].

Furthermore, the conductivity readings stayed relatively constant between irrigation events, suggesting that as water was laterally moving within cracks, part of it remained stored within the crack network, satisfying its storage capacity and acting as a water source so that swelling and redistribution could potentially occur.

After the soil was left to swell overnight, a large portion of the monitored cracks at the surface had sealed. Runoff was observed soon after initiation of the third irrigation. At the same time, the observed changes in soil apparent conductivity during the third irrigation were much larger than during the previous two irrigations. This may be explained by clay swelling processes decreasing the crack network void volume and sealing of some small transverse leakage paths. Under these conditions, a much smaller volume of irrigation water would be needed to fill a larger portion of the crack network, thus inducing a greater change of apparent conductivity with the onset of irrigation and surface flow. Furthermore, the soil beneath the irrigation plot was near field capacity, meaning that water loss from the cracks through infiltration and diffusion would be minimal and water could freely move downhill through the cracks under gravity.

During the fourth irrigation event, where runoff began almost immediately, water was noted flowing out of cracks within the collection barrel system. This visual observation confirmed the presence of lateral preferential flow, and supported the interpretation of increases in electrical resistivity as being indicative of active lateral

preferential flow paths. In contrast to *Greve et al.* [2012]'s lysimeter-scale study, in which a transition from preferential to matrix flow was observed to happen at the time of surface ponding, these field-scale results show that subsurface preferential flow and surface ponding/overland flow can occur simultaneously.

In the second monitoring event, where the soil within the irrigation plot was already near field capacity, an increase in apparent electrical conductivity was observed at approximately the same time as surface runoff began in the plot (Figure 14b). Very soon after, seepage flow (referring to flow observed through the walls of the collection barrel boxes out of the cracks downhill of the irrigation plots) was also observed.

Taken together, these two monitoring events show that flow through lateral surface or "concealed runoff" pathways is an important hydrologic process in both dry and wet conditions. The presence of these pathways in wet soil is interesting, particularly as a further repudiation to the paradigms that soil cracks seal from the bottom up and that infiltration effectively ends when the soil surface is sealed. However, the dry soil response may be even more important. The collected ERT data indicated that water must have begun moving laterally through the dry soil almost immediately after the start of the first irrigation, as evidenced by a decrease in resistivity 2 m downhill seen within the first 45 minutes of the experiment. This flow in dry, unsaturated conditions may provide a point of possible distinction from lateral subsurface runoff seen in non-

swelling soils, as in the latter either local water tables must be developed [*McGlynn et al.*, 2002; *Tromp van Meerveld and McDonnell*, 2005] or threshold amounts of precipitation and soil moisture must be reached [*McGuire and McDonnell*, 2010] for subsurface flow to occur.

One major drawback to the Wenner configuration used for these ERT measurements is that it does not provide for quantification of the amount of water being delivered preferentially. Therefore, it is hoped that future research will be directed towards better quantification and understanding of how water moves through subsurface crack flowpaths, including examining the contributions of film flow along crack walls versus flow driven by localized ponding, measuring how crack dimensions (particularly near the crack bottoms) are changing through time, determining how much water is moved laterally versus how much is absorbed into the crack walls, and observing if these flowpaths are active under low intensity precipitation events.

Summary and Conclusions

A study performed on a set of instrumented field plots demonstrated that, in a *vertic* soil, crack networks significantly control water movement. As seen in previous studies, shrinkage cracks can cause surface water to reach depths faster than would be expected from infiltration through the soil matrix. For example, capacitance soil moisture sensors installed within the plots showed that water was preferentially delivered to various depths within the soil profile.

Measurements made on representative cracks indicated that swelling of soil may proceed in phases. At the surface, for example, the cracks initially showed rapid swelling, closing by more than 50% with very little increase in the soil moisture of the profile. From there, however, the swelling proceeded much slower, and the near-surface soil reached field capacity before the crack completely sealed. Subsurface monitored cracks showed an opposite behavior, in that the volume changed very little initially as the soil profile wetted, but as the moisture levels approached field capacity swelling advanced rapidly. This may substantiate the findings of *Favre et al.* [1997], who using surface-based measurements observed that soil at the crack interface (which they dubbed the border zone) showed more rapid and more extensive swelling than the soil within the peds.

The relationship between runoff and soil moisture (as measured by small capacitance sensors embedded at four depths into the soil peds) was nearly binary, where no runoff occurred until the soil moisture reached a certain level, and then the soil moisture showed very little change even with increasing runoff ratio. This effect may be an artifact of the capacitance sensors' limited sampling volumes, which may have limited their ability to capture soil moisture changes occurring at the ped-crack interface.

Infiltration data collected during the experiment indicated that in dry conditions the soil matrix had a much higher infiltration capacity than would be predicted based on

the soil texture, likely due to the presence of microscopic cracks. At high moisture contents, when the cracks had mostly sealed at the surface and the soil matrix infiltration capacity had decreased, water was still able to infiltrate at relatively high rates. This was shown both by the runoff ratio, which for most plots peaked between 0.5 and 0.9 (indicating that 10-50 % of the water being applied was still infiltrating), and by electrical resistivity tomography measurements, which revealed the presence of active subsurface flowpaths coincident with surface runoff. However, data collected from one of the runoff plots showed that the runoff ratio approached unity when additional water was applied. This hints at the existence of a secondary runoff threshold in which the subsurface flowpaths have become sealed.

Finally, it was found that using a basic water budget (cumulative precipitation minus evaporation) was an effective predictor of the primary runoff threshold. Indeed, it seems possible that this simple metric serves to integrate many of the complex processes observed in this study. In many ways, this suggests that a *vertic* soil profile can be thought of as a leaking bucket, only one in which the leak becomes smaller and possibly sealed through time. This simple concept may be useful to inform the development of more refined models which quantitatively describe the overall hydrology of a *vertic* soil.

Acknowledgements

This work was supported by National Science Foundation (NSF) Grant No. 0943682. The authors wish to thank Sra. Irene Acevedo for generously providing the use of her property in Chile for purposes of this study. Likewise, the authors would like to recognize the contributions of Dr. Diego Rivera, Mr. Carlos Cea, Alejandra Lavados Carrasco, Abraham Arevalo Neira, and Viviana Gavilan Pino of the Department of Recursos Hídricos at the Universidad de Concepción, Chillán. Additionally, the authors would like to thank Dr. J. Reed Glassman of Willamette Geological Service for providing materials and assistance with the X-Ray Diffraction analysis. Brian Dougherty, John Hesseltine, Emeline Perret and Lifang Xie deserve recognition for their assistance with laboratory soil testing and analysis. Finally, the authors wish to acknowledge the participants of the NSF-funded Undergraduate Chilean Field Hydrology Course for assisting with field installation and data collection: Hayden Ausland, Felipe Bretón, Wiebke Boettche, Sebastián Bonelli, Maria Brown, Liam Kyle Cahill, Daniela Castañeda, Jenna Duffin, Nick Dummer, Alex Fisher, Hector Flores, Zak Grimes, Rachel Gross, Leah Kammel, Chuan Li, Marianela Matta, Claudia Maureira, Mackenzie Osypian, Hazel Owens, Julianne Quinn, William Rhoads, Ghislaine Rossel, and Jennifer Vettel.

References

Abou Najm, M. R., J. D. Jabro, W. M. Iversen, R. H. Mohtar, and R. G. Evans (2010), New method for the characterization of three-dimensional preferential flow paths in the field, *Water Resources Research*, *46*(2).

Ahmad, N. (1996), Occurrence and distribution of Vertisols, *Developments in Soil Science*, *24*, 1-41.

Ali, G., C. J. Oswald, C. Spence, E. L. Cammeraat, K. J. McGuire, T. Meixner, and S. M. Reaney (2013), Towards a unified threshold-based hydrological theory: necessary components and recurring challenges, *Hydrological Processes*, *27*(2), 313-318.

Amidu, S. A., and J. A. Dunbar (2007), Geoelectric Studies of Seasonal Wetting and Drying of a Texas Vertisol, *Vadose Zone Journal*, *6*(3), 511.

Arnold, J. G., K. N. Potter, K. W. King, and P. M. Allen (2005), Estimation of soil cracking and the effect on surface runoff in a Texas Blackland Prairie watershed, *Hydrological Processes*, *19*(3), 589-603.

Beven, K., and P. Germann (1982), Macropores and water flow in soils, *Water Resources Research*, *18*(5), 1311-1325.

Blake, G., E. Schlichting, and U. Zimmermann (1973), Water recharge in a soil with shrinkage cracks, *Soil Science Society of America Journal*, *37*(5), 669-672.

Blöschl, G., and E. Zehe (2005), On hydrological predictability, *Hydrological Processes*, *19*(19), 3923-3929.

Boivin, P., P. Garnier, and M. Vauclin (2006), Modeling the Soil Shrinkage and Water Retention Curves with the Same Equations, *Soil Science Society of America Journal*, *70*(4), 1082.

Bouma, J., and L. W. Dekker (1978), A case study on infiltration into dry clay soil I. Morphological observations, *Geoderma*, *20*(1), 27-40.

Bouma, J., and J. Loveday (1988), Characterizing soil water regimes in swelling clay soils, in *Vertisols: Their Distribution; Properties; Classification and Management*, edited by L. P. Wilding and R. Puentes, pp. 83–96, Texas A&M University Printing Center, College Station, TX.

Brocca, L., F. Melone, and T. Moramarco (2008), On the estimation of antecedent wetness conditions in rainfall–runoff modelling, *Hydrological Processes*, *22*(5), 629-642.

Bronswijk, J., W. Hamminga, and K. Oostindie (1995), Field-scale solute transport in a heavy clay soil, *Water Resources Research*, *31*(3), 517-526.

Campbell, C. S. (2001), Response of ECH2O soil moisture sensor to temperature variation, *Decagon Devices Inc. Application Note AN70TP-10.* Decagon Devices Inc., Pullman, Wash.

Chen, L., and M. H. Young (2006), Green-Ampt infiltration model for sloping surfaces, *Water Resources Research*, *42*(7).

Chertkov, V. Y. (2002), Modelling cracking stages of saturated soils as they dry and shrink, *European Journal of Soil Science*, *53*(1), 105-118.

Chertkov, V. Y. (2012), Physical modeling of the soil swelling curve vs. the shrinkage curve, *Advances in Water Resources*.

Dinka, T. M., and R. J. Lascano (2012), Review Paper: Challenges and Limitations in Studying the Shrink-Swell and Crack Dynamics of Vertisol Soils, *Open Journal of Soil Science*, *2*(2), 82-90.

Evett, S. R., R. C. Schwartz, J. A. Tolk, and T. A. Howell (2009), Soil profile water content determination: Spatiotemporal variability of electromagnetic and neutron probe sensors in access tubes, *Vadose Zone Journal*, *8*(4), 926-941.

Favre, F., P. Boivin, and M. Wopereis (1997), Water movement and soil swelling in a dry, cracked Vertisol, *Geoderma*, *78*(1-2), 113-123.

Giráldez, J. V., G. Sposito, and C. Delgado (1983), A general soil volume change equation: I. The two-parameter model, *Soil Science Society of America Journal*, *47*(3), 419-422.

Goodrich, D., T. Schmugge, T. Jackson, C. Unkrich, T. Keefer, R. Parry, L. Bach, and S. Amer (1994), Runoff simulation sensitivity to remotely sensed initial soil water content, *Water Resources Research*, *30*(5), 1393-1405.

Greco, R. (2002), Preferential flow in macroporous swelling soil with internal catchment: model development and applications, *Journal of Hydrology*, *269*(3), 150-168.

Greve, A. K., M. S. Andersen, and R. I. Acworth (2010), Investigations of soil cracking and preferential flow in a weighing lysimeter filled with cracking clay soil, *Journal of Hydrology*, *393*(1-2), 105-113.

Greve, A. K., M. S. Andersen, and R. I. Acworth (2012), Monitoring the transition from preferential to matrix flow in cracking clay soil through changes in electrical anisotropy, *Geoderma*, *179-180*, 46-52.

Heppell, C., T. Burt, and R. Williams (2000), Variations in the hydrology of an underdrained clay hillslope, *Journal of Hydrology*, *227*(1), 236-256.

Hoogmoed, W., and J. Bouma (1980), A simulation model for predicting infiltration into cracked clay soil, *Soil Science Society of America Journal*, *44*(3), 458-461.

James, A., and N. Roulet (2009), Antecedent moisture conditions and catchment morphology as controls on spatial patterns of runoff generation in small forest catchments, *Journal of Hydrology*, *377*(3), 351-366.

Jarvis, N. J. (1991), MACRO-A model of water movement and solute transport in macroporous soils. Reports and Dissertations No. 9. Department of Soil Sciences, Swedish University of Agricultural Sciences, Uppsala.

Jarvis, N. J., and P. B. Leeds-Harrison (1987), Modelling water movement in drained clay soil. I. Description of the model, sample output and sensitivity analysis, *Journal of Soil Science*, *38*(3), 487-498.

Kishné, A. S., C. L. S. Morgan, and W. L. Miller (2009), Vertisol Crack Extent Associated with Gilgai and Soil Moisture in the Texas Gulf Coast Prairie, *Soil Science Society of America Journal*, *73*(4), 1221.

Krzeminska, D., T. Bogaard, T. Debieche, V. Marc, J. Ponton, and J. Malet (2009), Quantitative analysis of preferential flow during small scale infiltration tests on an active mudslide, French Alps, paper presented at Landslide Processes International Conference, Strasbourg, France.

Kutílek, M. (1996), Water relations and water management of vertisols, *Developments in Soil Science*, *24*, 201-230.

McGarry, D., and K. W. J. Malafant (1987), The analysis of volume change in unconfined units of soil, *Soil Science Society of America Journal*, *51*(2), 290-297.

McGlynn, B. L., J. J. McDonnel, and D. D. Brammer (2002), A review of the evolving perceptual model of hillslope flowpaths at the Maimai catchments, New Zealand, *Journal of Hydrology*, *257*(1), 1-26.

McGuire, K. J., and J. J. McDonnell (2010), Hydrological connectivity of hillslopes and streams: Characteristic time scales and nonlinearities, *Water Resources Research*, *46*(10).

Messing, I., and N. J. Jarvis (1990), Seasonal variation in field-saturated hydraulic conductivity in two swelling clay soils in Sweden, *Journal of Soil Science*, *41*(2), 229-237.

Morari, F., and W. Knisel (1997), Modifications of the GLEAMS model for crack flow, *Transactions of the American Society of Agricultural Engineers (ASAE)*, *40*(5), 1337-1348.

Morbidelli, R., C. Corradini, C. Saltalippi, and L. Brocca (2012), Initial Soil Water Content as Input to Field-Scale Infiltration and Surface Runoff Models, *Water Resources Management*, 1-15.

Návar, J., J. Mendez, R. B. Bryan, and N. J. Kuhn (2002), The contribution of shrinkage cracks to bypass flow during simulated and natural rainfall experiments in northeastern Mexico, *Canadian Journal of Soil Science*, *82*(1), 65-74.

Novák, V., J. Šimůnek, and M. T. Van Genuchten (2000), Infiltration of water into soil with cracks, *Journal of Irrigation and Drainage Engineering*, *126*(1), 41-47.

Novák, V., J. Šimůnek, and M. T. Van Genuchten (2002), Infiltration into a swelling, cracked clay soil, *Journal of Hydrology and Hydromechanics*, *50*(1), 3-19.

Peng, X., and R. Horn (2007), Anisotropic shrinkage and swelling of some organic and inorganic soils, *European Journal of Soil Science*, *58*(1), 98-107.

Penna, D., H. J. Tromp-van Meerveld, A. Gobbi, M. Borga, and G. Dalla Fontana (2011), The influence of soil moisture on threshold runoff generation processes in an alpine headwater catchment, *Hydrology and Earth System Sciences*, *15*(3), 689-702.

Philip, J. R. (1957), The theory of infiltration: 4. Sorptivity and algebraic infiltration equations, *Soil Science*, *84*(3), 257.

Ringrose-Voase, A., and W. Sanidad (1996), A method for measuring the development of surface cracks in soils: application to crack development after lowland rice, *Geoderma*, *71*(3), 245-261.

Römkens, M. J. M., and S. N. Prasad (2006), Rain Infiltration into swelling/shrinking/cracking soils, *Agricultural Water Management*, *86*(1-2), 196-205.

Samouëlian, A., I. Cousin, G. Richard, A. Tabbagh, and A. Bruand (2003), Electrical resistivity imaging for detecting soil cracking at the centimetric scale, *Soil Science Society of America Journal*, *67*(5), 1319-1326.

Samouëlian, A., G. Richard, I. Cousin, R. Guerin, A. Bruand, and A. Tabbagh (2004), Three-dimensional crack monitoring by electrical resistivity measurement, *European Journal of Soil Science*, *55*(4), 751-762.

Sanders, E. C., M. R. Abou Najm, R. H. Mohtar, E. Kladivko, and D. Schulze (2012), Field method for separating the contribution of surface-connected preferential flow pathways from flow through the soil matrix, *Water Resources Research*, *48*(4), W04534.

Selker, J. S., C. K. Keller, and J. T. McCord (1999), *Vadose zone processes*, 339 p. pp., Lewis Publishers, Boca Raton, Fla.

Sentenac, P., and M. Zielinski (2009), Clay fine fissuring monitoring using miniature geo-electrical resistivity arrays, *Environmental Earth Sciences*, *59*(1), 205-214.

Smith, R., and D. Goodrich (2000), Model for rainfall excess patterns on randomly heterogeneous areas, *Journal of Hydrologic Engineering*, *5*(4), 355-362.

Stewart, R. D., M. R. Abou Najm, D. E. Rupp, and J. S. Selker (2012), Measurement Tool for Dynamics of Soil Cracks, *Vadose Zone Journal*, *11*(2).

Tariq, A.-u.-R., and D. S. Durnford (1993), Analytical volume change model for swelling clay soils, *Soil Science Society of America Journal*, *57*(5), 1183-1187.

te Brake, B., M. van der Ploeg, and G. de Rooij (2012), Water storage change estimation from in situ shrinkage measurements of clay soils, *Hydrology and Earth System Sciences*, *9*, 13117-13154.

Tromp van Meerveld, I., and J. J. McDonnell (2005), Comment to "Spatial correlation of soil moisture in small catchments and its relationship to dominant spatial hydrological processes, Journal of Hydrology 286: 113-134", *Journal of Hydrology*, *303*, 307-312.

van Dam, J. C. (2000), Simulation of field-scale water flow and bromide transport in a cracked clay soil, *Hydrological Processes*, *14*(6), 1101-1117.

Verbist, K., W. Cornelis, S. Torfs, and D. Gabriels (2013), Comparing methods to determine hydraulic conductivities on stony soils, *Soil Science Society of America Journal*, *77*(1), 25-42.

Vogel, H. J., H. Hoffmann, A. Leopold, and K. Roth (2005), Studies of crack dynamics in clay soil II. A physically based model for crack formation, *Geoderma*, *125*(3-4), 213-223.

Warrick, A. W. (1983), Interrelationships of irrigation uniformity terms, *Journal of Irrigation and Drainage Engineering*, *109*(3), 317-332.

Weisbrod, N., M. I. Dragila, U. Nachshon, and M. Pillersdorf (2009), Falling through the cracks: The role of fractures in Earth-atmosphere gas exchange, *Geophysical Research Letters*, *36*(2).

Wells, R., D. DiCarlo, T. Steenhuis, J.-Y. Parlange, M. Römkens, and S. Prasad (2003), Infiltration and surface geometry features of a swelling soil following successive simulated rainstorms, *Soil Science Society of America Journal*, *67*(5), 1344-1351.

Zehe, E., H. Elsenbeer, F. Lindenmaier, K. Schulz, and G. Blöschl (2007), Patterns of predictability in hydrological threshold systems, *Water Resources Research*, *43*(7).

Zein el Abedine, A., and G. H. Robinson (1971), A study on cracking in some vertisols of the Sudan, *Geoderma*, *5*(3), 229-241.

Figures

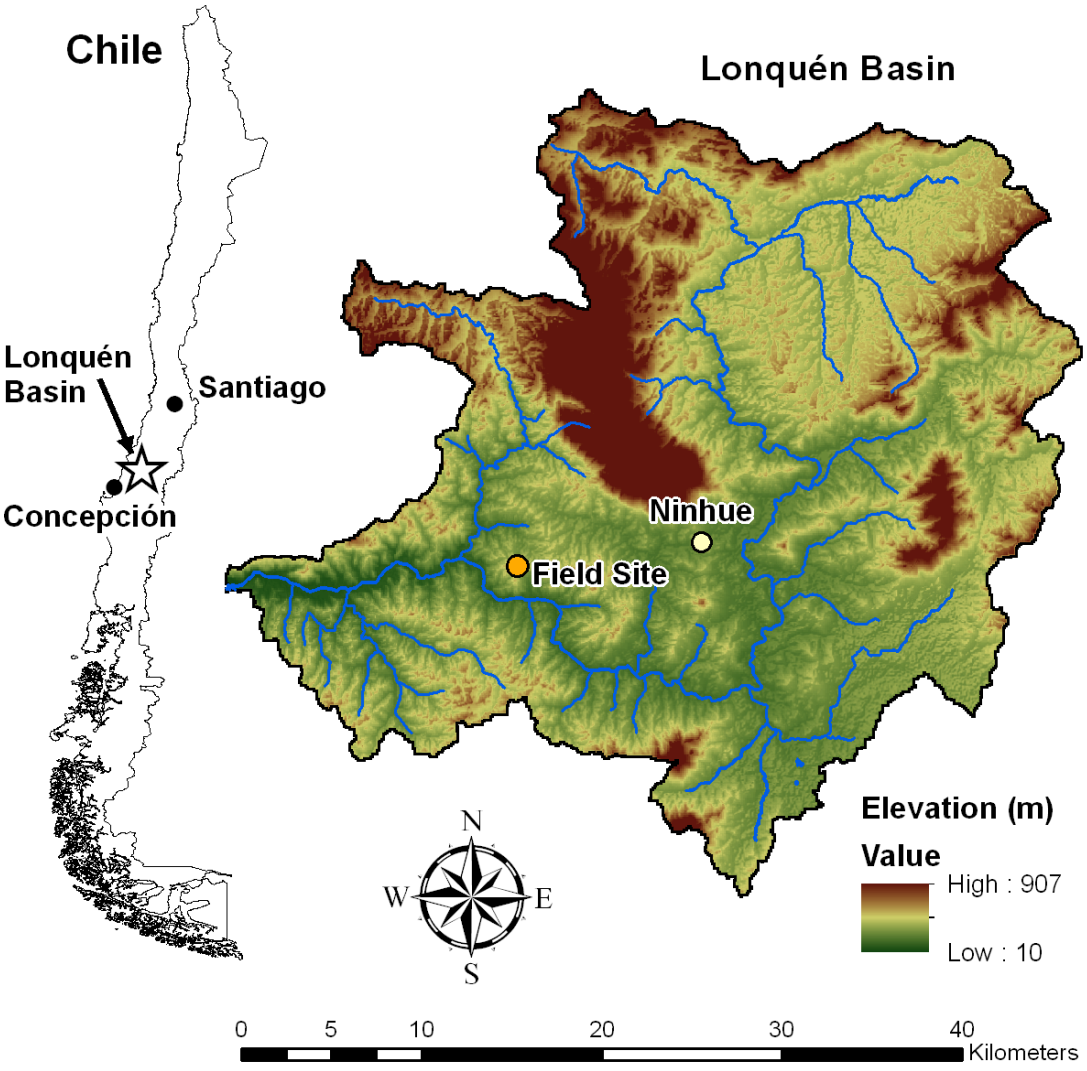

Figure 1 – Map showing relative position within Chile of the Lonquén Basin, and the location of the field site within the basin.

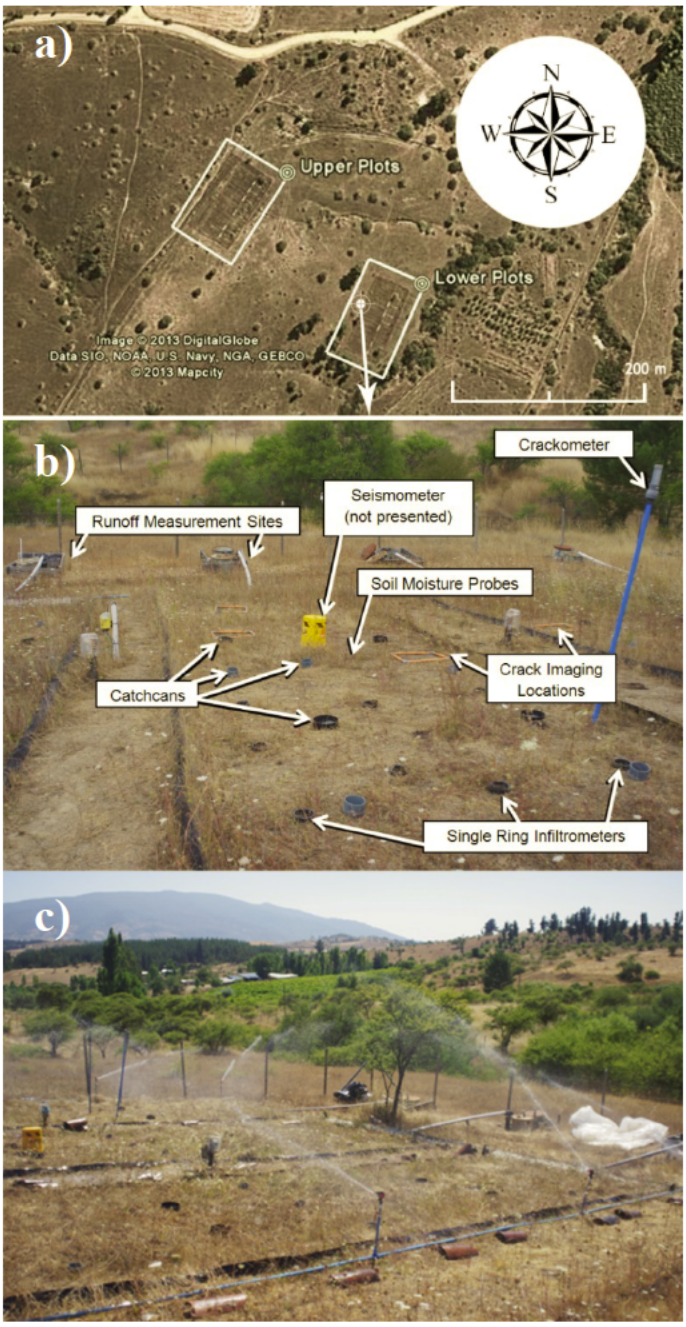

Figure 2 – a) Overhead view of the field site, with the two sets of runoff plots highlighted, b) Plot L5, with examples of notable equipment and instruments highlighted, and c) Plots L1-L3, showing how the configuration of the irrigation system divided the plots into sets of three.

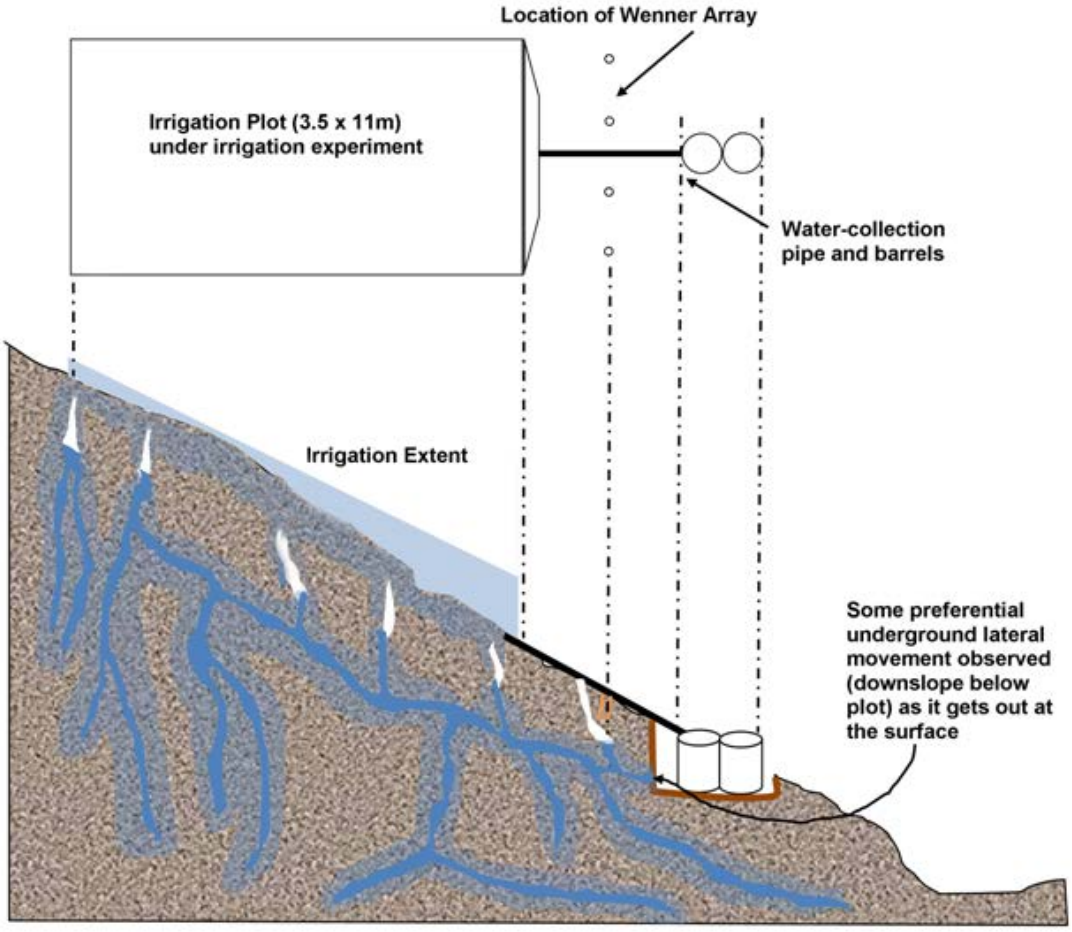

Figure 3 - Schematic of an experimental field plot and conceptualization of water distribution in the hillslope crack-system in response to the irrigation. In 2011 (Year 1), two of the plots were outfitted with Wenner arrays of electrodes to measure the existence of subsurface preferential flowpaths.

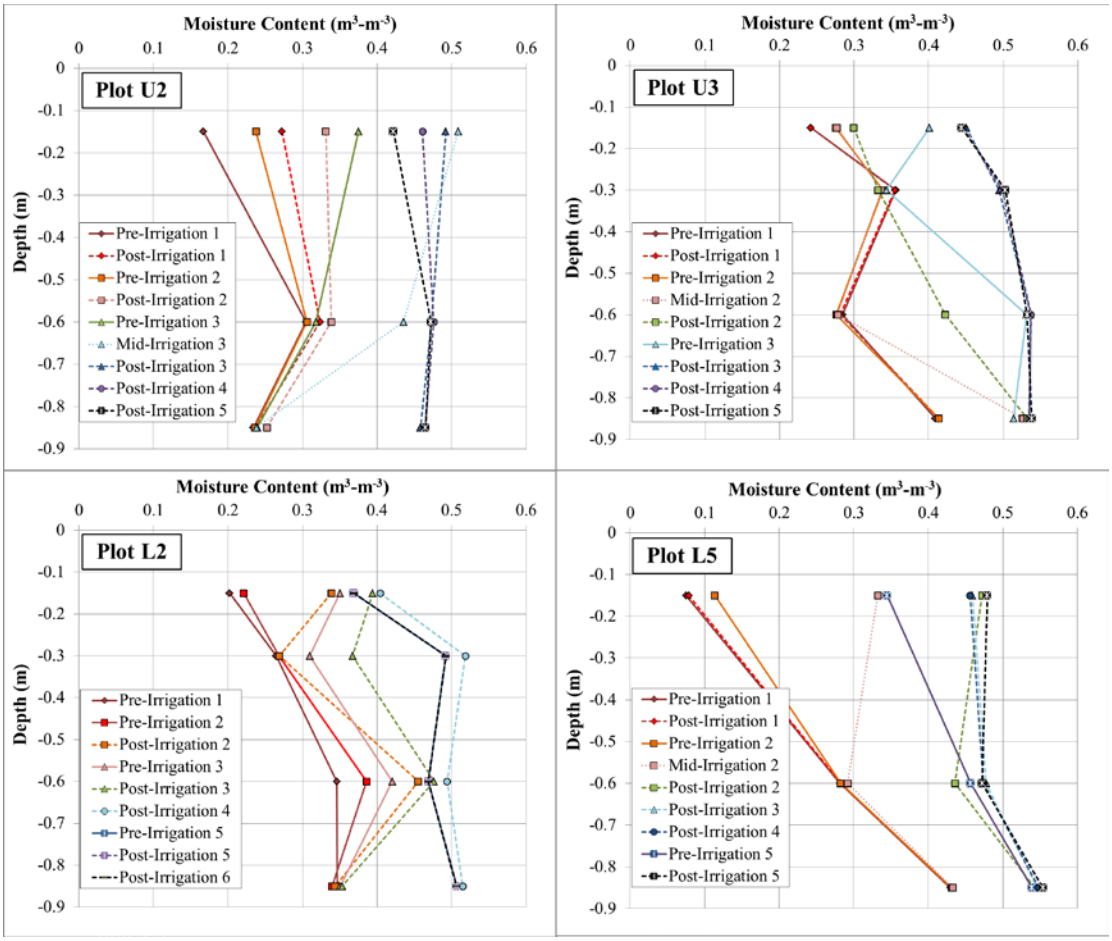

Figure 4 – Wetting profile for Plots U2, U3, L2 and L5 during the 2012 (Year 2) irrigation experiment. Solid lines indicate pre-irrigation readings, dotted lines indicate mid-irrigation readings, and dashed lines indicate post-irrigation readings.

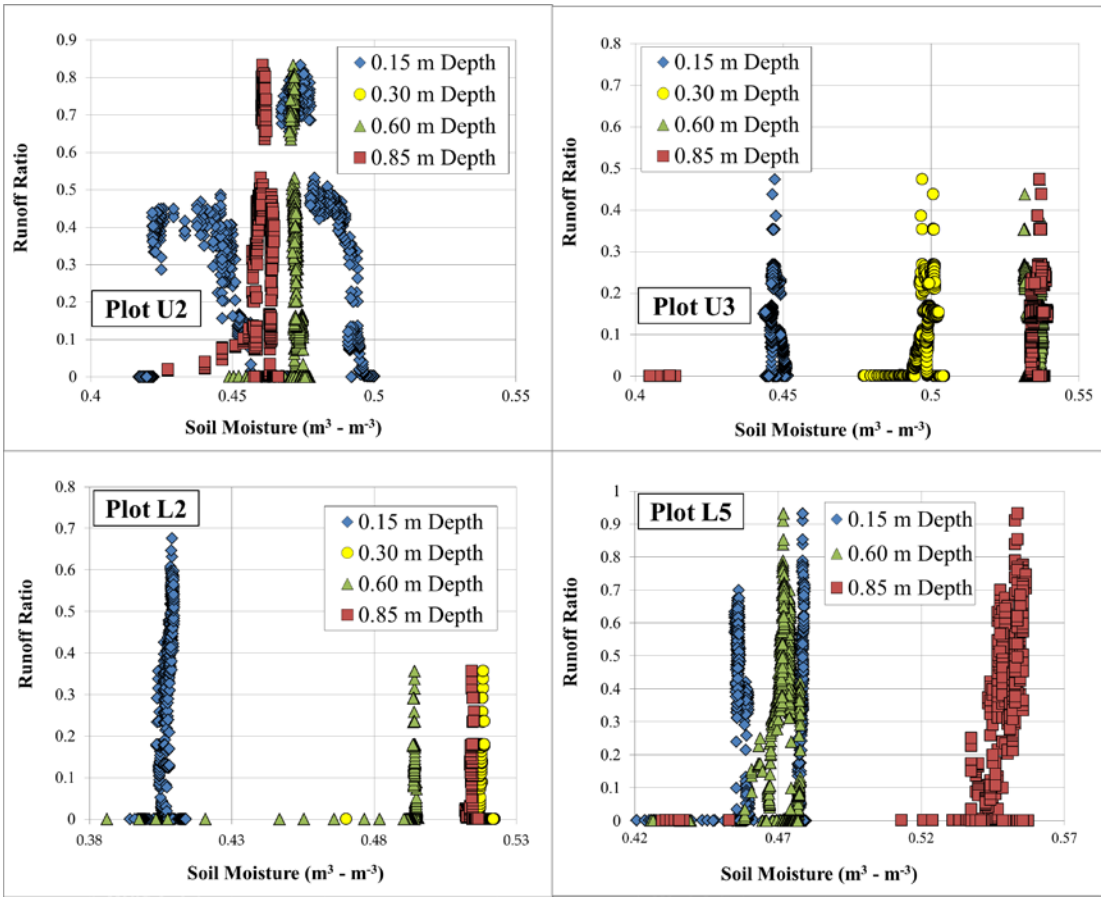

Figure 5 – Volumetric soil moisture and runoff ratio for Plots U2, U3, L2 and L5 during the 2012 (Year 2) irrigation experiment.

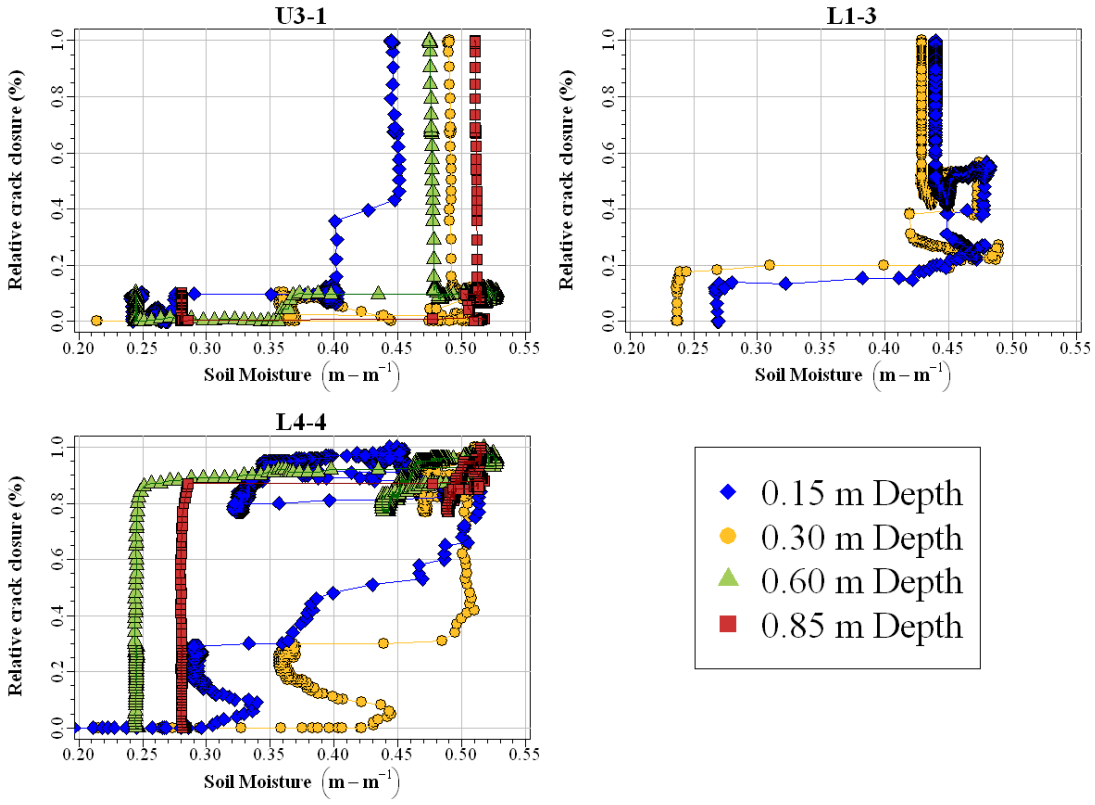

Figure 6 – Volumetric soil moisture and the percent closure of representative cracks for Plots U2, U3, L2 and L5 during the 2012 (Year 2) irrigation experiment.

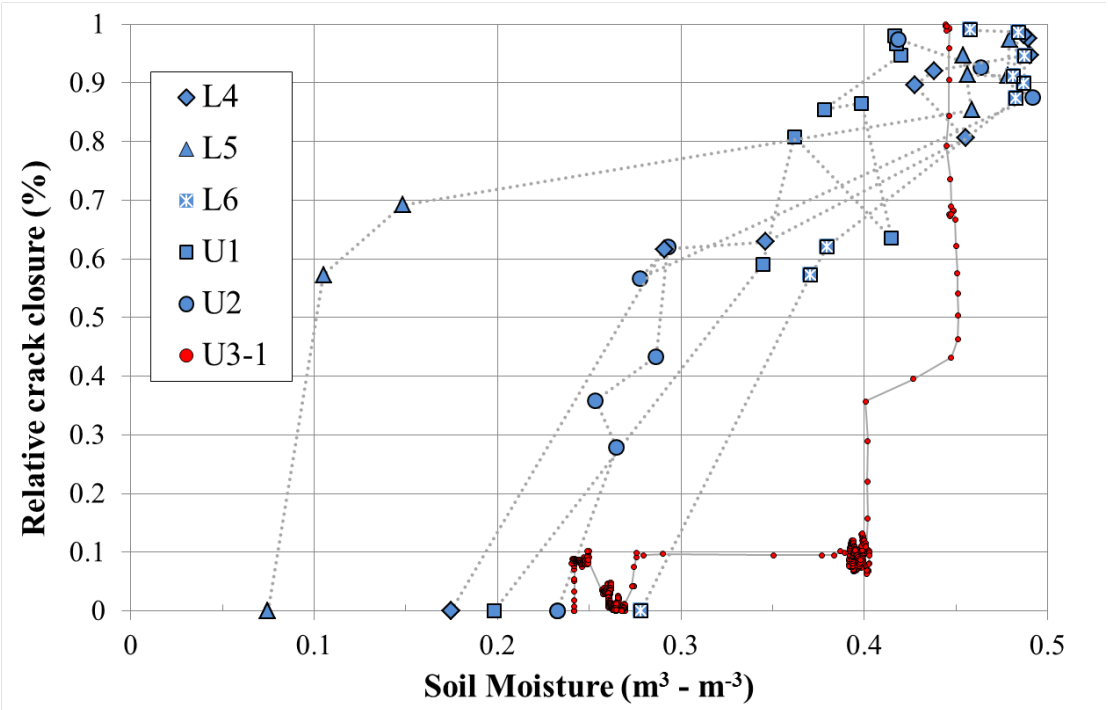

Figure 7 – Crack closure versus soil moisture, where relative crack closure is estimated using the surface-based crack imaging (in red). *Crackometer* data from Plot U3 is also shown for comparison (in green). Soil moisture measurements come from the 0.15 m depth.

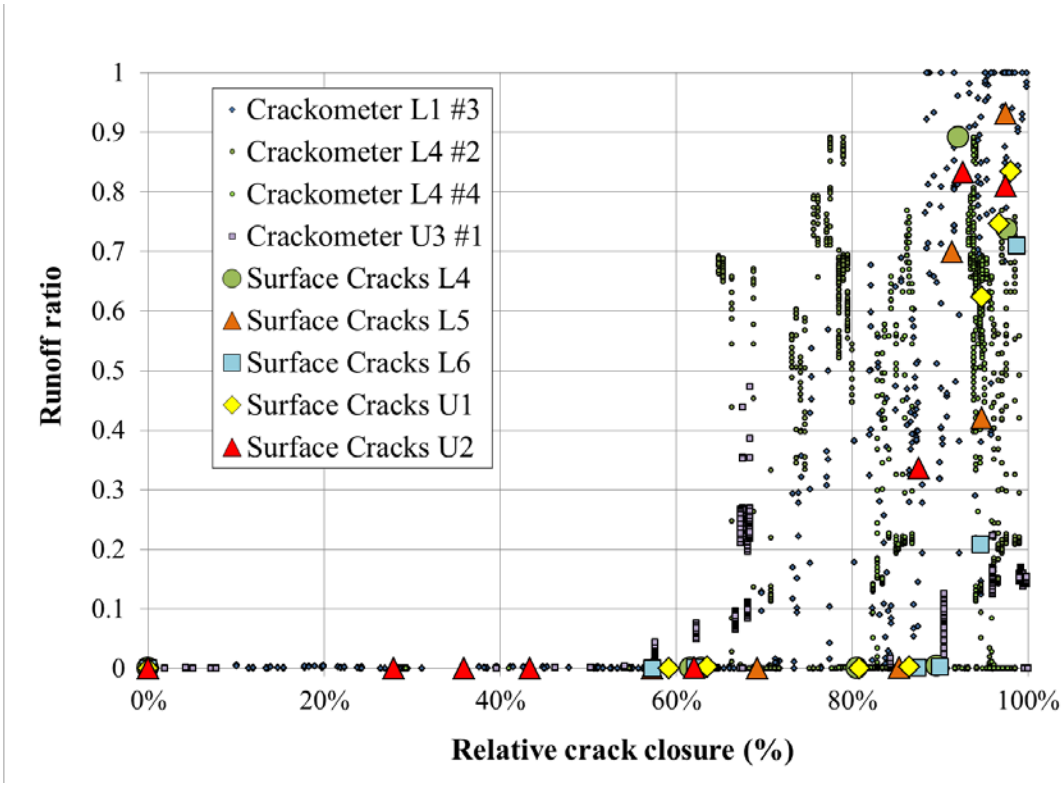

Figure 8 – Runoff ratio compared to relative crack closure, from both the surface imaging of selected cracks and from the installed *crackometer* instruments.

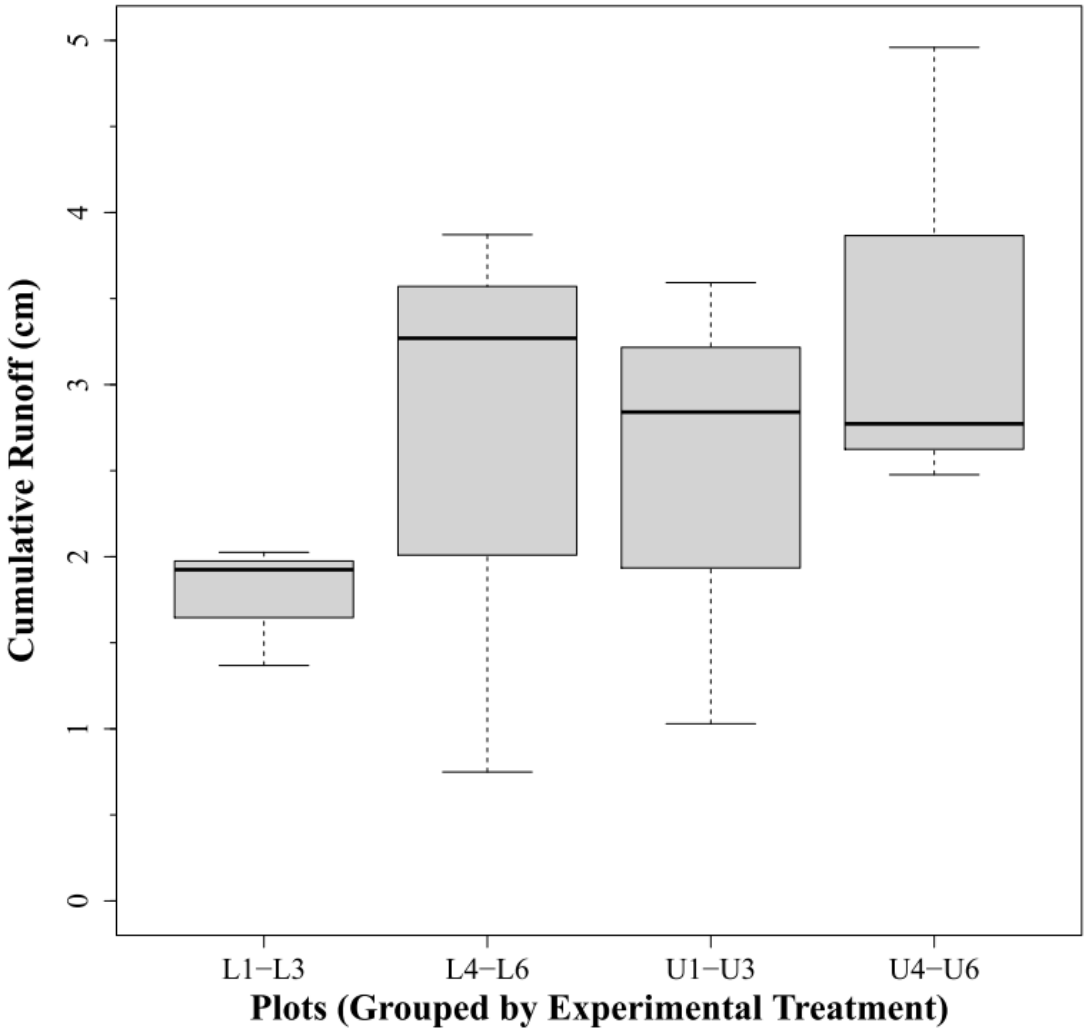

Figure 9 – Difference in mean group runoff for the four experimental treatments.

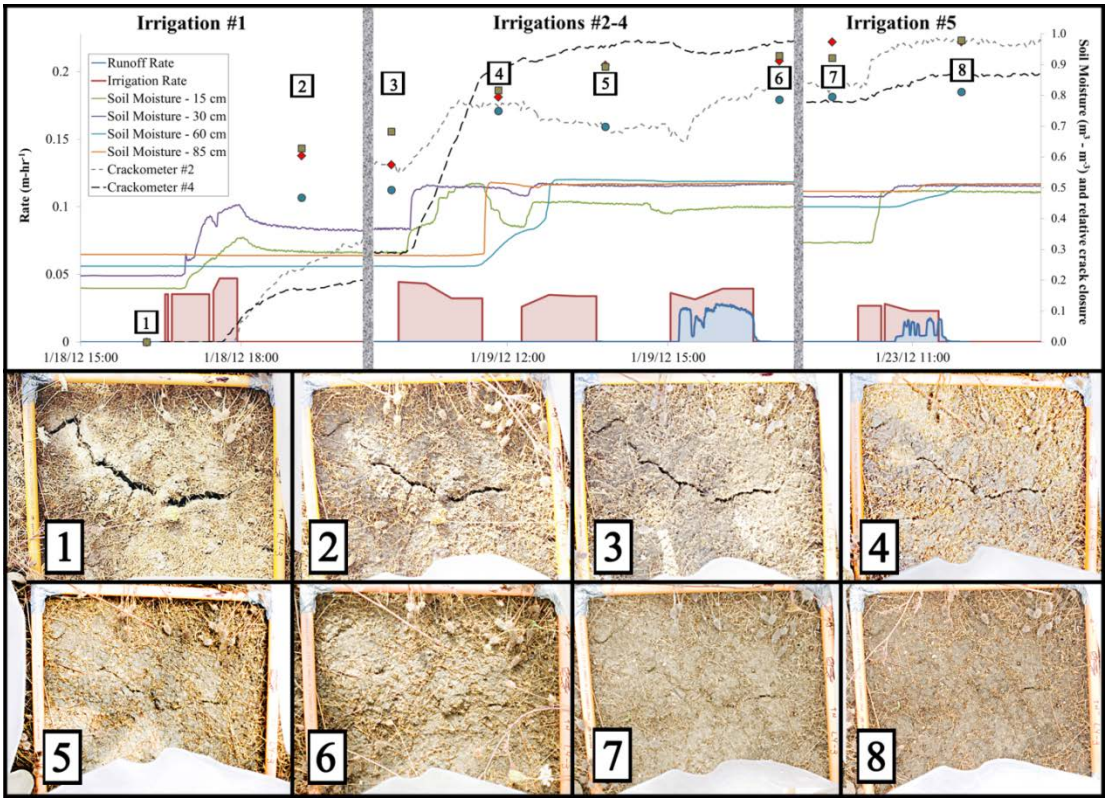

Figure 10 – Time-Series for Plot L4 during 2012 (Year 2) experiment. Simulated rainfall (irrigation) and runoff are presented as rates, in red and blue, respectively. Soil moisture at 0.15 (green), 0.30 (purple), 0.60 (blue) and 0.85 m (orange) depths is shown as temperature-corrected volumetric data. Relative crack closure, taken to be $(V_{max} - V_i)/(V_{max}\text{-}V_{min})$, where V_i is the instantaneous measured volume, is shown as dashed lines for the *crackometer* data and as the discrete points for the crack imaging measurements.

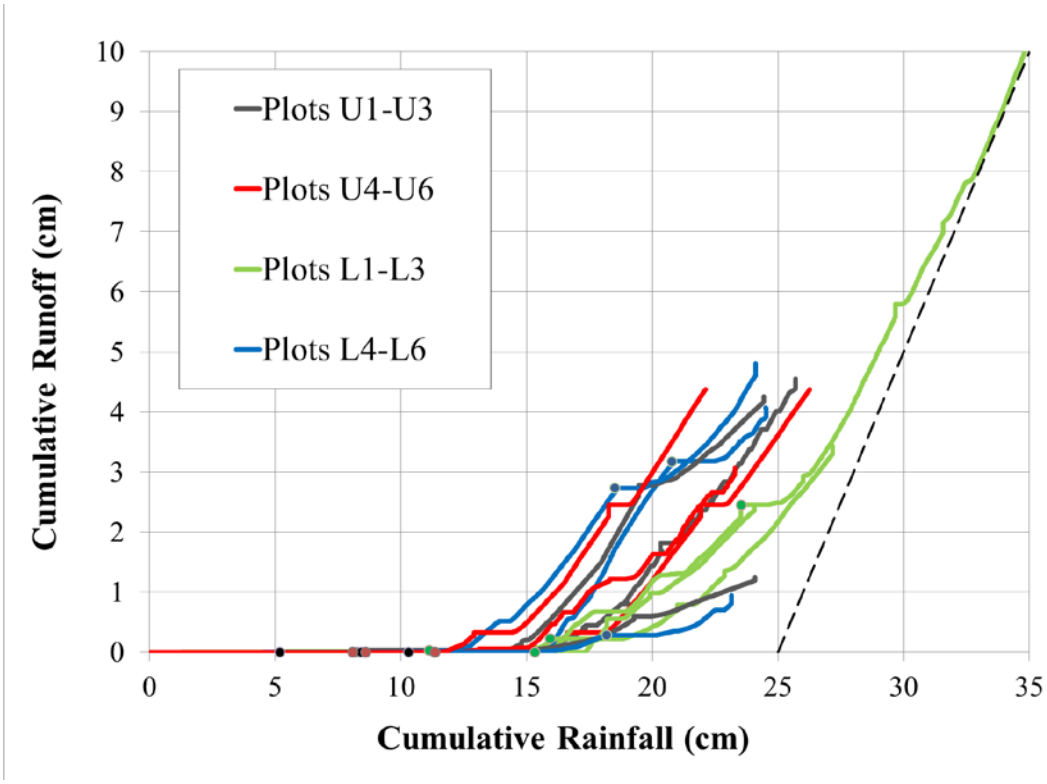

Figure 11 – Cumulative amounts of rainfall (irrigation) and runoff for all plots during the 2012 (Year 2) irrigation experiment. Periods between irrigations of two days or longer are indicated by the points. The 1:1 line is shown in black, starting at 25 cm of cumulative rainfall.

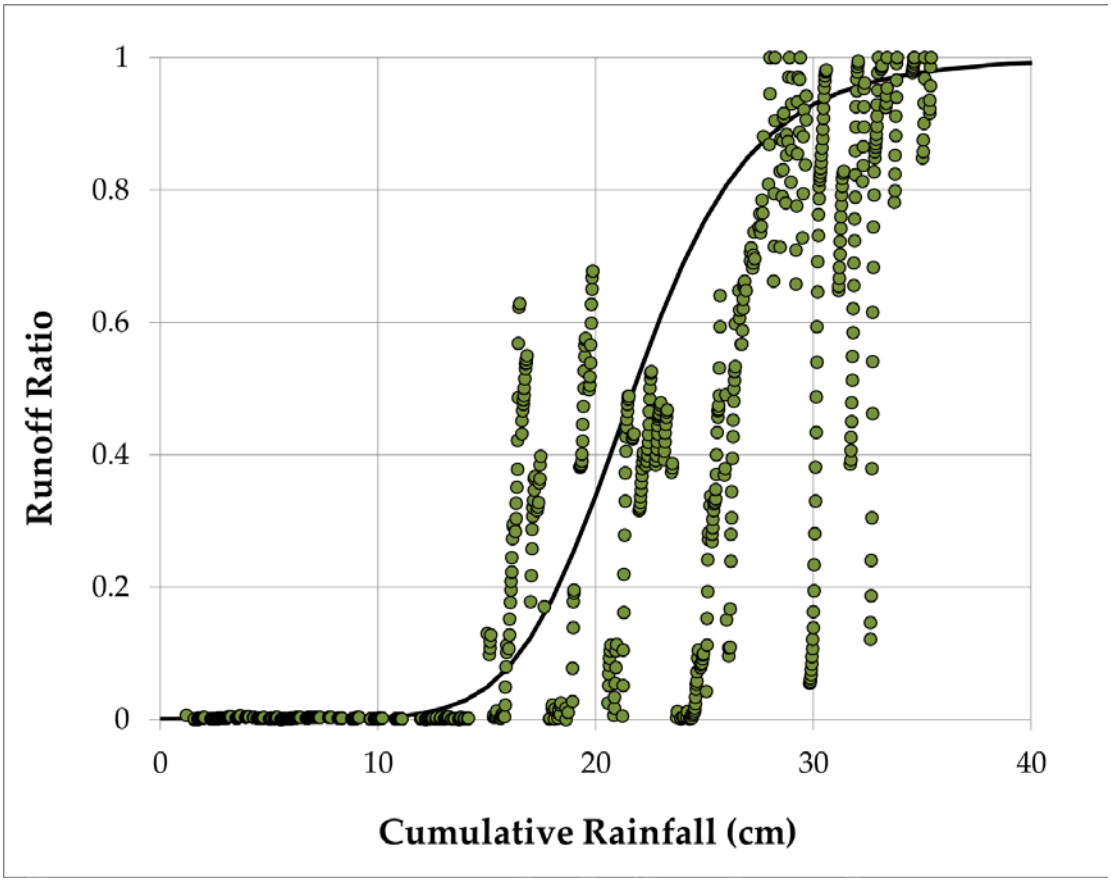

Figure 12 – Runoff ratio as a function of cumulative rainfall for Plot L1. The black line represents a sigmoidal function which potentially describes the transition between no runoff (runoff ratio = 0) and full runoff (runoff ratio = 1).

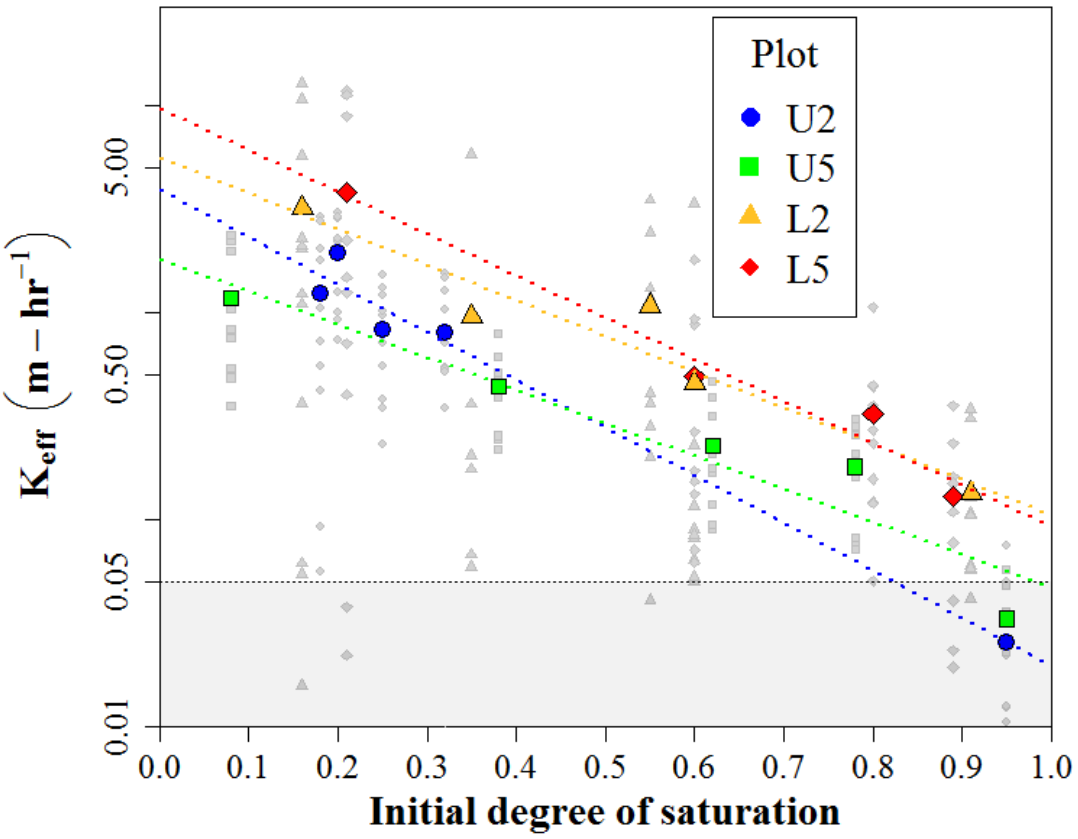

Figure 13 – Effective hydraulic conductivity (K_{eff}) as a function of initial degree of saturation. The gray points represent individual measurements, while the colored points represent the arithmetic mean of those measurements. The range of irrigation rates applied during the irrigation experiments are shown in the shaded box.

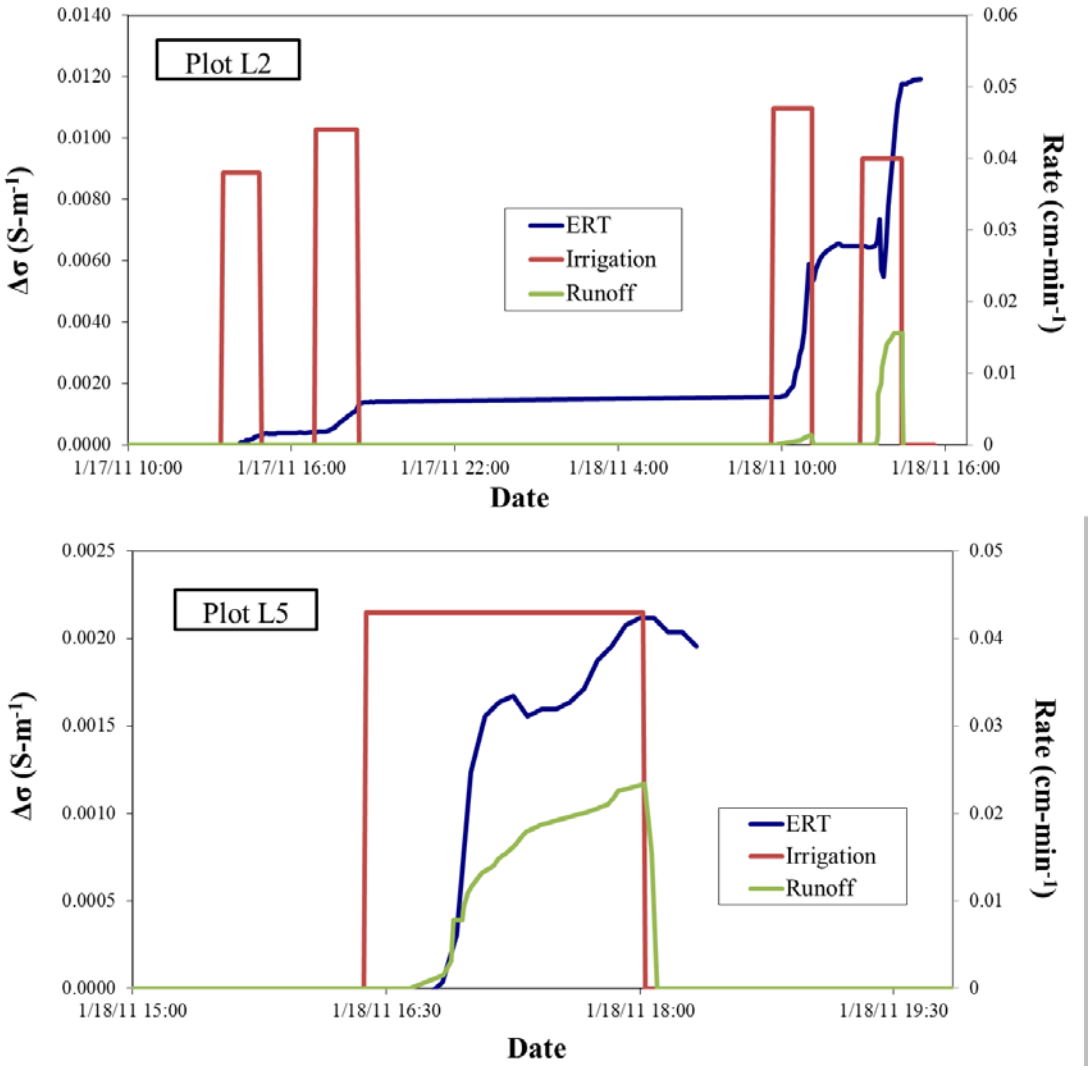

Figure 14 – Change in apparent electric conductivity for a) Plot L2 and b) Plot L5, along with the duration and amount of irrigation and runoff.

Tables

Table 1 – Percentages of Sand, Silt and Clay, and Mineralogical Composition of the Clay (< 2 μm) fraction.

Depth (cm)	No. of samples	Particle Size Distribution (%)			Texture
		Sand	Silt	Clay	
5	15	52 ± 11	33 ± 12	15 ± 8	Loam
10	13	51 ± 14	32 ± 15	18 ± 12	Loam
20	10	29 ± 6	29 ± 4	42 ± 7	Clay
30	9	23 ± 6	31 ± 7	46 ± 12	Clay
60	5	23 ± 6	27 ± 5	50 ± 2	Clay
85	3	48 ± 6	31 ± 5	21 ± 11	Loam

Depth (cm)	No. of samples	Mineral % in the < 2 μm fraction			
		Smectite	Vermiculite	Kaolinite	Illite
5	1	15	10	70	5
10	2	20	5	70	5
20	1	45	10	40	5
30	2	30	20	45	5
60	2	30	15	50	5
85	2	50	10	35	5

Table 2 – Irrigation schedule for 2011 and 2012. For the 2012 data, the gray shading indicates periods where the plots were covered with plastic to prevent evaporation.

Year 1 (2011)

Date	1/5	1/6	1/7 - 1/10	1/11	1/12	1/13 - 1/16	1/17	1/18
Day	*1*	*2*	*3-6*	*7*	*8*	*9-12*	*13*	*14*
L1-L3							1* 2*	3* 4*
L4-L6				1	2 3 4		5	6ǂ
U1-U3	1 2	3 4		5				

Year 2 (2012)

Date	1/11	1/12 - 1/16	1/17	1/18	1/19	1/20 - 1/22	1/23	1/24	1/25	1/26
Day	*1*	*2-6*	*7*	*8*	*9*	*10-12*	*13*	*14*	*15*	*16*
L1-L3	1 2		3 4					5 6		
L4-L6				1	2 3 4		5			
U1-U3			1					2		3 4 5
U4-U6			1	2				3	4	5

* *indicates the first ERT monitoring event*

ǂ *indicates the second ERT monitoring event*

Table 3 – Cumulative irrigation amounts and the Distributed Uniformity (DU) coefficient for both years of the experiment.

	Cumulative Irrigation (cm)		DU Coefficient	
Plot	Year 1*	Year 2	Year 1	Year 2
L1	17.4	35.5	0.75	0.81
L2	15.2	27.2	0.72	0.76
L3	15.6	24.1	0.69	0.48
L4	26.1	24.5	0.73	0.66
L5	22.4	24.1	0.74	0.77
L6	22.1	23.2	0.7	0.48
U1	16.8	25.7	0.67	0.76
U2	12.0	24.4	0.61	0.72
U3	14.2	24.1	0.64	0.66
U4	N/A	27.3	N/A	0.79
U5	N/A	23.3	N/A	0.76
U6	N/A	23.1	N/A	0.5

** An additional 2.1 cm of natural precipitation occurred during the study period*

Table 4 – Summary of infiltration measurements taken over the two-year experimental period. SRI = single ring infiltrometer, DRI = double ring infiltrometer, GP = Guelph Permeameter, and MTP = mini-disk tension infiltrometer.

		K_{eff} (m hr^{-1})				
Method	# of Tests	Minimum	Maximum	Arith. Mean	Geo. Mean	Std. Dev.
SRI*	62	1.58×10^{-2}	1.29×10^{1}	2.08×10^{0}	9.48×10^{-1}	2.92×10^{0}
DRI†	5	4.64×10^{-2}	5.41×10^{-1}	1.79×10^{-1}	1.17×10^{-1}	1.84×10^{-1}
GP‡	6	1.20×10^{-4}	6.91×10^{-1}	1.16×10^{-1}	1.07×10^{-3}	2.57×10^{-1}
MTP	4	5.14×10^{-3}	1.32×10^{-1}	5.58×10^{-2}	2.55×10^{-2}	5.28×10^{-2}

* *only measurements with $\Theta_0 < 0.3$ were included for the SRI.*

† *an additional DRI test was attempted, but emptied so rapidly that accurate data could not be collected.*

‡ *GP data are based on the minimum calculated K_{eff}, which assumes initially unsaturated soil and maximum matric potential.*

5. Conclusions

When analyzing shrink-swell clay (*vertic*) soils, it is tempting to state that the only constant is change. After all, at different moisture contents a *vertic* soil experiences tremendous variation in physical properties such as bulk density, effective hydraulic conductivity, size and connectivity of cracks, surface elevation, hardness and plasticity, geometric factor, and water retention. To further complicate matters, many of these properties exhibit hysteresis between cycles of shrinkage and swelling [*Wells et al.*, 2003; *Peng and Horn*, 2007]. Therefore, it would seem that trying to predict the hydrologic response of a *vertic* soil, and how processes such as infiltration, runoff and preferential flow become manifest, would be incredibly difficult. However, this study identified several phenomena which offer the potential to simplify the description of hydrologic processes in such soils.

First, it was recognized that when scaled relative to dry conditions, all soil types had a similar relationship between sorptivity and initial soil moisture. This substantiated the long-held simplification that the initial amount of non-filled (effective) porosity was the most important component for describing variations in sorptivity. A slight modification to the *Green and Ampt* [1911] model was then proposed to approximate the sorptivity of any soil as a function of soil moisture. Included in the analysis was a swelling clay soil (the Beit Netofa clay), which demonstrated a similar theoretical sorptivity profile as its non-swelling counterparts.

The second chapter of the study, which examined field-based infiltration tests conducted in a *vertic* soil, corroborated that finding: it was determined that variations in the effective porosity of the soil explained most of the difference in sorptivity at different moisture conditions. However, when looking at the gravity-driven infiltration component, the *vertic* soil deviated widely from non-swelling soils. It was determined that the effective hydraulic conductivity (determined as the resistance to gravity-driven, rather than capillary-driven, flow) decreased as moisture content increased. In some locations the effective hydraulic conductivity decreased by more than two orders of magnitudes as the soil went from dry to fully saturated.

To explain this behavior, an expression was developed which used the reciprocal of a simplified soil shrinkage curve to describe crack porosity as a function of soil moisture. After assuming that the widths of micro-cracks within the soil matrix varied with soil moisture in a manner proportional to the overall porosity, Plane-Poiseuille flow was utilized to estimate flow rate through these micro-cracks. This allowed for Darcy's law to be used to approximate the effective hydraulic conductivity in terms of the crack porosity of the soil, and enabled the effective hydraulic term to be replaced with a soil "constant", A_0. Altogether, the developed theory accurately described the observed field behavior (within the realms of accepted natural variability in soil properties), and in the future should allow for easy incorporation into large-scale hydrologic models.

The third chapter of this study also relied on field observations and measurements, this time to examine how water moves through, and interacts with, a *vertic* soil. Twelve 3.5 x 11 m runoff plots located at a field site in the *Secano Interior* region of Chile were used as the basis for the study. The plots were heavily instrumented, including dielectric capacitance soil moisture sensors at two or four depths, runoff and rainfall measurement equipment, infiltrometers, and monitoring equipment placed in and around representative cracks throughout the plots. By applying water to the plots when they were dry and the cracks were wide open, several interesting and, in some cases, novel phenomena were revealed.

For instance, the cracks appeared to seal from the top down. This means that other studies which utilize surface-based crack measurements may underestimate the influence of crack networks on water movement. Electrical resistivity measurements demonstrated that crack networks can act as preferential flowpaths, conducting water laterally (in the case of a sloped soil profile). These flowpaths were active both in dry (when no surface runoff was apparent) and wet conditions (when the cracks had nearly or completely sealed at the surface and significant surface runoff was being produced). Therefore, “concealed” runoff produced by these cracks should be considered by anyone attempting to model or understand the hydrology of a *vertic* soil.

Non-concealed surface runoff (overland flow) exhibited a strongly non-linear threshold. That is, no runoff was produced when the dry soil was irrigated. However, after 0.12 – 0.17 m of irrigation, all of the plots showed a sharp increase in surface runoff. At this point, water appeared to be moving quickly off of the runoff plots as both surface and subsurface flow, with very little apparent internal soil storage. Data collected from one plot suggested that with enough additional water, the subsurface cracks may eventually close, at which point water will move almost entirely over the surface. All told, if these transition points are consistent between plots and across multiple years, they may provide an effective means to simplify the hydrologic description of these soils.

As a final note, the *Secano Interior* region of Chile, where the latter portion of the study took place, is currently experiencing a tremendous shift in land use. The traditional vegetative cover, which consists of native grasses intermingled with fields producing wheat and other grains, is rapidly being converted to intensively-planted pine (*pinus radiata*) forests [*Aronson et al.*, 1998]. This land use change may be altering the region's soils, biodiversity and hydrology [*Aronson et al.*, 1993], though to what extent and duration is the subject of considerable debate [*Scott and Prinsloo*, 2008; *Huber et al.*, 2010]. It is hoped that the findings of this study, which describe water movement in *vertic* soils under native grass cover, may in the future be used to

compare hydrologic and physical changes (and by extension social, economic and ecological changes) produced by conversion of the land cover to forest.

References

Alcaíno, E., and K. Vargas (2001), Potencial productivo y económico de sistemas agrícolas con recusos hídricos escasos *Boletin INIA-Instituto de Investigaciones Agropecuarias*(71).

Aronson, J., C. Floret, E. Le Floc'h, C. Ovalle, and R. Pontanier (1993), Restoration and Rehabilitation of Degraded Ecosystems in Arid and Semi-Arid Lands. II. Case Studies in Southern Tunisia, Central Chile and Northern Cameroon, *Restoration Ecology*, *1*(3), 168-187.

Aronson, J., A. Del Pozo, C. Ovalle, J. Avendaño, A. Lavin, and M. Etienne (1998), Land use changes and conflicts in central Chile, *Ecological studies*, 155-170.

Green, W. H., and G. Ampt (1911), Studies on soil physics, *Journal of Agricultural Science*, *4*(1), 1-24.

Huber, A., A. Iroume, C. Mohr, and C. Frene (2010), Effect of Pinus radiata and Eucalyptus globulus plantations on water resource in the Coastal Range of Biobio region, Chile, *Bosque*, *31*(3), 219-230.

Peng, X., and R. Horn (2007), Anisotropic shrinkage and swelling of some organic and inorganic soils, *European Journal of Soil Science*, *58*(1), 98-107.

Scott, D. F., and F. Prinsloo (2008), Longer-term effects of pine and eucalypt plantations on streamflow, *Water Resources Research*, *44*(7).

Wells, R., D. DiCarlo, T. Steenhuis, J.-Y. Parlange, M. Römkens, and S. Prasad (2003), Infiltration and surface geometry features of a swelling soil following successive simulated rainstorms, *Soil Science Society of America Journal*, *67*(5), 1344-1351.

Bibliography

Abou Najm, M. R. (2009), Soil-water interaction: Lessons across scales, PhD Dissertation thesis, Purdue University, West Lafayette, IN.

Abou Najm, M. R., J. D. Jabro, W. M. Iversen, R. H. Mohtar, and R. G. Evans (2010), New method for the characterization of three-dimensional preferential flow paths in the field, *Water Resources Research, 46*(2).

Abu-Hejleh, A. N., and D. Znidarcic (1995), Desiccation theory for soft cohesive soils, *Journal of Geotechnical Engineering*, *121*(6), 493-502.

Aeby, P., J. Forrer, H. Flühler, and C. Steinmeier (1997), Image analysis for determination of dye tracer concentrations in sand columns, *Soil Science Society of America Journal*, *61*(1), 33-35.

Ahmad, N. (1996), Occurrence and distribution of Vertisols, *Developments in Soil Science*, *24*, 1-41.

Alcaíno, E., and K. Vargas (2001), Potencial productivo y económico de sistemas agrícolas con recusos hídricos escasos *Boletin INIA-Instituto de Investigaciones Agropecuarias 71*.

Ali, G., C. J. Oswald, C. Spence, E. L. Cammeraat, K. J. McGuire, T. Meixner, and S. M. Reaney (2013), Towards a unified threshold-based hydrological theory: necessary components and recurring challenges, *Hydrological Processes*, *27*(2), 313-318.

Amidu, S. A., and J. A. Dunbar (2007), Geoelectric Studies of Seasonal Wetting and Drying of a Texas Vertisol, *Vadose Zone Journal, 6*(3), 511.

Arnold, J. G., K. N. Potter, K. W. King, and P. M. Allen (2005), Estimation of soil cracking and the effect on surface runoff in a Texas Blackland Prairie watershed, *Hydrological Processes*, *19*(3), 589-603.

Aronson, J., C. Floret, E. Le Floc'h, C. Ovalle, and R. Pontanier (1993), Restoration and Rehabilitation of Degraded Ecosystems in Arid and Semi-Arid Lands. II. Case Studies in Southern Tunisia, Central Chile and Northern Cameroon, *Restoration Ecology, 1*(3), 168-187.

Aronson, J., A. Del Pozo, C. Ovalle, J. Avendaño, A. Lavin, and M. Etienne (1998), Land use changes and conflicts in central Chile, *Ecological studies*, 155-170.

Bandyopadhyay, K. K., M. Mohanty, D. K. Painuli, A. K. Misra, K. M. Hati, K. G. Mandal, P. K. Ghosh, R. S. Chaudhary, and C. L. Acharya (2003), Influence of tillage practices and nutrient management on crack parameters in a Vertisol of central India, *Soil and Tillage Research, 71*(2), 133-142.

Basma, A. A., A. S. Al-Homoud, and A. Husein (1995), Laboratory assessment of swelling pressure of expansive soils, *Applied Clay Science, 9*(5), 355-368.

Berndt, R., and K. Coughlan (1977), The nature of changes in bulk density with water content in a cracking clay, *Soil Research, 15*(1), 27-37.

Beven, K., and P. Germann (1982), Macropores and water flow in soils, *Water Resources Research, 18*(5), 1311-1325.

Bhushan, L., and P. K. Sharma (2002), Long-term effects of lantana (Lantana spp. L.) residue additions on soil physical properties under rice–wheat cropping: I. Soil consistency, surface cracking and clod formation, *Soil and Tillage Research, 65*(2), 157-167.

Blake, G., E. Schlichting, and U. Zimmermann (1973), Water recharge in a soil with shrinkage cracks, *Soil Science Society of America Journal, 37*(5), 669-672.

Blöschl, G., and E. Zehe (2005), On hydrological predictability, *Hydrological Processes, 19*(19), 3923-3929.

Bogner, C., B. Wolf, M. Schlather, and B. Huwe (2008), Analysing flow patterns from dye tracer experiments in a forest soil using extreme value statistics, *European Journal of Soil Science, 59*(1), 103-113.

Boivin, P., P. Garnier, and M. Vauclin (2006), Modeling the Soil Shrinkage and Water Retention Curves with the Same Equations, *Soil Science Society of America Journal, 70*(4), 1082.

Bouma, J., and L. W. Dekker (1978), A case study on infiltration into dry clay soil I. Morphological observations, *Geoderma, 20*(1), 27-40.

Bouma, J., and J. Loveday (1988), Characterizing soil water regimes in swelling clay soils, in *Vertisols: Their Distribution; Properties; Classification and Management,* edited by L. P. Wilding and R. Puentes, pp. 83–96, Texas A&M University Printing Center, College Station, TX.

Bouma, J., A. Jongerius, and D. Schoonderbeek (1979), Calculation of saturated hydraulic conductivity of some pedal clay soils using micromorphometric data, *Soil Science Society of America Journal, 43*(2), 261-264.

Bouwer, H. (1964), Unsaturated flow in ground-water hydraulics, *Journal of the Hydraulics Division, Proceedings of the American Society of Civil Engineers, 90*(HY5), 121-144.

Brasher, B., D. Franzmeier, V. Valassis, and S. E. Davidson (1966), Use of saran resin to coat natural soil clods for bulk-density and water-retention measurements, *Soil Science, 101*(2), 108.

Braud, I., D. De Condappa, J. M. Soria, R. Haverkamp, R. Angulo-Jaramillo, S. Galle, and M. Vauclin (2005), Use of scaled forms of the infiltration equation for the estimation of unsaturated soil hydraulic properties (the Beerkan method), *European Journal of Soil Science, 56*(3), 361-374.

Braudeau, E. (1988), Essai de caractérisation quantitative de l'état structural d'un sol basé sur l'étude de la courbe de retrait, *CR Académie des Sciences, Série 2*, 307, 1933-1936.

Braudeau, E., J.-P. Frangi, and R. H. Mohtar (2004), Characterizing Nonrigid Aggregated Soil–Water Medium Using its Shrinkage Curve, *Soil Science Society of America Journal, 68*(2), 359-370.

Braudeau, E., J. Costantini, G. Bellier, and H. Colleuille (1999), New device and method for soil shrinkage curve measurement and characterization, *Soil Science Society of America Journal, 63*(3), 525-535.

Brocca, L., F. Melone, and T. Moramarco (2008), On the estimation of antecedent wetness conditions in rainfall–runoff modelling, *Hydrological Processes, 22*(5), 629-642.

Bronswijk, J. (1988), Modeling of Water-Balance, Cracking and Subsidence of Clay Soils, *Journal of Hydrology, 97*(3-4), 199-212.

Bronswijk, J., W. Hamminga, and K. Oostindie (1995a), Field-scale solute transport in a heavy clay soil, *Water Resources Research, 31*(3), 517-526.

Bronswijk, J., W. Hamminga, and K. Oostindie (1995b), Rapid nutrient leaching to groundwater and surface water in clay soil areas, *European Journal of Agronomy, 4*(4), 431-439.

Bronswijk, J., J. Evers-Vermeer, and J. van den Akker (1997), Determination of the shrinkage characteristics of clay soil aggregates, *Manual for soil physical measurements. Version, 3*, 71-77.

Brooks, R. H., and A. T. Corey (1964), Hydraulic properties of porous media, *Hydrology Papers*, Colorado State University.

Brutsaert, W. (1977), Vertical infiltration in dry soil, *Water Resources Research, 13*(2), 363-368.

Campbell, C. S. (2001), Response of ECH2O soil moisture sensor to temperature variation, *Decagon Devices Inc. Application Note AN70TP-10,* Decagon Devices Inc., Pullman, Wash.

Chen, L., and M. H. Young (2006), Green-Ampt infiltration model for sloping surfaces, *Water Resources Research, 42*(7).

Chertkov, V. Y. (2002a), Modelling cracking stages of saturated soils as they dry and shrink, *European Journal of Soil Science, 53*(1), 105-118.

Chertkov, V. Y. (2002b), The Horizontal Hydraulic Conductivity of Vertical Interaggregate Capillary Cracks in Clay Soils, in *Physical Methods in Agriculture*, edited, pp. 39-50, Springer.

Chertkov, V. Y. (2012), Physical modeling of the soil swelling curve vs. the shrinkage curve, *Advances in Water Resources*.

Chertkov, V. Y., and I. Ravina (2000), Shrinking-swelling phenomenon of clay soils attributed to capillary-crack network, *Theory and Applied Fracture Mechanics, 34*(1), 61-71.

Chertkov, V. Y., and I. Ravina (2001), Effect of interaggregate capillary cracks on the hydraulic conductivity of swelling clay soils, *Water Resources Research, 37*(5), 1245-1256.

Cornelis, W. M., J. Corluy, H. Medina, J. Díaz, R. Hartmann, M. Van Meirvenne, and M. E. Ruiz (2006), Measuring and modelling the soil shrinkage characteristic curve, *Geoderma, 137*(1-2), 179-191.

Dasog, G., and G. Shashidhara (1993), Dimension and volume of cracks in a Vertisol under different crop covers, *Soil Science, 156*(6), 424.

Davidson, M. R. (1984), A Green-Ampt Model of infiltration in a cracked soil, *Water Resources Research, 20*(11), 1685-1690.

Das Gupta, S., B. P. Mohanty, and J. M. Köhne (2006), Soil hydraulic conductivities and their spatial and temporal variations in a vertisol, *Soil Science Society of America Journal*, *70*(6), 1872-1881.

Deeks, L., A. Williams, J. Dowd, and D. Scholefield (1999), Quantification of pore size distribution and the movement of solutes through isolated soil blocks, *Geoderma, 90*(1), 65-86.

Dinka, T. M., and R. J. Lascano (2012), Review Paper: Challenges and Limitations in Studying the Shrink-Swell and Crack Dynamics of Vertisol Soils, *Open Journal of Soil Science, 2*(2), 82-90.

Elias, E. A., A.A. Salih and F. Alaily (2001), Cracking patterns in the Vertisols of the Sudan Gezira at the end of the dry season, *International Agrophysics, 15*, 151-155.

Evett, S. R., R. C. Schwartz, J. A. Tolk, and T. A. Howell (2009), Soil profile water content determination: Spatiotemporal variability of electromagnetic and neutron probe sensors in access tubes, *Vadose Zone Journal, 8*(4), 926-941.

Favre, F., P. Boivin, and M. Wopereis (1997), Water movement and soil swelling in a dry, cracked Vertisol, *Geoderma, 78*(1-2), 113-123.

Flowers, M., and R. Lal (1999), Axle load and tillage effects on the shrinkage characteristics of a Mollic Ochraqualf in northwest Ohio, *Soil and Tillage Research, 50*(3), 251-258.

Forrer, I., A. Papritz, R. Kasteel, H. Flühler, and D. Luca (2000), Quantifying dye tracers in soil profiles by image processing, *European Journal of Soil Science, 51*(2), 313-322.

Fortner, J., K. Harward, D. Lytle, and D. Williamson (2006), Web Soil Survey.

Fuentes, C., R. Haverkamp, and J. Y. Parlange (1992), Parameter constraints on closed-form soilwater relationships, *Journal of Hydrology, 134*(1), 117-142.

Gérard-Marchant, P., R. Angulo-Jaramillo, R. Haverkamp, M. Vauclin, P. Groenevelt, and D. Elrick (1997), Estimating the hydraulic conductivity of slowly permeable and swelling materials from single-ring experiments, *Water Resources Research, 33*(6), 1375-1382.

Getreue, P. (2004), MATLAB functions to read and write 3D data PLY files (plyread.m).

Giaccari, L. (2008a), Surface Reconstruction from Scattered Point Clouds (MyRobustCrust.m).

Giaccari, L. (2008b), Volume Enclosed by a Triangulated Surface (SurfaceVolume.m).

Giraldez, J. V., and G. Sposito (1985), Infiltration in swelling soils, *Water Resources Research, 21*(1), 33-44.

Giráldez, J. V., G. Sposito, and C. Delgado (1983), A general soil volume change equation: I. The two-parameter model, *Soil Science Society of America Journal, 47*(3), 419-422.

Goodrich, D., T. Schmugge, T. Jackson, C. Unkrich, T. Keefer, R. Parry, L. Bach, and S. Amer (1994), Runoff simulation sensitivity to remotely sensed initial soil water content, *Water Resources Research, 30*(5), 1393-1405.

Gray, C. W., and R. Allbrook (2002), Relationships between shrinkage indices and soil properties in some New Zealand soils, *Geoderma, 108*(3), 287-299.

Greco, R. (2002), Preferential flow in macroporous swelling soil with internal catchment: model development and applications, *Journal of Hydrology, 269*(3), 150-168.

Green, W. H., and G. Ampt (1911), Studies on soil physics, *Journal of Agricultural Science, 4*(1), 1-24.

Greve, A. K., M. S. Andersen, and R. I. Acworth (2010), Investigations of soil cracking and preferential flow in a weighing lysimeter filled with cracking clay soil, *Journal of Hydrology, 393*(1-2), 105-113.

Greve, A. K., M. S. Andersen, and R. I. Acworth (2012), Monitoring the transition from preferential to matrix flow in cracking clay soil through changes in electrical anisotropy, *Geoderma, 179-180*, 46-52.

Haines, W. B. (1930), Studies in the physical properties of soil. V. The hysteresis effect in capillary properties, and the modes of moisture distribution associated therewith, *Journal of Agricultural Science, 20*(01), 97-116.

Harris, G., P. Nicholls, S. Bailey, K. Howse, and D. Mason (1994), Factors influencing the loss of pesticides in drainage from a cracking clay soil, *Journal of Hydrology, 159*(1), 235-253.

Harvey, A. (1971), Seasonal flood behaviour in a clay catchment, *Journal of Hydrology*, *12*(2), 129-144.

Haverkamp, R., F. Bouraoui, C. Zammit, and R. Angulo-Jaramillo (1999), Soil properties and moisture movement in the unsaturated zone, *Handbook of Groundwater Engineering*.

Heppell, C., T. Burt, and R. Williams (2000), Variations in the hydrology of an underdrained clay hillslope, *Journal of Hydrology*, *227*(1), 236-256.

Hoogmoed, W., and J. Bouma (1980), A simulation model for predicting infiltration into cracked clay soil, *Soil Science Society of America Journal*, *44*(3), 458-461.

Huber, A., A. Iroume, C. Mohr, and C. Frene (2010), Effect of Pinus radiata and Eucalyptus globulus plantations on water resource in the Coastal Range of Biobio region, Chile, *Bosque*, *31*(3), 219-230.

Hudak, P., B. Sadler, and B. Hunter (1998), Analyzing underground water-pipe breaks in residual soils, *Water Engineering and Management*, *145*, 15-20.

Hunt, A. G., and G. W. Gee (2002), Application of critical path analysis to fractal porous media: comparison with examples from the Hanford site, *Advances in Water Resources*, *25*(2), 129-146.

Jabro, J. D. (1996), Variability of field-saturated hydraulic conductivity in a Hagerstown soil as affected by initial water content, *Soil Science*, *161*(11), 735-739.

James, A., and N. Roulet (2009), Antecedent moisture conditions and catchment morphology as controls on spatial patterns of runoff generation in small forest catchments, *Journal of Hydrology*, *377*(3), 351-366.

Jarvis, N., P. E. Jansson, P. Dik, and I. Messing (1991), Modelling water and solute transport in macroporous soil. I. Model description and sensitivity analysis, *Journal of Soil Science*, *42*(1), 59-70.

Jarvis, N. J. (1991), MACRO-A model of water movement and solute transport in macroporous soils. Reports and Dissertations No. 9. Department of Soil Sciences, Swedish University of Agricultural Sciences, Uppsala.

Jarvis, N. J., and P. B. Leeds-Harrison (1987), Modelling water movement in drained clay soil. I. Description of the model, sample output and sensitivity analysis, *Journal of Soil Science, 38*(3), 487-498.

Jones, L. D., and I. Jefferson (2012), *Expansive soils*, ICE Publishing, Telluride, CO.

Kasteel, R., M. Burkhardt, S. Giesa, and H. Vereecken (2005), Characterization of field tracer transport using high-resolution images, *Vadose Zone Journal, 4*(1), 101-111.

Kishné, A. S., C. L. S. Morgan, and W. L. Miller (2009), Vertisol Crack Extent Associated with Gilgai and Soil Moisture in the Texas Gulf Coast Prairie, *Soil Science Society of America Journal, 73*(4), 1221.

Klocke, N. L., and P. Fischbach (1984), G84-690 Estimating Soil Moisture by Appearance and Feel, *Historical Materials from University of Nebraska-Lincoln Extension, Paper 1201*.

Knezevich, C. A. (1975), Soil Survey of Benton County Area, Oregon, US Soil Conservation Service.

Konrad, J.-M., and R. Ayad (1997), An idealized framework for the analysis of cohesive soils undergoing desiccation, *Canadian Geotechnical Journal, 34*(4), 477-488.

Krohn, J. P., and J. E. Slosson (1980), Assessment of expansive soils in the United States, paper presented at Expansive Soils, ASCE.

Krzeminska, D., T. Bogaard, T. Debieche, V. Marc, J. Ponton, and J. Malet (2009), Quantitative analysis of preferential flow during small scale infiltration tests on an active mudslide, French Alps, paper presented at Landslide Processes International Conference, Strasbourg, France.

Kutílek, M. (1996), Water relations and water management of vertisols, *Developments in Soil Science 24*, 201-230.

Leeds-Harrison, P., C. Shipway, N. Jarvis, and E. Youngs (1986), The influence of soil macroporosity on water retention, transmission and drainage in a clay soil, *Soil Use and Management, 2*(2), 47-50.

Ligthart, T., G. Peek, and E. Taber (1993), A method for the three-dimensional mapping of earthworm burrow systems, *Geoderma, 57*(1), 129-141.

Lindenmaier, F., E. Zehe, M. Helms, O. Evadakov, and J. Ihringer (2006), Effect of soil shrinkage on runoff generation in micro and mesoscale catchments, IAHS PUBLICATION, 303, 305.

Lu, J., and L. Wu (2003), Visualizing bromide and iodide water tracer in soil profiles by spray methods, *Journal of Environmental Quality, 32*(1), 363-367.

Mallants, D., B. P. Mohanty, D. Jacques, and J. Feyen (1996), Spatial variability of hydraulic properties in a multi-layered soil profile, *Soil Science, 161*(3), 167.

McGarry, D., and K. W. J. Malafant (1987), The analysis of volume change in unconfined units of soil, *Soil Science Society of America Journal, 51*(2), 290-297.

McGlynn, B. L., J. J. McDonnel, and D. D. Brammer (2002), A review of the evolving perceptual model of hillslope flowpaths at the Maimai catchments, New Zealand, *Journal of Hydrology*, *257*(1), 1-26.

McGuire, K. J., and J. J. McDonnell (2010), Hydrological connectivity of hillslopes and streams: Characteristic time scales and nonlinearities, *Water Resources Research*, *46*(10).

McIntyre, D., C. Watson, and J. Loveday (1982a), Swelling of a clay soil profile under ponding, *Soil Research, 20*(2), 71-79.

McIntyre, D., J. Loveday, and C. Watson (1982b), Field studies of water and salt movement in an irrigated swelling clay soil. I. Infiltration during ponding, *Soil Research, 20*(2), 81-90.

Messing, I., and N. J. Jarvis (1990), Seasonal variation in field-saturated hydraulic conductivity in two swelling clay soils in Sweden, *Journal of Soil Science, 41*(2), 229-237.

Mitchell, A. R., and M. T. Van Genuchten (1993), Flood irrigation of a cracked soil, *Soil Science Society of America Journal, 57*(2), 490-497.

Morari, F., and W. Knisel (1997), Modifications of the GLEAMS model for crack flow, *Transactions of the American Society of Agricultural Engineers, 40*(5), 1337-1348.

Morbidelli, R., C. Corradini, C. Saltalippi, and L. Brocca (2012), Initial Soil Water Content as Input to Field-Scale Infiltration and Surface Runoff Models, *Water Resources Management*, 1-15.

Morel-Seytoux, H. J., and J. Khanji (1974), Derivation of an Equation of Infiltration, *Water Resources Research, 10*(4), 795-800.

Morel-Seytoux, H. J., P. D. Meyer, M. Nachabe, J. Touma, M. T. van Genuchten, and R. J. Lenhard (1996), Parameter equivalence for the Brooks-Corey and van Genuchten soil characteristics: Preserving the effective capillary drive, *Water Resources Research, 32*(5), 1251-1258.

Mualem, Y. (1976), A new model for predicting the hydraulic conductivity of unsaturated porous media, *Water Resources Research, 12*(3), 513-522.

Návar, J., J. Mendez, R. B. Bryan, and N. J. Kuhn (2002), The contribution of shrinkage cracks to bypass flow during simulated and natural rainfall experiments in northeastern Mexico, *Canadian Journal of Soil Science, 82*(1), 65-74.

Neuman, S. P. (1976), Wetting front pressure head in the infiltration model of Green and Ampt, *Water Resources Research, 12*(3), 564-566.

Novák, V. (1976), Cracks in swelling soil and the calculation of their characteristics, *Water in Heavy Soils, Proc. II, ICID and ISSS, Bratislava*, 21-41.

Novák, V., J. Šimůnek, and M. T. Van Genuchten (2000), Infiltration of water into soil with cracks, *Journal of Irrigation and Drainage Engineering, 126*(1), 41-47.

Novák, V., J. Šimůnek, and M. T. Van Genuchten (2002), Infiltration into a swelling, cracked clay soil, *Journal of Hydrology and Hydromechanics, 50*(1), 3-19.

Parlange, J. Y. (1975), On solving the flow equation in unsaturated soils by optimization: Horizontal infiltration, *Soil Science Society of America Journal, 39*(3), 415-418.

Peng, X., and R. Horn (2007), Anisotropic shrinkage and swelling of some organic and inorganic soils, *European Journal of Soil Science, 58*(1), 98-107.

Penna, D., H. J. Tromp-van Meerveld, A. Gobbi, M. Borga, and G. Dalla Fontana (2011), The influence of soil moisture on threshold runoff generation processes in an alpine headwater catchment, *Hydrology and Earth System Sciences, 15*(3), 689-702.

Péron, H., T. Hueckel, and L. Laloui (2007), An improved volume measurement for determining soil water retention curves, *Geotechnical Testing Journal, 30*(1), 1.

Peyton, R. L., C. J. Gantzer, S. H. Anderson, B. A. Haeffner, and P. Pfeifer (1994), Fractal dimension to describe soil macropore structure using X ray computed tomography, *Water Resources Research, 30*(3), 691-700.

Philip, J. R. (1957), The theory of infiltration: 4. Sorptivity and algebraic infiltration equations, *Soil Science, 84*(3), 257.

Philip, J. R. (1969), Moisture equilibrium in the vertical in swelling soils. I. Basic theory, *Soil Research, 7*(2), 99-120.

Philip, J. R. (1990), Inverse Solution for One-Dimensional Infiltration, and the Ratio a/K1, *Water Resources Research, 26*(9), 2023-2027.

Preston, S., B. Griffiths, and I. Young (1997), An investigation into sources of soil crack heterogeneity using fractal geometry, *European Journal of Soil Science, 48*(1), 31-37.

Rawls, W. J., L. R. Ahuja, D. L. Brakensiek, A. Shirmohammadi, and D. Maidment (1992), *Infiltration and soil water movement*, McGraw-Hill Inc.

Ringrose-Voase, A., and W. Sanidad (1996), A method for measuring the development of surface cracks in soils: application to crack development after lowland rice, *Geoderma, 71*(3), 245-261.

Römkens, M. J. M., and S. N. Prasad (2006), Rain Infiltration into swelling/shrinking/cracking soils, *Agricultural Water Management, 86*(1-2), 196-205.

Rossi, A. M., D. R. Hirmas, R. C. Graham, and P. D. Sternberg (2008), Bulk density determination by automated three-dimensional laser scanning, *Soil Science Society of America Journal, 72*(6), 1591-1593.

Samouëlian, A., I. Cousin, G. Richard, A. Tabbagh, and A. Bruand (2003), Electrical resistivity imaging for detecting soil cracking at the centimetric scale, *Soil Science Society of America Journal, 67*(5), 1319-1326.

Samouëlian, A., G. Richard, I. Cousin, R. Guerin, A. Bruand, and A. Tabbagh (2004), Three-dimensional crack monitoring by electrical resistivity measurement, *European Journal of Soil Science, 55*(4), 751-762.

Sander, T., and H. H. Gerke (2007), Noncontact shrinkage curve determination for soil clods and aggregates by three-dimensional optical scanning, *Soil Science Society of America Journal, 71*(5), 1448.

Sanders, E. C., M. R. A. Najm, R. H. Mohtar, E. Kladivko, and D. Schulze (2012), Field method for separating the contribution of surface-connected preferential flow pathways from flow through the soil matrix, *Water Resources Research, 48*(4), W04534.

Schafer, W., and M. Singer (1976), A reinvestigation of the effect of saran coatings on the extensibility of swelling soil clods, *Soil Science, 122*(6), 360-364.

Scott, D. F., and F. Prinsloo (2008), Longer-term effects of pine and eucalypt plantations on streamflow, *Water Resources Research*, *44*(7).

Scott, G., R. Webster, and S. Nortcliff (1986), An analysis of crack pattern in clay soil: its density and orientation, *Journal of Soil Science*, *37*(4), 653-668.

Selker, J. S., C. K. Keller, and J. T. McCord (1999), *Vadose zone processes*, 339 p. pp., Lewis Publishers, Boca Raton, Fla.

Sentenac, P., and M. Zielinski (2009), Clay fine fissuring monitoring using miniature geo-electrical resistivity arrays, *Environmental Earth Sciences*, *59*(1), 205-214.

Šimůnek, J., M. T. Van Genuchten, and M. Sejna (2005), The HYDRUS-1D software package for simulating the one-dimensional movement of water, heat, and multiple solutes in variably-saturated media, *University of California, Riverside, Research reports*, 240.

Smettem, K., P. Ross, R. Haverkamp, and J. Parlange (1995), Three-Dimensional Analysis of Infiltration from the Disk Infiltrometer: 3. Parameter Estimation Using a Double-Disk Tension Infiltrometer, *Water Resources Research*, *31*(10), 2491-2495.

Smiles, D. E. (1974), Infiltration into a swelling material, *Soil Science*, *117*(3), 140-147.

Smiles, D. E., and J. H. Knight (1976), A note on the use of the Philip infiltration equation, *Soil Research*, *14*(1), 103-108.

Smith, R., and D. Goodrich (2000), Model for rainfall excess patterns on randomly heterogeneous areas, *Journal of Hydrologic Engineering*, *5*(4), 355-362.

Stavridakis, E. I. (2006), Assessment of anisotropic behavior of swelling soils on ground and construction work, in *Expansive Soils: Recent Advances in Characterization And Treatment*, 371-384.

Stewart, R. D., M. R. Abou Najm, D. E. Rupp, and J. S. Selker (2012a), An Image-Based Method for Determining Bulk Density and the Soil Shrinkage Curve, *Soil Science Society of America Journal*, *76*(4), 1217-1221.

Stewart, R. D., M. R. Abou Najm, D. E. Rupp, and J. S. Selker (2012b), Measurement Tool for Dynamics of Soil Cracks, *Vadose Zone Journal, 11*(2).

Su, N. (2010), Theory of infiltration: Infiltration into swelling soils in a material coordinate, *Journal of Hydrology, 395*(1-2), 103-108.

Swartzendruber, D., M. F. De Boodt, and D. Kirkham (1954), Capillary Intake Rate of Water and Soil Structure, *Soil Science Society of America Journal, 18*(1), 1-7.

Talsma, T., and A. Lelij (1976), Infiltration and water movement in an in situ swelling soil during prolonged ponding, *Soil Research, 14*(3), 337-349.

Tariq, A.-u.-R., and D. S. Durnford (1993), Analytical volume change model for swelling clay soils, *Soil Science Society of America Journal, 57*(5), 1183-1187.

Tariq, A.-u.-R., and D. S. Durnford (1993), Soil volumetric shrinkage measurements: a simple method, *Soil Science*, 155.

Tavenas, F., P. Jean, P. Leblond, and S. Leroueil (1983), The permeability of natural soft clays. Part II: Permeability characteristics, *Canadian Geotechnical Journal, 20*(4), 645-660.

te Brake, B., M. van der Ploeg, and G. de Rooij (2012), Water storage change estimation from in situ shrinkage measurements of clay soils, *Hydrology and Earth System Sciences, 9*, 13117-13154.

Toker, N., J. Germaine, K. Sjoblom, and P. Culligan (2004), A new technique for rapid measurement of continuous soil moisture characteristic curves, *Geotechnique, 54*(3), 179-186.

Touma, J., M. Voltz, and J. Albergel (2007), Determining soil saturated hydraulic conductivity and sorptivity from single ring infiltration tests, *European Journal of Soil Science, 58*(1), 229-238.

Tromp van Meerveld, I., and J. J. McDonnell (2005), Comment to "Spatial correlation of soil moisture in small catchments and its relationship to dominant spatial hydrological processes, Journal of Hydrology 286: 113-134", *Journal of Hydrology, 303*, 307-312.

Tuller, M., and D. Or (2001), Hydraulic conductivity of variably saturated porous media: Film and corner flow in angular pore space, *Water Resources Research, 37*(5), 1257-1276.

Tunny, J. (1970), The influence of Saran resin coatings on swelling of natural soil clods, *Soil Science, 109*(4), 254-256.

van Dam, J. C. (2000), Simulation of field-scale water flow and bromide transport in a cracked clay soil, *Hydrological Processes, 14*(6), 1101-1117.

van Genuchten, M. T. (1980), A closed-form equation for predicting the hydraulic conductivity of unsaturated soils, *Soil Science Society of America Journal, 44*(5), 892-898.

Vandervaere, J. P., M. Vauclin, and D. E. Elrick (2000), Transient Flow from Tension Infiltrometers I. The Two-Parameter Equation, *Soil Science Society of America Journal, 64*(4), 1263-1272.

Verbist, K., W. Cornelis, S. Torfs, and D. Gabriels (2013), Comparing methods to determine hydraulic conductivities on stony soils, *Soil Science Society of America Journal, 77*(1), 25-42.

Vogel, H. J., H. Hoffmann, A. Leopold, and K. Roth (2005), Studies of crack dynamics in clay soil II. A physically based model for crack formation, *Geoderma, 125*(3-4), 213-223.

Warrick, A. W. (1983), Interrelationships of irrigation uniformity terms, *Journal of Irrigation and Drainage Engineering, 109*(3), 317-332.

Washburn, E. W. (1921), The Dynamics of Capillary Flow, *Physical Review, 17*(3), 273-283.

Weaver, T., N. Hulugalle, and H. Ghadiri (2005), Comparing deep drainage estimated with transient and steady state assumptions in irrigated vertisols, *Irrigation Science, 23*(4), 183-191.

Weisbrod, N., M. I. Dragila, U. Nachshon, and M. Pillersdorf (2009), Falling through the cracks: The role of fractures in Earth-atmosphere gas exchange, *Geophysical Research Letters*, *36*(2).

Wells, R., D. DiCarlo, T. Steenhuis, J.-Y. Parlange, M. Römkens, and S. Prasad (2003), Infiltration and surface geometry features of a swelling soil following successive simulated rainstorms, *Soil Science Society of America Journal, 67*(5), 1344-1351.

White, I., and M. Sully (1987), Macroscopic and microscopic capillary length and time scales from field infiltration, *Water Resources Research, 23*(8), 1514-1522.

White, I., M. J. Sully, and K. M. Perroux (1992), Measurement of surface-soil hydraulic properties: Disk permeameters, tension infiltrometers, and other techniques, in *Advances in measurement of soil physical properties: Bringing theory into practice*, 69-103.

Wooding, R. (1968), Steady infiltration from a shallow circular pond, *Water Resources Research*, *4*(6), 1259-1273.

Zehe, E., H. Elsenbeer, F. Lindenmaier, K. Schulz, and G. Blöschl (2007), Patterns of predictability in hydrological threshold systems, *Water Resources Research, 43*(7).

Zein el Abedine, A., and G. H. Robinson (1971), A study on cracking in some vertisols of the Sudan, *Geoderma, 5*(3), 229-241.

Appendices

Appendix A – Measurement Tool for Dynamics of Soil Cracks

Ryan D. Stewart[1*], Majdi R. Abou Najm[1,2,3], David E. Rupp[4,5], John S. Selker[1]

[1] *Biological & Ecological Engineering Department, Oregon State University, Corvallis, OR, USA.*

[2] *Civil & Environmental Engineering, Massachusetts Institute of Technology. Cambridge, MA, USA*

[3] *Now at Civil & Environmental Engineering, American University of Beirut, Beirut, Lebanon*

[4] *Cooperative Institute for Marine Resources Studies, Oregon State University, Newport, OR, USA.*

[5] *Now at Oregon Climate Change Research Institute, College of Oceanic and Atmospheric Sciences, Oregon State University, Corvallis, OR, USA*

*Corresponding author (stewarry@onid.orst.edu)

Vadose Zone Journal

Volume 11, Issue 2

doi:10.2136/vzj2011.0048

Abstract

Shrinkage cracks in soil function as a dominant control on the partitioning and distribution of moisture fluxes in the vadose zone. Their dynamics influence moisture balance and control water availability for runoff, deep infiltration, and near-surface storage. We present a new low-cost field instrument to monitor the temporal change in crack volume as affected by shrinkage and swelling cycles. The proposed *crackometer* is composed of a sealed impermeable bag connected by a hose to a standpipe. An automated level logger records changes in water level in the standpipe, which correspond to volumetric changes of the crack. Results from two laboratory experiments show that the volume change observed by the *crackometer* instruments scales linearly with the actual volume change, with an average error of 3%. The instrument was then used in a field experiment in Chile, where it measured the closing of cracks due to soil swelling.

Introduction

Expansive clay soils are characterized by spatially and temporally dynamic crack networks, which function as dominant controls on the partitioning of surface and subsurface water fluxes within expansive soils. The presence of a crack network can increase infiltration rates and allow for faster and deeper percolation of water and solutes [*Messing and Jarvis,* 1990; *Bronswijk et al.*, 1995; *Greve et al.*, 2010], while also enhancing soil moisture evaporation rates [*Weisbrod et al.*, 2009]. As a result, crack networks affect surface, soil, and ground water quantity and quality.

Capturing the dynamic nature of crack networks has been a theoretical and experimental challenge that has impacted our understanding of water movement in soils at the pedon, field, hillslope, and watershed scales. Numerous studies have attempted to characterize landscape-scale cracking behavior [*Bronswijk*, 1988; *Arnold et al.*, 2005], but up to the present, field methods have been mostly limited to estimating the instantaneous volume or the shape of a crack. In addition, many of the methods have the drawbacks of being destructive, being based only on surface characteristics, or being so labor-intensive that taking multiple measurements over a period of time can be impractical, particularly during the faster wetting phase. Examples of destructive methods include sand filling [*Dasog and Shashidhara*, 1993]; serial sectioning of soil [*Lightart et al.*, 1993]; pouring liquid latex [*Abou Najm et al.*, 2010]; and coupling spray techniques of different dye tracers [*Lu and*

Wu, 2003; *Kasteel et al.*, 2005] with various image analysis methods [*Aeby et al.*, 1997; *Forrer et al.*, 2000; *Bogner et al.*, 2008] for visualization of preferential flow paths. Surface-based methods to monitor crack evolution include surface image analysis [*Flowers and Lal*, 1999; *Abou Najm*, 2009]; observing soil's natural foaming [*Mitchell and van Genuchten*, 1993]; and soil surface elevation monitoring [*Wells et al.*, 2003; *Arnold et al.*, 2005], which can be used to estimate the evolution of the crack network by assuming isotropy of shrinkage. Examples of labor intensive methods include a variety of crack tracing techniques utilizing thin flexible metal probes for depth detection and simple geometric assumption for volume estimation [*Zein El Abedine and Robinson*, 1971; *Ringrose-Voase and Sanidad*, 1996; *Deeks et al.*, 1999; *Bhushan and Sharma*, 2002; *Bandyopadhyay et al.*, 2003; *Kishné et al.*, 2009] and calipers for measuring crack geometry [*Návar et al.*, 2002].

In this technical note, we propose the *crackometer* as a novel instrument for measuring transient crack-volume in the field. This instrument is simple to construct, low-cost, non-destructive, requires minimal effort to install or maintain, and allows for temporal and spatial measurements of volume changes for individual cracks. By having all these characteristics, this instrument overcomes many of the drawbacks of the aforementioned techniques. The instrument uses a sealed plastic bag connected by a hose to a polyvinyl chloride (PVC) standpipe which contains a water level logger. Laboratory and field experiments validated the design.

Method

An empty water-impermeable bag is placed into an existing crack and water is added via a standpipe until the bag has expanded to the boundaries of the crack and the water level within the standpipe has equilibrated above the hose connection (Figure A.1). An automated pressure logger is placed at the bottom of the standpipe to continuously measure the pressure head inside the standpipe (p_{water}). In applications where sealed (non-differential) pressure transducers are used, an additional pressure transducer or nearby weather station is needed to correct for barometric pressure ($p_{barometric}$) fluctuations. Water column height (h_{water}) is found by $h_{water} = (p_{water} - p_{barometric})/(g\rho_{water})$.

To reduce trapped air bubbles in the system, the bag should be free of air during insertion into the soil and the water should be introduced to the pipe slowly. Orienting the bag so that the hose is at the uppermost position can help eliminate air bubbles. At the surface, the bag can also be manually adjusted after filling to force bubbles from the system, assuming care is taken to minimize impact on crack structure.

As the crack shrinks or swells, its volume changes; this causes the water-filled bag to shrink or expand equally, which in turn causes an equivalent displacement of water volume in the standpipe. This change in water level in the standpipe (Δh) is measured

and converted to volumetric change (ΔV), using $\Delta V = \pi r^2 \Delta h$, where r is the internal radius of the standpipe.

This setup was tested in a controlled laboratory experiment at Oregon State University (43°33'59"N, 123°16'50"W) in Corvallis, Oregon, and at field site in the Chilean commune of Ninhue (36°25'04"S, 72°31'05"W). Onset Corporation HOBO U20-001 (0-9 m ± 0.005 m) pressure transducers were used to monitor water level within the standpipes. An additional U20 logger was used to record barometric pressure at the field site (for barometric pressure correction), while the laboratory experiment used barometric data from the National Climatic Data Center weather station at the Corvallis airport (KCVO).

Laboratory Experiment

For the controlled laboratory experiment, a 0.55 x 0.42 x 0.25 m (55 liter) plastic storage bin was filled with Witham clay, a soil of basaltic origin, composed of approximately 55% clay, 40% silt and 5% sand [*Fortner et al.*, 2011]. The soil was sieved while at field-saturated water content (using a 4 mm screen) and compacted using 100 strikes per layer with a 4.5 cm diameter, 1,880 g mini-sledge hammer. The hammer was hand-held and struck against the soil with moderate force. Final soil column height was approximately 0.16 m. The soil was allowed to air dry for six weeks until a large shrinkage crack formed near the center, at which point the water-

impermeable bag – a 1000 mL Injection IV bag (B. Braun Medical Inc.) – was installed. The IV bag was connected to a 0.0254 m (inner diameter) PVC standpipe via 0.0064 m (inner diameter) plastic tubing.

The effective length (L) of the IV injection bag was approximately 0.26 m, while the bag was inserted into the crack to an approximate depth (D) of 0.082 m. Thus, assuming that the crack is V-shaped, the change in average crack width (ΔW) can be approximated using Equation 1:

$$\Delta W = 2\Delta V / LD \qquad (1)$$

where ΔV is the volume displacement measured by the instrument, L is the effective (water-filled) length of the bag, and D is the inserted depth of the bag.

After the instrument was installed, the soil was rewetted by blowing air with atomized water droplets (provided by a Vick's-brand vaporizing humidifier) with an application rate of approximately 1 L day^{-1} (equivalent to 0.0043 m day^{-1} of water) and by a direct application of 0.0025 m day^{-1} of water to the soil surface.

Another laboratory experiment was used to assess the measurement error of the proposed *crackometer*. An artificial triangular shaped crack (Figure A.2a) was made from two 0.6 x 0.2 m pieces of 5/8" (0.016 m) plywood, joined at one edge by two door hinges. The artificial crack was put into a bench vise, and the *crackometer* was installed covering a space confined between W_{top} and W_{bottom} (Figure A.2a), using the

same instrument configuration as in the previous experiment. The objective of this second experiment was to estimate the measurement error from this *crackometer* configuration.

The vice was closed in quarter-turn increments until a minimum volume was obtained, and then was reopened in quarter-turn increments until the crack was at its initial opening width. At each step, the actual dimensions (W_{top} and W_{bottom}) for crack width were measured across the bottom and top of the IV bag (as shown in Figure A.2a). Actual crack volume corresponding to the space sampled by the *crackometer* instrument was calculated by $V_{actual} = ½(W_{top} + W_{bottom}) \times D \times L$, where D is the effective depth and L is the effective length of the IV bag. For this configuration D = 0.11 m and L = 0.26 m. Measured crack volume was calculated from water level in the standpipe using the same procedure as in the previous experiment.

For this experiment, the percent volume change, $V(\%)$, was calculated as percentage of the range between the maximum (V_{max}) and minimum (V_{min}) measured crack volumes (simulating maximum shrinkage and swelling, respectively) :

$$V(\%) = 100 \times \frac{V_{\max} - V_i}{V_{\max} - V_{\min}} \qquad (2)$$

where V_i is the measured crack volume at each measured increment.

Field Experiment

Three *crackometer* instruments were placed in an active research site in the Chilean Eighth Region. The instruments were installed on January 16th and 17th, 2011, within a single 3.5 by 11 m irrigation plot. The irrigation plot was orientated so that the long dimension was approximately in the direction of highest gradient (i.e., downslope). Installation #1 was located approximately 3 meters from the upslope edge of the plot. Installations #2 and #3 were located at approximately the center of the plot, as shown in Figure 1. The IV injection bags were inserted vertically into the cracks, reaching an average maximum depth of 0.22 m from the surface. The PVC standpipes had inner diameters of 0.0285 m. Figure A.1 shows the irrigation plot, from the upslope, left corner, facing downhill. The soil was classified as clay, made up of approximately 30% sand, 20% silt, and 50% clay.

The plot was irrigated with four 90-minute applications over a two-day period (January 17th and 18th, 2011), with a total cumulative application of approximately 0.17 m of water. Soil moisture content was monitored with Decagon 5TM soil moisture probes at 0.15, 0.30, 0.60 and 0.85 m depths. Runoff from the irrigation experiments was captured into collection barrels to allow for calculation of runoff rates and volumes.

Results and Discussions

Laboratory Experiments

Results from the initial controlled laboratory experiment showed that during one month of active wetting of the soil within the plastic container, Δh_{water} in the standpipe changed by 0.28 m, which corresponds to a volumetric change (ΔV) of 1.4 x 10^{-4} m^3 (Figure A.3). The trend was monotonic, with some noise which was inherent to the barometric correction of the pressure readings. Approximately 70% of the total volume change occurred in the first week. Overhead photographs confirm that by the end of the experiment the crack had changed in width from approximately 0.025 m to 0.012 m, due to soil swelling (Figure 3). Figure 3 presents good agreement between actual (accurately measured from digital image analysis) and measured (using *crackometer*) crack widths, with average error of 3%.

Similarly, the simulated crack experiment showed that the relative volume change, as measured by the *crackometer* instrument, scaled linearly with the actual crack volume (Figure A.2b), with no observed directional hysteresis. This configuration of the *crackometer* showed promising results, with an average error of 3% and a maximum error of 6% between actual and measured volume change. However, it should be noted that this error is only specific to this particular configuration and pressure sensor; different bag geometries, standpipe configurations and measurement devices would have different (and potentially smaller) magnitudes of intrinsic error.

Field Experiment

Figure A.4 shows changes in crack volume for Installations #1 and #2 (the results of Installation #3 are not included due to instrument malfunction). In general, the field data showed significant changes in crack volume as a result of simulated rainfall. Most of the swelling occurred during the four irrigation events, though some swelling continued in the hours between the irrigations (Figure A.4b). The near surface (0.10 – 0.30 m) water content increased quickly following the first irrigation, from nearly dry conditions (26% average volumetric water content) to near saturation (about 50% average volumetric water content) (Figure A.4c). The break between the first two irrigations allowed some water to percolate, thus decreasing the water content of the upper soil to about 45%. This redistribution process did not reverse the swelling, as can be seen by comparing Figures A.4b and A.4c.

Similarly, the overnight break between the second and third irrigations allowed for some redistribution of water, during which time the water content of the upper soil again decreased from about 50% to 45%, yet the swelling process did not reverse. On the contrary, the swelling continued perceptibly, after irrigation stopped, for about 3 hours at Installation #2 and for about 12 hours at Installation #1.

Finally, the soil saturated quickly after the third irrigation and stayed at a steady 50% water content, with no further redistribution observed. The soil showed notable

swelling during the third and fourth irrigation events; little change in crack volume was observed during the last hours of observation following the fourth irrigation.

The field results indicate that crack closure can become temporally decoupled from bulk soil moisture. Assuming that the observed changes in crack volumes are primarily due to changes in crack width, the temporal trends seen in Installations #1 and #2 are consistent with the results of *Návar et al*. [2002], who measured crack dimensions during and after simulated rainfall events, and observed that the majority of the cracks demonstrated significant closure during the first hour of irrigation (up to 50% decrease in width), but that complete closure did not happen for three more months (until 0.450 m of cumulative rainfall had been applied).

Installation and Modeling Considerations

Initial results under controlled laboratory (Figures A.2 and A.3) and uncontrolled field (Figure A.4) conditions demonstrated the capability of the proposed *crackometer* instrument to monitor the relative changes in crack volumes through time. These measurements of temporal crack dynamics, coupled with field observations, can provide valuable inputs to existing shrinkage and crack-pattern models. Such models provide predictions of total volume change and degree of shrinkage isotropy [*Bronswijk*, 1988, using the shrinkage curve and an estimated geometry factor, r_s), crack depth and spacing of primary cracks [*Konrad and Ayad*, 1997], and surface crack patterns [*Vogel et al.*, 2005]. Likewise, these results may be

used to calibrate and validate hydrological models that accommodate macropore dynamics [*Jarvis et al.*, 1991; *Greco*, 2002], by comparing measured relative crack volumes to those calculated based on soil matrix water content and potential.

Care should be taken when extending (scaling-up) the results from the local experiment to the entire field. For example, the *crackometer* instrument only samples a portion of the crack volume due to the fixed geometry of the impermeable bag (as seen in Figure A.2a). This can be of particular concern when shrinkage is not isotropic, such as in very dry soils where crack width has reached a maximum but crack depth continues to increase [*Zein el Abedine and Robinson*, 1971]. Furthermore, the limited flexibility of the impermeable bags means that the instrument may be unable capture fine-scale volumetric changes when cracks possess rough, angled and/or blocky surfaces. At the same time, a sampling bias can occur because these instruments can only be installed in larger shrinkage cracks (those of at least 1 cm width). While large cracks have been shown to preferentially transport water and solutes [*Messing and Jarvis*, 1990; *Greve et al.*, 2010], *Bronswijk et al.* [1995] found that small, intra-aggregate cracks also contributed significantly to solute transport.

One way to improve the accuracy of the method is through proper selection of representative crack spacing and crack shape models, given field-specific conditions. For example, with respect to crack-shape models, we have assumed V-shaped (triangular) crack cross-sectional geometries. While this is a commonly assumed cross-sectional geometry [*Zein el Abedine and Robinson*, 1971; *Elias et al.*, 2001],

other studies have proposed that cracks are rectangular, with parallel walls [*Scott et al.*, 1986; *Dasog and Shashidhara*, 1993]. In addition, *Ringrose-Voase and Sanidad* [1996] concluded that rectangular geometries are most likely to be found in wide, mature cracks (no longer shrinking horizontally), whereas the triangular shape is likely more valid for horizontally-evolving cracks. Therefore, assuming a cross-sectional shape based on the knowledge of crack's surface conditions may help limit error in total crack volume estimates.

Finally, there was some concern that the pressure head of the water within a vertical standpipe will provide resistance to the swelling soil. In our current configuration, the water column can reach a maximum height of approximately 1.5 m (which corresponds to 15 kPa). Laboratory experiments on swelling pressures of expansive clay soils show swelling pressures which range from 200 – 1200 kPa [*Basma et al.*, 1995). Therefore, even on the low end of swelling pressures the resistance due to the water column should be minor. At the same time, future modifications to the design, such as non-vertical standpipes (to lessen the pressure head acting against the soil), specially-manufactured bags (which can be made more flexible and in different geometries), and alternative methods of measuring the water displacement (such as weighing the mass displaced or using optical measurements) can help to both limit pressure impacts on the soil structure and to improve the overall accuracy of the instrument.

Altogether, attention to installation details, coupled with proper understanding of field cracking patterns, can help improve the accuracy of the method and eliminate potential sources of error. Nonetheless, as shown by the initial results (Figures A.2, A.3 and A.4), even in its current configuration the instrument is able to accurately capture the initial and intermediate stages of crack closure.

Conclusion

We present a practical "*crackometer*", which can be used to quantify the temporal changes in the volume of individual cracks, as demonstrated by laboratory and field experiments. All successful installations showed that swelling occurs shortly after the soil is wetted. Furthermore, we observed continued swelling at the field site for hours after water application had ceased, even when the local bulk soil moisture content slightly declined. This highlights that (1) there is a temporal component to soil swelling, and that (2) bulk soil volume is not a one-to-one function with bulk water content.

Finally, although the current experimental design allowed for the installation of only one *crackometer* instrument per crack, it is conceivable that multiple instruments or bag compartments, connected to individual standpipes, could be used at multiple depths or spatial locations within a single crack. Such use of different configurations and orientations may lead to insight on the manner in which shrinkage cracks open

and close, which can have important implications for modeling hydrologic response and vadose zone transport.

Acknowledgements

This material is based upon work supported by the National Science Foundation (NSF) under Grant No. 0943682. The authors would like to acknowledge Dr. Hamil Uribe and the Chilean Instituto Nacional de Investigaciones Agropecuarias (INIA) for providing collaboration and field site support. Furthermore, the authors would like to acknowledge the participants of the NSF-funded Undergraduate Chilean Field Hydrology Course for assisting with field installation and data collection: Zak Grimes, Hayden Ausland, Mackenzie Osypian, Alex Fisher, Jennifer Vettel, Julianne Quinn, Jenna Duffin, William Rhoads, Hazel Owens, Leah Kammel, Rachel Gross, Daniela Castañeda, Liam Kyle Cahill, Maria Brown, Nick Dummer, Chuan Li, Wiebke Boettche, Felipe Bretón, Sebastián Bonelli, Hector Flores, Ghislaine Rossel, Claudia Maureira, and Marianela Matta. Finally, the authors would like to extend their gratitude to José Luis Arumí and Diego Rivera of the Department of Recursos Hídricos at the Universidad de Concepción, Chillán, for providing logistical support.

References

Abou Najm, M. R. (2009), Soil-water interaction: Lessons across scales. Ph.D. dissertation. Purdue Univ., West Lafayette, Indiana.

Abou Najm, M. R., J. D. Jabro, W. M. Iversen, R. H. Mohtar, and R. G. Evans (2010), New method for the characterization of three-dimensional preferential flow paths in the field, *Water Resources Research, 46*(2).

Abu-Hejleh, A. N., and D. Znidarcic (1995), Desiccation theory for soft cohesive soils, *Journal of Geotechnical Engineering, 121*(6), 493-502.

Aeby, P., J. Forrer, H. Flühler, and C. Steinmeier (1997), Image analysis for determination of dye tracer concentrations in sand columns, *Soil Science Society of America Journal, 61*(1), 33-35.

Arnold, J. G., K. N. Potter, K. W. King, and P. M. Allen (2005), Estimation of soil cracking and the effect on surface runoff in a Texas Blackland Prairie watershed, *Hydrological Processes, 19*(3), 589-603.

Bandyopadhyay, K. K., M. Mohanty, D. K. Painuli, A. K. Misra, K. M. Hati, K. G. Mandal, P. K. Ghosh, R. S. Chaudhary, and C. L. Acharya (2003), Influence of tillage practices and nutrient management on crack parameters in a Vertisol of central India, *Soil and Tillage Research, 71*(2), 133-142.

Basma, A. A., A. S. Al-Homoud, and A. Husein (1995), Laboratory assessment of swelling pressure of expansive soils, *Applied Clay Science, 9*(5), 355-368.

Bhushan, L., and P. K. Sharma (2002), Long-term effects of lantana (Lantana spp. L.) residue additions on soil physical properties under rice–wheat cropping: I. Soil consistency, surface cracking and clod formation, *Soil and Tillage Research, 65*(2), 157-167.

Bogner, C., B. Wolf, M. Schlather, and B. Huwe (2008), Analysing flow patterns from dye tracer experiments in a forest soil using extreme value statistics, *European Journal of Soil Science, 59*(1), 103-113.

Bronswijk, J. (1988), Modeling of Water-Balance, Cracking and Subsidence of Clay Soils, *Journal of Hydrology, 97*(3-4), 199-212.

Bronswijk, J., W. Hamminga, and K. Oostindie (1995), Field-scale solute transport in a heavy clay soil, *Water Resources Research, 31*(3), 517-526.

Dasog, G., and G. Shashidhara (1993), Dimension and volume of cracks in a Vertisol under different crop covers, *Soil Science, 156*(6), 424.

Deeks, L., A. Williams, J. Dowd, and D. Scholefield (1999), Quantification of pore size distribution and the movement of solutes through isolated soil blocks, *Geoderma, 90*(1), 65-86.

Elias, E. A., A.A. Salih and F. Alaily (2001), Cracking patterns in the Vertisols of the Sudan Gezira at the end of the dry season, *International Agrophysics, 15*, 151-155.

Flowers, M., and R. Lal (1999), Axle load and tillage effects on the shrinkage characteristics of a Mollic Ochraqualf in northwest Ohio, *Soil and Tillage Research, 50*(3), 251-258.

Forrer, I., A. Papritz, R. Kasteel, H. Flühler, and D. Luca (2000), Quantifying dye tracers in soil profiles by image processing, *European Journal of Soil Science, 51*(2), 313-322.

Fortner, J., K. Harward, D. Lytle, and D. Williamson (2006), Web Soil Survey.

Greco, R. (2002), Preferential flow in macroporous swelling soil with internal catchment: model development and applications, *Journal of Hydrology, 269*(3), 150-168.

Greve, A. K., M. S. Andersen, and R. I. Acworth (2010), Investigations of soil cracking and preferential flow in a weighing lysimeter filled with cracking clay soil, *Journal of Hydrology, 393*(1-2), 105-113.

Jarvis, N., P. E. Jansson, P. Dik, and I. Messing (1991), Modelling water and solute transport in macroporous soil. I. Model description and sensitivity analysis, *Journal of Soil Science, 42*(1), 59-70.

Kasteel, R., M. Burkhardt, S. Giesa, and H. Vereecken (2005), Characterization of field tracer transport using high-resolution images, *Vadose Zone Journal*, *4*(1), 101-111.

Kishné, A. S., C. L. S. Morgan, and W. L. Miller (2009), Vertisol Crack Extent Associated with Gilgai and Soil Moisture in the Texas Gulf Coast Prairie, *Soil Science Society of America Journal*, *73*(4), 1221.

Konrad, J.-M., and R. Ayad (1997), An idealized framework for the analysis of cohesive soils undergoing desiccation, *Canadian Geotechnical Journal*, *34*(4), 477-488.

Ligthart, T., G. Peek, and E. Taber (1993), A method for the three-dimensional mapping of earthworm burrow systems, *Geoderma*, *57*(1), 129-141.

Lu, J., and L. Wu (2003), Visualizing bromide and iodide water tracer in soil profiles by spray methods, *Journal of Environmental Quality*, *32*(1), 363-367.

Messing, I., and N. J. Jarvis (1990), Seasonal variation in field-saturated hydraulic conductivity in two swelling clay soils in Sweden, *Journal of Soil Science*, *41*(2), 229-237.

Mitchell, A. R., and M. T. Van Genuchten (1993), Flood irrigation of a cracked soil, *Soil Science Society of America Journal*, *57*(2), 490-497.

Návar, J., J. Mendez, R. B. Bryan, and N. J. Kuhn (2002), The contribution of shrinkage cracks to bypass flow during simulated and natural rainfall experiments in northeastern Mexico, *Canadian Journal of Soil Science*, *82*(1), 65-74.

Ringrose-Voase, A., and W. Sanidad (1996), A method for measuring the development of surface cracks in soils: application to crack development after lowland rice, *Geoderma*, *71*(3), 245-261.

Scott, G., R. Webster, and S. Nortcliff (1986), An analysis of crack pattern in clay soil: its density and orientation, *Journal of Soil Science*, *37*(4), 653-668.

Vogel, H. J., H. Hoffmann, A. Leopold, and K. Roth (2005), Studies of crack dynamics in clay soil II. A physically based model for crack formation, *Geoderma, 125*(3-4), 213-223.

Weisbrod, N., M. I. Dragila, U. Nachshon, and M. Pillersdorf (2009), Falling through the cracks: The role of fractures in Earth-atmosphere gas exchange, *Geophysical Research Letters*, *36*(2).

Wells, R., D. DiCarlo, T. Steenhuis, J.-Y. Parlange, M. Römkens, and S. Prasad (2003), Infiltration and surface geometry features of a swelling soil following successive simulated rainstorms, *Soil Science Society of America Journal*, *67*(5), 1344-1351.

Zein el Abedine, A., and G. H. Robinson (1971), A study on cracking in some vertisols of the Sudan, *Geoderma, 5*(3), 229-241.

Figures

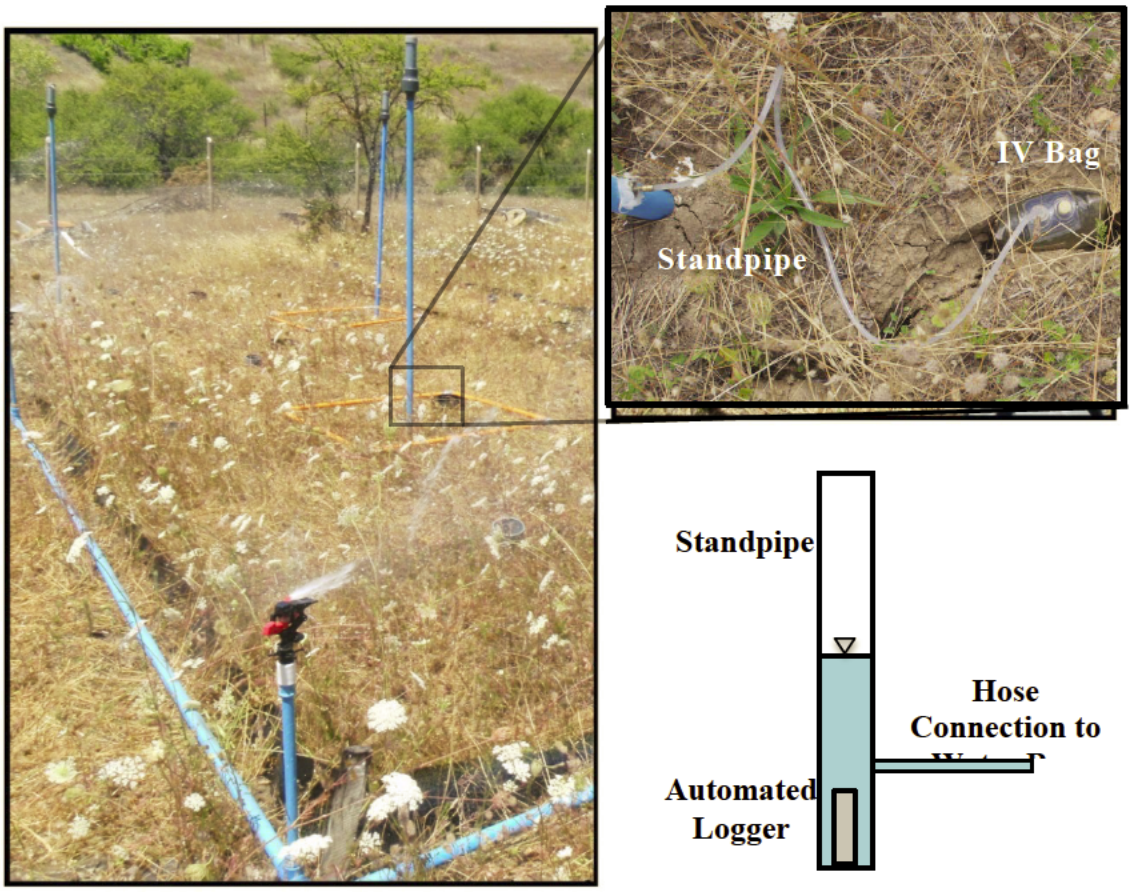

Figure A.1 – Schematic of the *crackometer* with field images showing the installations and the details of the setup. Installation #1 is located closest to the camera; Installation #2 is in the top left corner of the image; and Installation #3 is in the middle. Notes: The orange squares surrounding Installations #1 and #3 are frames for digital crack monitoring. The sprinkler in operation at foreground is part of the rainfall/runoff simulation irrigation system. The attachments on top of the standpipes provided housing for a secondary water level measurement sensor (which failed to function properly during this experiment).

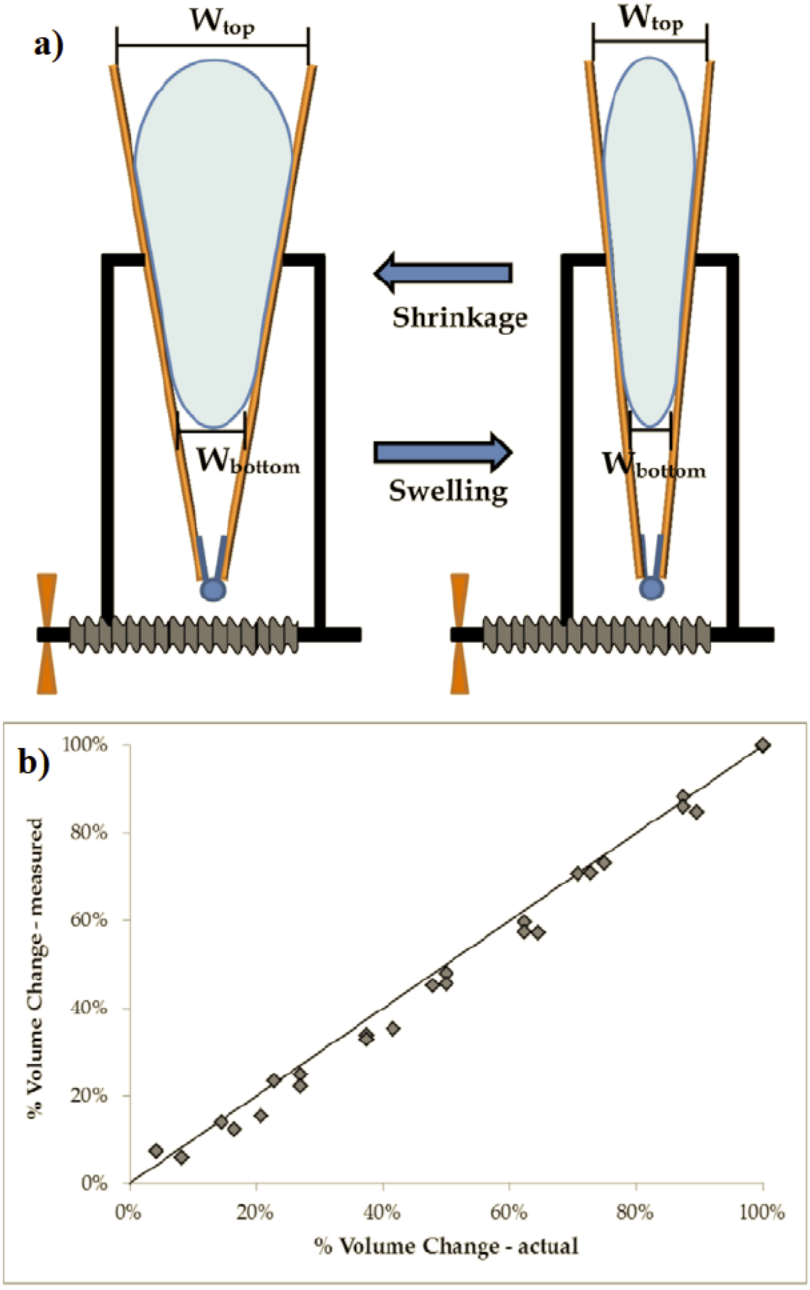

Figure A.2 – (a) Schematic of the laboratory experiment used to quantify *crackometer* instrument error for the current instrument configuration; (b) Percent change in volume based on a simulated triangular crack. Average error was 3% and maximum error was 6%.

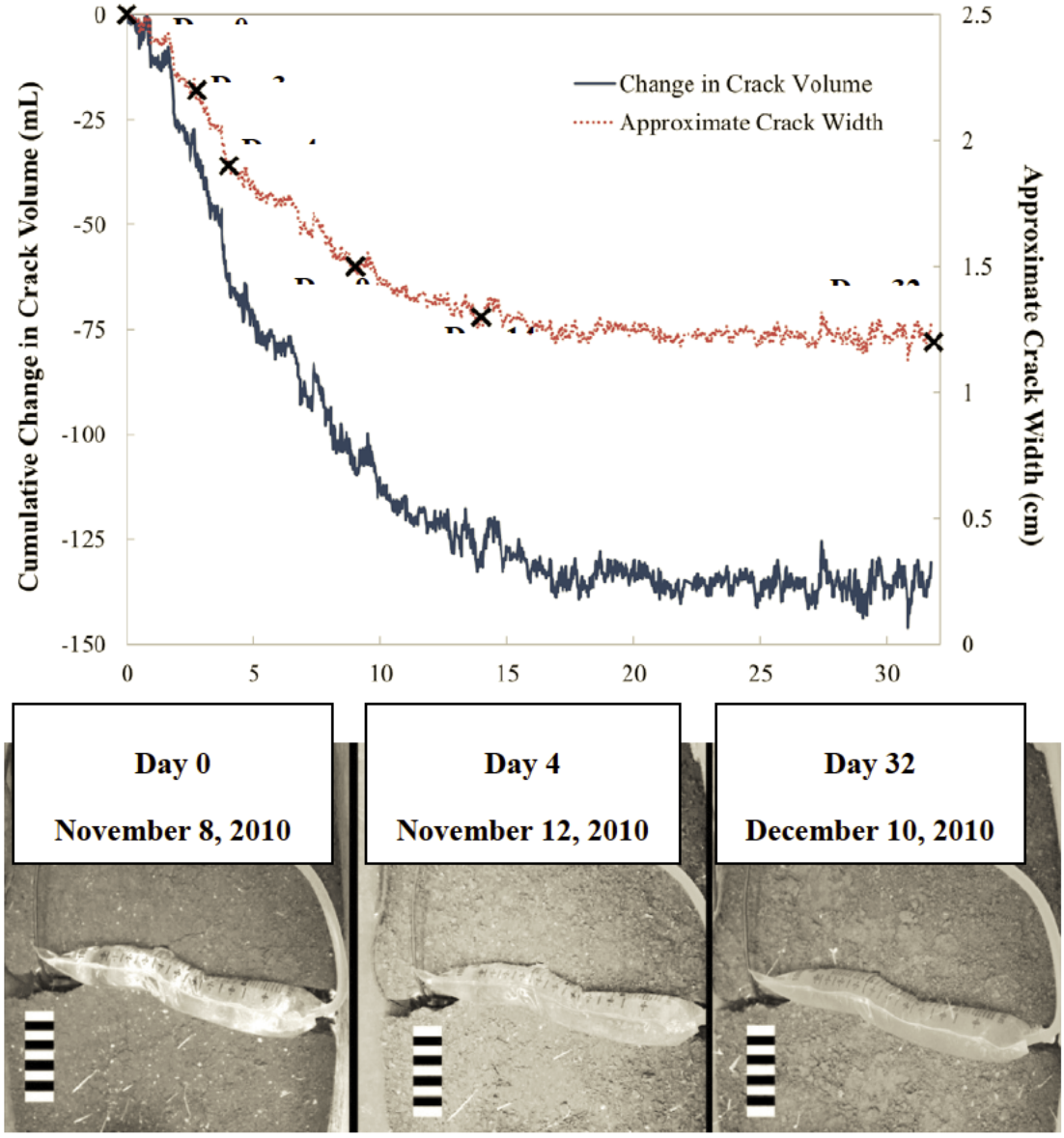

Figure A.3 – Total change in crack volume, and corresponding crack width, as measured by the laboratory *crackometer* instrument. Day 0 corresponds to November 8th, 2010. The points marked with X's correspond to the validation points from the digital images shown in the lower part of the Figure (Note that the images from Days 3, 9 and 32 are not shown). The reference scale shows 1 cm increments.

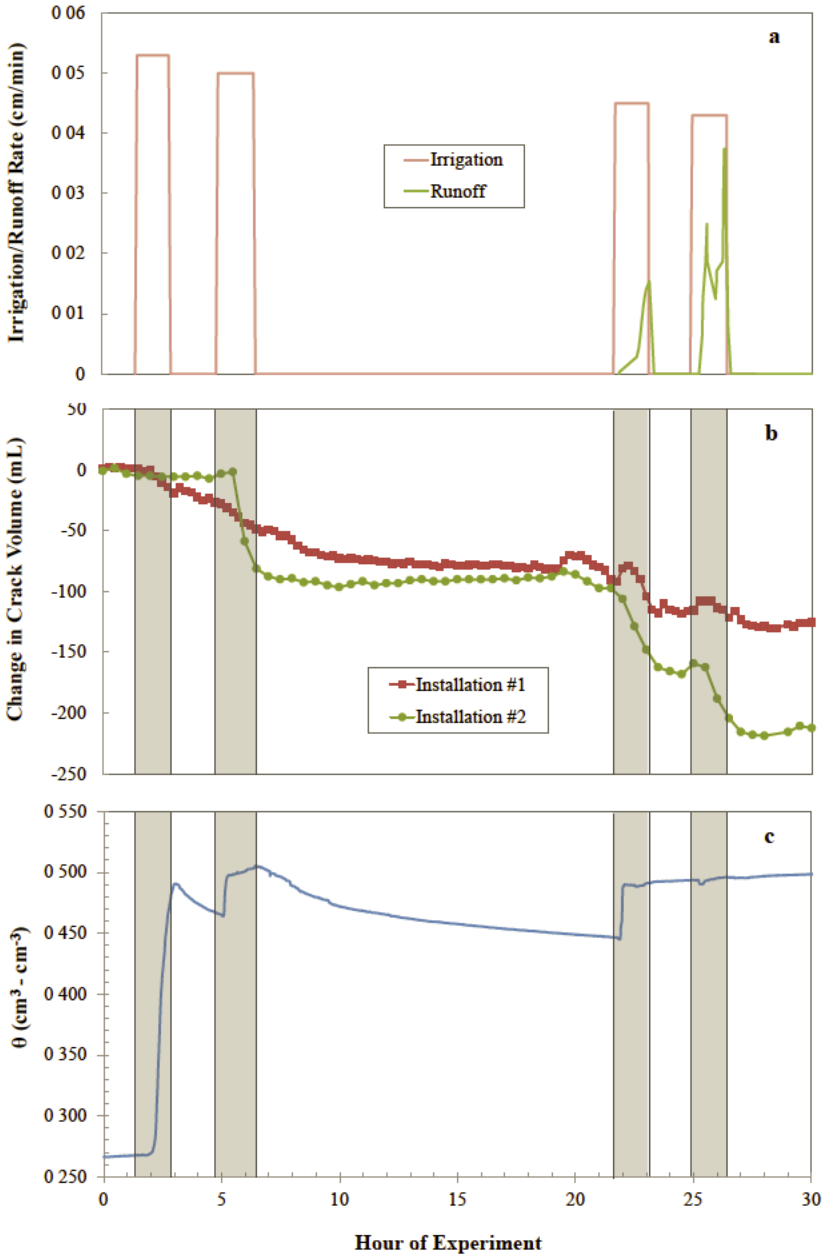

Figure A.4 – (a) The four irrigation-runoff experiments showing the volume and timing of irrigation and runoff; (b) Cumulative change in crack volumes as the result of 4 rainfall simulation events; and (c) average near surface (0.1 – 0.3 m) soil moisture. Time = 0 corresponds to 12:00:00 PM on January 17, 2011.

Appendix B – An Image-Based Method for Determining Bulk Density and the Soil Shrinkage Curve

Ryan D. Stewart[1]*, Majdi R. Abou Najm[1,2], David E. Rupp[3,4], John S. Selker[1]

[1] *Biological & Ecological Engineering Department, Oregon State University, Corvallis, OR, 97331 United States.*

[2] *Civil & Environmental Engineering, American University of Beirut. Beirut, Lebanon.*

[3] *Cooperative Institute for Marine Resources Studies, Oregon State University, Newport, OR, United States.*

[4] *Present address: Oregon Climate Change Research Institute, College of Earth, Ocean, and Atmospheric Sciences, Oregon State University, Corvallis, OR, United States.*

*Corresponding Author (stewarry@onid.orst.edu)

Soil Science Society of America Journal

Volume 76, Issue 4

doi:10.2136/sssaj2011.0276n

Abstract

Current laboratory methods for determining volume and bulk density of soil clods include dipping saran-coated clods in water (a destructive process due to the permanent coating), performing physical measurements on samples with well-defined geometries, or using expensive equipment and proprietary software (such as laser scanners). We propose an alternative method for determining the volume and bulk density of a soil clod, which is non-destructive, low-cost and utilizes free and open-source software. This method (the *clodometer* method) uses a standard digital camera to image a rotating clod, which allows for reconstruction of its three-dimensional surface and subsequent calculation of its volume. We validated the method through comparison to the standard displacement method, and then used the method to create a soil shrinkage curve for the Waldo silty clay loam soil. The method had acceptable precision (relative standard errors of the mean between 0.4 – 1.6%), which may be further improved through future software development.

Abbreviations: coefficient of linear extensibility (COLE); soil shrinkage curve (SSC)

Introduction

Expansive clay soils are characterized by hysteretic shrinking/swelling dynamics that continuously alter the pore structure and cause quantifiable changes in bulk density. These soils have been observed to seasonally affect and be affected by the hydrology of entire basins [*Harvey*, 1971; *Lindenmaier et al*., 2005], and are known to strongly influence transport of water [*Messing and Jarvis*, 1990; *Greve et al.*, 2010] and solutes [*Harris et al.*, 1994; *Bronswijk et al.*, 1995; *Weaver et al.*, 2005]. The most common methods to describe the shrinkage behavior of such soils are based on laboratory analysis of individual soil clods or cores. In general, the shrinkage behavior of these soil samples are described using either (1) the soil shrinkage curve (SSC), where the gravimetric water content of a sample is related to its specific volume or void ratio; or (2) the coefficient of linear extensibility (COLE), where a sample's volume is compared at a matric potential of -30 kPa and after oven drying [*Gray and Allbrook*, 2002]. For the SSC, a number of analytical models have been proposed to relate water content to specific volume [*Giraldez et al*., 1983; *McGarry and Malafant*, 1987; *Tariq and Durnford*, 1993a; *Braudeau et al*., 1999; *Braudeau et al.*, 2004; *Boivin et al*., 2006; *Sander and Gerke*, 2007], which typically account for distinct shrinkage phases. On the other hand, the COLE index is typically used as a single, lumped value per soil type [*Gray and Allbrook*, 2002] and cannot distinguish the different phases of shrinkage.

Both SSC and COLE require an accurate determination of the sample's volume at different moisture contents. Volume is most commonly determined by placing a resin- or paraffin-coated clod into water or kerosene and measuring the fluid displacement, utilizing Archimedes' principle [*Brasher et al*., 1966; *Bronswijk et al*., 1997]. However, coating the clod has a number of significant drawbacks. For paraffin-coated samples, the SSC is found by analyzing the specific volume of distinct samples prepared at different matric potentials [*Cornelis et al.*, 2006], rather than on a single specimen. For resin-coated samples, it has been observed that the coating can inhibit swelling of the sample [*Tunny*, 1970], particularly as the sample nears saturation [*Schafer and Singer*, 1976], or can pull away during shrinkage [*Tunny*, 1970]. Furthermore, the resin loses mass during oven drying [*Bronswijk et al*., 1997; *Sander and Gerke*, 2007] and thus without proper correction can cause over-prediction of water content. In addition, coating the samples is effectively a destructive process, as they can no longer be used for other physical or hydrological testing [*Sander and Gerke*, 2007].

Schafer and Singer [1976] coated clods at oven-dry, air-dry, 1/3 bar (33 kPa) matric potential, and saturated conditions, and found that the clods coated at saturation became compacted (mostly due to handling) and subsequently had lower measured volumes. Therefore, because the standard method for calculating soil shrinkage curves [*Bronswijk et al*., 1997, modified from *Brasher et al*., 1966] specifies that the

clods should be saturated at the time of coating, it is likely that the coated clod will have higher bulk density and lower volume than a similar non-coated specimen.

It has been observed that the resin can penetrate into the pores, which causes the clod to retain less water in subsequent water content measurements, particularly for small clods [*Schafer and Singer*, 1976]. On the other hand, it has also been observed that the resin may not adequately coat deep pores, which can allow water to penetrate into the clod during submersion [*Sander and Gerke*, 2007] and cause underestimation of clod volume; this is particularly of concern for oven-dried specimens [*Bronswijk et al.*, 1997]. During displacement measurements, *Sander and Gerke* [2007] observed air bubbles within the saran coating, macropores which may have been incompletely sealed, and a color change in the clods indicative of water penetrating the coating, all of which led to erratic or artificially low volume measurements. In summary, the evidence shows that the saran coating impacts soil shrinkage measurements, and the displacement method generally under-predicts the volume of soil clods.

Another displacement method for determining soil volume is the rubber balloon method of *Tariq and Durnford* [1993b], where a soil is packed into a rubber balloon which is suspended in water; volume changes are measured using Archimedes' principle. This method generally requires the clod to be disturbed, either through smoothing down of edges [*Tariq and Durnford*, 1993a] or else through sieving [*Cornelis et al.*, 2006].

Other common methods utilize direct physical measurement of the specimen dimensions. Typically, this is done using calipers, rulers, or strain gauges on a core with a well-known geometry [*Berndt and Coughlan*, 1972; *Toker et al.*, 2004; *Cornelis et al.*, 2006; *Perón et al.*, 2007]. Axisymmetric shrinkage is typically assumed. Due to the irregular geometries of soil clods, direct physical measurements have not often been used to measure shrinkage for undisturbed soil clods.

More recent methods to quantify soil clod volume and shrinkage behavior include lasers [*Rossi et al*., 2008] and 3D optical scanning [*Sander and Gerke*, 2007] which scan the surface of the clod and compute its volume. While initial results with these methods are promising, the equipment needed is relatively expensive and utilizes proprietary software for analysis, with little control over the process. Thus, we see the need for a low-cost alternative which makes use of freely available software. In this paper, we present an alternative, non-destructive, low-cost method for determining the volume of a soil clod. The method utilizes completely free and open-source software. Compared to the traditional saran-coated clod displacement technique, this method does not use harsh chemicals.

Materials and Methods

Volume Analysis Method (The Clodometer)

To determine clod volumes, the samples were placed on a rotating imaging stand (Figure B.1), which includes a calibration object with known volume. The calibration object used for this test was a standard golf ball, painted in a multi-colored, random pattern (to maximize surface features). Its actual volume ($V_{calibration,\ actual} = 40.4\ cm^3$) was determined by measuring its displacement when suspended in water. The clod and calibration sphere were then photographed using a 6-megapixel PENTAX® K100d dSLR camera with a 35mm f/2.8 lens. The clod and calibration sphere were positioned 0.38 meters from the camera focal plane. Images were taken at approximately every 4° of the stand's rotation (this value represents a combination of efficiency and adequate coverage, but can be adjusted as needed). In this manner, the clod and calibration volume were imaged from all 360°, using a total of approximately 90 images. With the tested setup, we could collect an image approximately every 2-4 seconds, which meant the collection process required around 3-5 minutes per sample.

The photos were joined together using Microsoft®'s free web-based program, *Photosynth*®. *Photosynth*® uses common points between photos to create three-dimensional point clouds of x,y,z- and r,g,b-referenced vertices. Next, the freeware program *SynthExport*© was used to convert the *Photosynth*® files into .ply (polygon)

format, which were then manipulated using the freeware program *Meshlab*©. Within *Meshlab*©, color selection filters and manual removal of extraneous vertices were used to isolate the point clouds which correspond to the clod and the calibration object. Poisson surface meshes were then applied to both the clod and the calibration object point clouds. Finally, a script (based on *Getreue* [2004], *Giaccari* [2008a], and *Giaccari* [2008b]) was used in *Octave*© to calculate the relative volumes of the point clouds for the calibration object ($V_{calibration,\ relative}$) and clod ($V_{clod,\ relative}$). This was performed by summing the tetrahedra formed by the surface mesh (as referenced to a common datum). For each image set, individual calculations were performed to find the relative volume of the clod and the calibration volume. The actual clod volume (V_i) was then determined by Equation 1:

$$V_i = V_{clod,relative} * (V_{calibration,actual} / V_{calibration,relative}) \quad (1)$$

where V_i has the same units as the calibration object ($V_{calibration,actual}$).

Method Validation

The validation of the method was divided into two phases. First, the volumes of six saran-coated clods measured using the proposed imaging analysis method were compared to the volumes obtained using the standard displacement method [*Bronswijk et al*., 1997]. These clods came from two silty clay loam series [Waldo (18-55% clay) and Witham (27-60% clay)] and ranged in volume from 15 cm^3 to 40

cm^3. Percent difference between the two methods was calculated by dividing the volume difference of both methods by the displacement-measured volume.

Before imaging, each soil clod was double-coated in a 1:4 Dow® Saran Resin F-310/MEK (Methyl Ethyl Ketone) solution. After the coating dried, the clod was imaged using the *clodometer* method. After completion of the imaging procedure, the clod was weighed and its volume was determined through a water displacement test. Due to concerns about water filling pores and/or penetrating the coating, the displacement method was repeated on the clods until the measured volume was unchanged between successive tests. The clod was reweighed after each displacement test.

Second, the precision of the method was tested by calculating the volume of a clod using three independent sets of images. This was done for five different clods (tests) where results were summarized with the mean volume, as calculated from the three independent measurements, and the standard error of the mean for those three measurements.

Soil Shrinkage Curve

After validation, the *clodometer* method was used to obtain a soil shrinkage curve for the Waldo silty clay loam soil. Four uncoated clods (volume at field capacity ranging from 25 to 53 cm^3) were allowed to air dry from field capacity water content at room

temperature with limited temperature and humidity fluctuations. The clods were weighed and imaged at ten intermediate water contents, before being oven-dried at 105°C and then weighed and imaged again. The image sets were analyzed to determine clod volumes, using the methodology described above.

To convert the data into a full SSC, we chose to employ the four-phase SSC model of *Tariq and Durnford* [1993a]. Thus, the measured volumes were converted to void ratios (e) using Equation 2:

$$e = \frac{V_i - V_s}{V_s} = \frac{V_i - (m_{oven\ dry} / \rho_s)}{m_{oven\ dry} / \rho_s} \tag{2}$$

where V_i is the clod volume, V_s is the volume of the solid particles, $m_{oven\ dry}$ is the weight of the oven dry sample, and ρ_s is the density of the solid particles. Moreover, the corresponding water contents were converted into volumetric moisture ratios (ϑ) using Equation 3:

$$\vartheta = \frac{m_w / \rho_w}{m_s / \rho_s} = \frac{(m_i - m_{oven\ dry}) / \rho_w}{m_{oven\ dry} / \rho_s} \tag{3}$$

where m_i is the weight of the sample at each intermediate water content, $m_{oven\ dry}$ is the weight of the oven dry sample, and ρ_w is the density of water. For the purpose of this analysis, ρ_s was assumed to equal 2.67 g/cm^3.

Results and Discussion

During displacement measurements, air bubbles emerged from several clods, indicating large air-filled voids hidden within the clod and/or incomplete coatings. This in turn led to an initial underestimation of displacement volume. This was also detected by variation in weight of coated clods before and after dipping. Therefore, we decided to repeat the displacement measurements until the measured weight of displacement was unchanged between measurements. This required between 3 and 7 measurements for each clod (Table B.1).

Similarly, *Sander and Gerke* [2007] observed larger volumes from their 3D imaging method as compared to the displacement method. They attributed those differences to saran coating imperfections and to general limitations with the displacement method. By assuming a greater loss of coating mass during drying and that 0.3 to 0.8 g of water penetrated into the clods during submersion, *Sander and Gerke* [2007] were able to achieve a high level of agreement between the displacement method and their 3D scanning method.

While the initial displacement measurements with saran-coated clods were 3-17% smaller than the imaging-measured volumes, the second displacement measurements were within 5% of the imaging method (Table B.1). The final displacement measurements (taken when the displacement did not change between subsequent tests) were generally larger than the imaging-measured volumes (3 – 10% larger, with

the exception of sample 6, which was still 5% smaller). We conclude that the second measurement is likely to be the most accurate estimation of actual clod volume, as during this measurement any voids in the clod were water-filled and thus did not cause an underestimation of sample volume, while at the same time the clods did not yet have time to swell due to any water penetration. Assuming that the second test is the most accurate estimate of actual clod volume, our imaging results show good consistency with the traditional method of volume determination.

Results based on triplicate independent volume measurements of five different clods (using the imaging method) are shown in Table B.2. The standard errors of the mean were between 0.4 and 1.6% of the mean volumes, which shows the method to have sufficient precision to measure individual clod volumes and determine soil shrinkage curves.

Soil Shrinkage Curve

The *clodometer* was used to monitor the shrinkage behavior of four Waldo silty clay loam clods (Figure B.2). Results of these tests were combined to construct a characteristic Soil Shrinkage Curve, using the four-phase model of *Tariq and Durnford* [1993a]. The *Tariq and Durnford* model assumes that soil shrinkage has four distinct phases: 1) structural shrinkage, where water is lost only from macropores and other large discontinuities, without greatly altering the soil bulk volume; 2)

normal shrinkage, where water is lost from the soil pores without being replaced by air (it is often assumed that there is a 1:1 relationship between the volume of water lost and the decrease in soil bulk volume [*Braudeau et al.,* 1999]); 3) residual shrinkage, where air enters the pores and the volume of water lost is greater than the decrease in bulk soil volume; and 4) zero shrinkage, where the soil has reached its minimum bulk volume and any additional water loss has no effect on the bulk volume.

The Waldo silty clay loam clods did not exhibit structural shrinkage, likely because the analysis began with the samples at field capacity water content, rather than being fully-saturated. Most of the data points occurred in the normal shrinkage phase, and closely followed the theoretical 1:1 line between decrease in water and soil bulk volume. At the dry end of the spectrum, the observed soil shrinkage curve began to level off, indicative of the residual and zero shrinkage regions. It should be noted that the transition between residual and zero shrinkage occurred while the clods were in the oven, so no data was collected at that point. Finally, though there was an observed offset in the void-moisture ratio values of the different clods, all samples demonstrated similar relative change in volume and moisture content.

Utility of Method

Our prototype implementation of the *clodometer* was relatively time- and labor-intensive; though collecting the photographs took only a few minutes, the generation of a single volume required anywhere from 15 to 60 minutes of imaging and processing time. This contrasts with the traditional displacement method, where each measurement can be performed in less than 5 minutes (though initial preparation and coating of the clod may take 24 hours or more). Furthermore, when measuring the bulk density of a soil clod (where typically only a single measurement is made per sample), the time difference between methods will be minimal, and the *clodometer* method has the additional advantage of leaving the clod undisturbed for use in further analyses. Therefore, even with this current level of required effort, the *clodometer* method is of great potential value to researchers due to its low-cost, accuracy, and preservation of the samples. At the same time, we envision future implementations that will automate much of the imaging and analysis processes, thus increasing the utility of the *clodometer* method and widening its function to include application in areas like soil anisotropy detection and strain calculation.

Conclusions

We combined a standard digital camera with freely available software to provide a low-cost and accurate way to measure bulk density of soil clods. Performing this analysis on soil clods at multiple water contents was then used to characterize their

shrinking and swelling behavior. The system (which we call the *clodometer*) gave results that were consistent with the traditional water-displacement method, after considering causes of error in the displacement method. Moreover, measurements of clod volumes done in triplicate showed that the method had acceptable precision, as relative standard errors of the mean were between 0.4 – 1.6%.

While currently more time-intensive than other volume determination methods, the *clodometer* method offers several advantages compared to other approaches. It does not require expensive, specialized equipment or hazardous chemicals (such as methyl ethyl ketone). Samples are not destroyed or modified during testing, and expansive soil clods can shrink and swell without impediment. Finally, future software modifications and improvements will likely increase accuracy and decrease processing time for the *clodometer* method, which will only its overall utility.

References

Berndt, R., and K. Coughlan (1977), The nature of changes in bulk density with water content in a cracking clay, *Soil Research, 15*(1), 27-37.

Boivin, P., P. Garnier, and M. Vauclin (2006), Modeling the Soil Shrinkage and Water Retention Curves with the Same Equations, *Soil Science Society of America Journal, 70*(4), 1082.

Brasher, B., D. Franzmeier, V. Valassis, and S. E. Davidson (1966), Use of saran resin to coat natural soil clods for bulk-density and water-retention measurements, *Soil Science, 101*(2), 108.

Braudeau, E., J.-P. Frangi, and R. H. Mohtar (2004), Characterizing Nonrigid Aggregated Soil–Water Medium Using its Shrinkage Curve, *Soil Science Society of America Journal, 68*(2), 359-370.

Braudeau, E., J. Costantini, G. Bellier, and H. Colleuille (1999), New device and method for soil shrinkage curve measurement and characterization, *Soil Science Society of America Journal, 63*(3), 525-535.

Bronswijk, J., W. Hamminga, and K. Oostindie (1995), Rapid nutrient leaching to groundwater and surface water in clay soil areas, *European Journal of Agronomy, 4*(4), 431-439.

Bronswijk, J., J. Evers-Vermeer, and J. van den Akker (1997), Determination of the shrinkage characteristics of clay soil aggregates, *Manual for soil physical measurements, Version 3*, 71-77.

Cornelis, W. M., J. Corluy, H. Medina, J. Díaz, R. Hartmann, M. Van Meirvenne, and M. E. Ruiz (2006), Measuring and modelling the soil shrinkage characteristic curve, *Geoderma, 137*(1-2), 179-191.

Getreue, P. (2004), MATLAB functions to read and write 3D data PLY files (plyread.m).

Giaccari, L. (2008a), Surface Reconstruction from Scattered Point Clouds (MyRobustCrust.m).

Giaccari, L. (2008b), Volume Enclosed by a Triangulated Surface (SurfaceVolume.m).

Giráldez, J. V., G. Sposito, and C. Delgado (1983), A general soil volume change equation: I. The two-parameter model, *Soil Science Society of America Journal, 47*(3), 419-422.

Gray, C. W., and R. Allbrook (2002), Relationships between shrinkage indices and soil properties in some New Zealand soils, *Geoderma, 108*(3), 287-299.

Greve, A. K., M. S. Andersen, and R. I. Acworth (2010), Investigations of soil cracking and preferential flow in a weighing lysimeter filled with cracking clay soil, *Journal of Hydrology, 393*(1-2), 105-113.

Harris, G., P. Nicholls, S. Bailey, K. Howse, and D. Mason (1994), Factors influencing the loss of pesticides in drainage from a cracking clay soil, *Journal of Hydrology, 159*(1), 235-253.

Harvey, A. (1971), Seasonal flood behaviour in a clay catchment, *Journal of Hydrology, 12*(2), 129-144.

Lindenmaier, F., E. Zehe, M. Helms, O. Evadakov, and J. Ihringer (2006), Effect of soil shrinkage on runoff generation in micro and mesoscale catchments, IAHS PUBLICATION, 303, 305.

McGarry, D., and K. W. J. Malafant (1987), The analysis of volume change in unconfined units of soil, *Soil Science Society of America Journal, 51*(2), 290-297.

Messing, I., and N. J. Jarvis (1990), Seasonal variation in field-saturated hydraulic conductivity in two swelling clay soils in Sweden, *Journal of Soil Science, 41*(2), 229-237.

Péron, H., T. Hueckel, and L. Laloui (2007), An improved volume measurement for determining soil water retention curves, *Geotechnical Testing Journal, 30*(1), 1.

Rossi, A. M., D. R. Hirmas, R. C. Graham, and P. D. Sternberg (2008), Bulk density determination by automated three-dimensional laser scanning, *Soil Science Society of America Journal, 72*(6), 1591-1593.

Sander, T., and H. H. Gerke (2007), Noncontact shrinkage curve determination for soil clods and aggregates by three-dimensional optical scanning, *Soil Science Society of America Journal, 71*(5), 1448.

Schafer, W., and M. Singer (1976), A reinvestigation of the effect of saran coatings on the extensibility of swelling soil clods, *Soil Science, 122*(6), 360-364.

Tariq, A.-u.-R., and D. S. Durnford (1993), Analytical volume change model for swelling clay soils, *Soil Science Society of America Journal, 57*(5), 1183-1187.

Tariq, A.-u.-R., and D. S. Durnford (1993), Soil volumetric shrinkage measurements: a simple method, *Soil Science*, 155.

Toker, N., J. Germaine, K. Sjoblom, and P. Culligan (2004), A new technique for rapid measurement of continuous soil moisture characteristic curves, *Geotechnique, 54*(3), 179-186.

Tunny, J. (1970), The influence of Saran resin coatings on swelling of natural soil clods, *Soil Science, 109*(4), 254-256.

Weaver, T., N. Hulugalle, and H. Ghadiri (2005), Comparing deep drainage estimated with transient and steady state assumptions in irrigated vertisols, *Irrigation Science, 23*(4), 183-191.

Figures

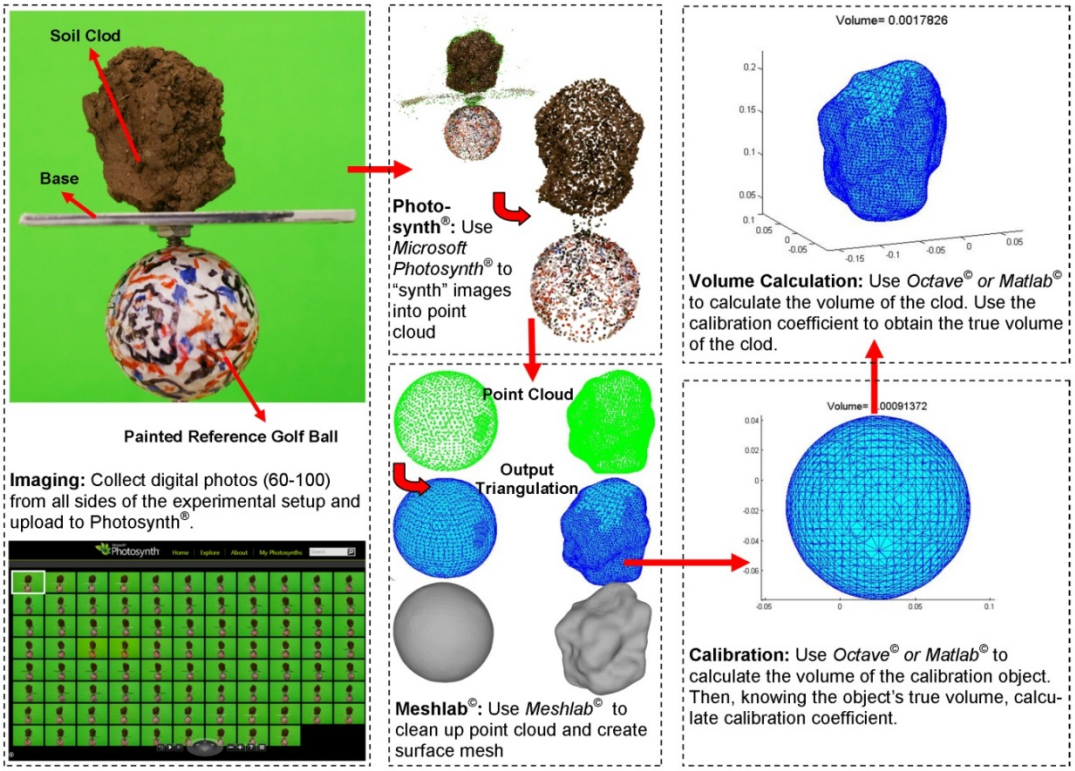

Figure B.1 – Steps to calculate clod volume using the *clodometer* method.

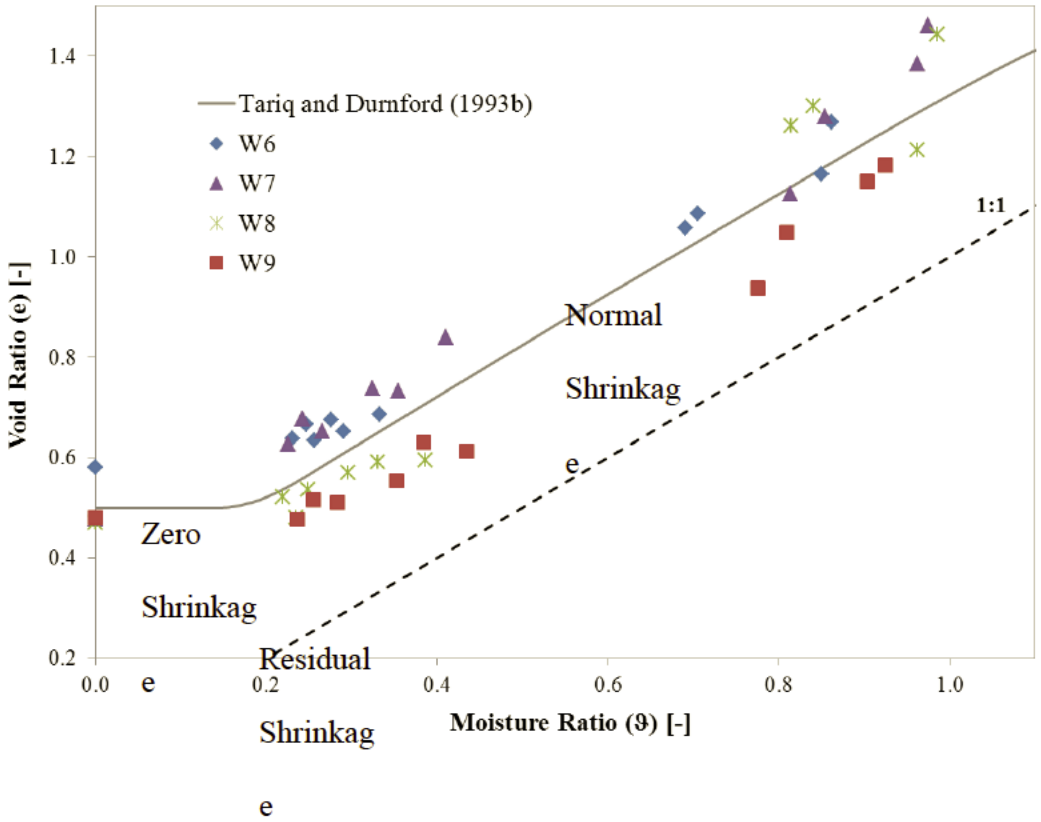

Figure B.2 – Soil shrinkage curve for Waldo Silty Clay Loam clods. The four phase analytical model (Tariq and Durnford, 1993b) was fit to the data to show the zero, residual and normal shrinkage zones for the soil (structural shrinkage was not observed).

Tables

Table B.1 – Imaging Method Validation, comparing displacement-measured to imaging-measured volumes. The Initial Displacement Measurements were always smaller than the imaging- measured volumes, whereas the Final Displacement Measurements (when successive displacement measurements were unchanged) had better agreement with the results of the Imaging Method. Percent difference indicates the difference in volume between the Imaging and the Displacement Methods, divided by the volume from the Displacement Method.

Sample	Soil Type	Displacement Measurement[1]	Volume[‡] – Displac. Method (cm^3)	Volume – Imaging Method (cm^3)	% Diff. – Imaging v. Displac.	Clod Weight (g)
1	Waldo	1	16.4	19.2	17%	31.81
		2	19.5		-2%	34.92
		6	20.9		-8%	36.86
2	Waldo	1	36.1	39.5	9%	70.99
		2	40.1		-2%	74.75
		7§	44.0		-10%	79.1
3	Waldo	1	26.9	27.8	3%	50.8
		2	28.9		-4%	53.17
		5	29.6		-6%	54.34
4	Witham	1	16.5	17.5	6%	26.56
		2	17.1		2%	28.16
		5	17.7		-1%	29.38
5	Waldo	1	29.0	30.1	4%	45.98
		2	30.1		0%	48.21
		6	30.9		-3%	50.49
6	Witham	1	15.0	16.3	8%	23.38
		2	15.5		5%	24.24
		3	15.5		5%	24.43

[†] *Iteration number for the displacement method: first, second, and last iteration.*

[‡] *Volume corresponding to the iteration number obtained by the displacement method.*

§ The sample did not have successive identical displacement methods due to coating imperfections. Swelling was visually evident after the seventh measurement, so the test was discontinued.

Table B.2 – Imaging Method Precision. Triplicate independent measurements were performed on five different clods. Mean volumes and standard errors of the mean are shown for each test.

Test	Mean Volume (cm^3)	Standard Error of the Mean
1	42.8	0.18
2	37.2	0.32
3	28.7	0.46
4	95.5	0.92
5	41.0	0.63
Mean		0.50

Appendix C – Calculating Effective Hydraulic Conductivity (K_{eff}) from the second infiltration term

Vertical infiltration from a constant head disk source can be described by [*Vandervaere et al.*, 2000]:

$$I = C_1\sqrt{t} + C_2 t \tag{C.1}$$

Generally, the first term (C_1) is considered to be the soil sorptivity, S. The second term is related to gravity flow, though its exact interpretation will depend on whether one- or three-dimensional infiltration is occurring. For example, with one-dimensional infiltration, C_2 will be proportional to the effective hydraulic conductivity, K_{eff}

$$P = \frac{C_2}{K_{eff}} \tag{C.2}$$

where P is a soil constant generally found within the range $0.3 < P < 0.4$ [*Philip*, 1990].

With three-dimensional infiltration, C_2 will include a capillary component to describe the horizontal progression of water. This was described by *Smettem et al.* [1995] as

$$C_2 = \frac{2-\beta}{3}K_{eff} + \frac{\gamma S^2}{r_d(\theta_s - \theta_0)} = \frac{2-\beta}{3}K_{eff} + \frac{\gamma S^2}{r_d(\theta_s - \theta_r)(1-\Theta_0)} \tag{C.3}$$

where β is a shape factor between 0 and 1, γ is a proportionality constant between 0.6 and 0.8, r_d is the radius of the supply disc, θ_s is the saturated water content, θ_r is the residual water content, θ_0 is the initial water content and Θ_0 is the initial water content expressed as degree of saturation. S is soil sorptivity, which is equivalent to C_1. Unfortunately, for cases where C_1^2 is greater than C_2, Equation (C.3) will lead to non-positive estimates of K_{eff}.

Of the 145 valid infiltration measurements collected as part of this experiment, just under half gave non-positive estimates of K_{eff}. That is to say, for almost half of the measurements, the ratio of C_2/C_1^2 was less than unity (Figure C.1), particularly under wetter conditions. This is likely due to two reasons: the gravity term becomes less important as the soil wets and micro cracks become sealed, and there is less available porosity in wet conditions. The remaining 73 measurements had ratios of the ratio of C_2/C_1^2 that were greater than unity and thus provided positive estimates for K_{eff}.

Assuming $\beta = 0.55$, $\gamma = 0.7$, $(\theta_s - \theta_r) = 0.4$ and using measured values of C_1, C_2 and Θ_0, the 73 positive measurements were used to estimate the "three-dimensional" K_{eff}. These values were then plotted against the "one-dimensional" K_{eff} for those same measurements, calculated using Equation (C.2). It was determined that using a value of $P = 0.55$ provided a 1:1 line between the one and three-dimensional estimates of K_{eff} (Figure C.2), and thus was adopted for estimating K_{eff} using the two-term Philip model.

References

Philip, J. R. (1990), Inverse Solution for One-Dimensional Infiltration, and the Ratio a/K1, *Water Resources Research, 26*(9), 2023-2027.

Smettem, K., P. Ross, R. Haverkamp, and J. Parlange (1995), Three-Dimensional Analysis of Infiltration from the Disk Infiltrometer: 3. Parameter Estimation Using a Double-Disk Tension Infiltrometer, *Water Resources Research, 31*(10), 2491-2495.

Vandervaere, J. P., M. Vauclin, and D. E. Elrick (2000), Transient Flow from Tension Infiltrometers I. The Two-Parameter Equation, *Soil Science Society of America Journal*, *64*(4), 1263-1272.

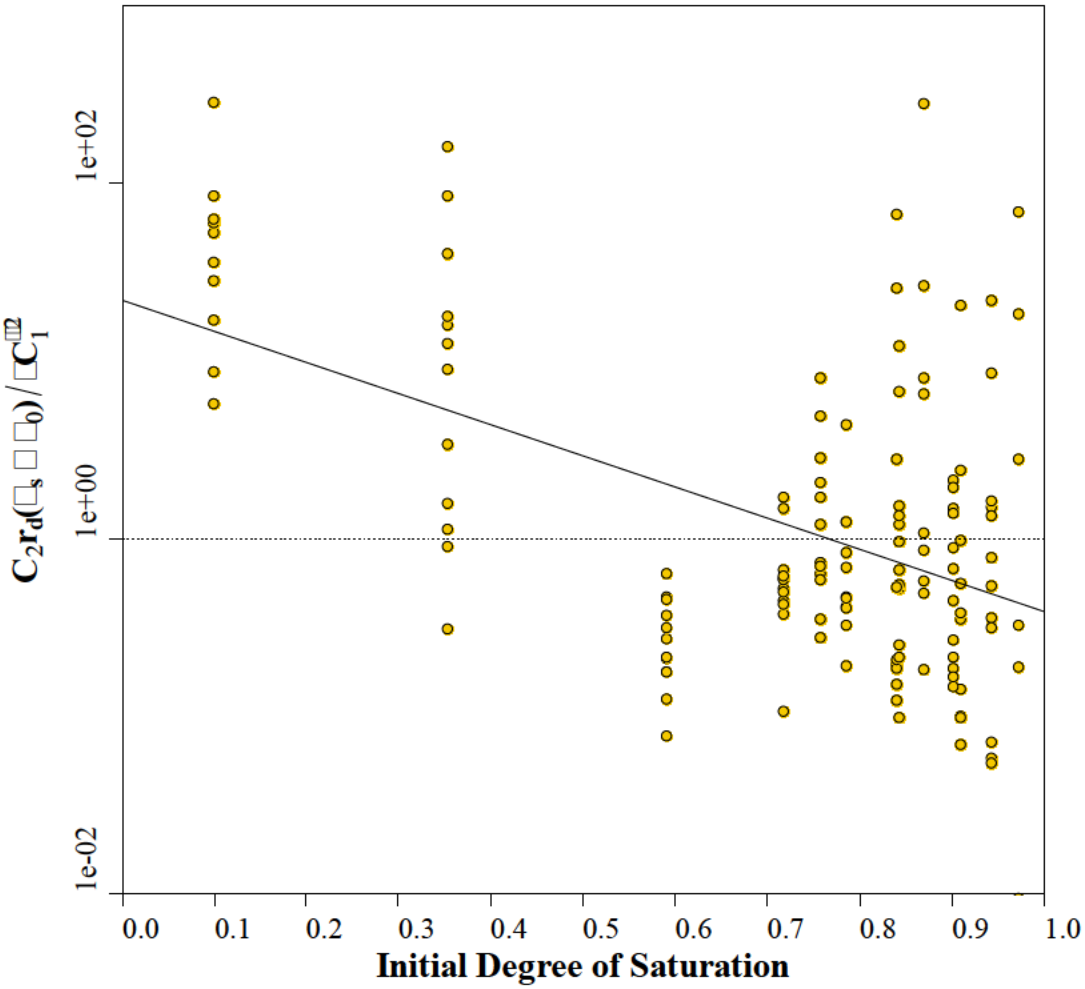

Figure C.1 – Ratio of the terms C_1 and C_2 in Equation C.3, adjusted for disc size, effective porosity, and the proportionality constant, γ. Values below the dashed line indicate that the effective hydraulic conductivity (K_{eff}) would be non-positive.

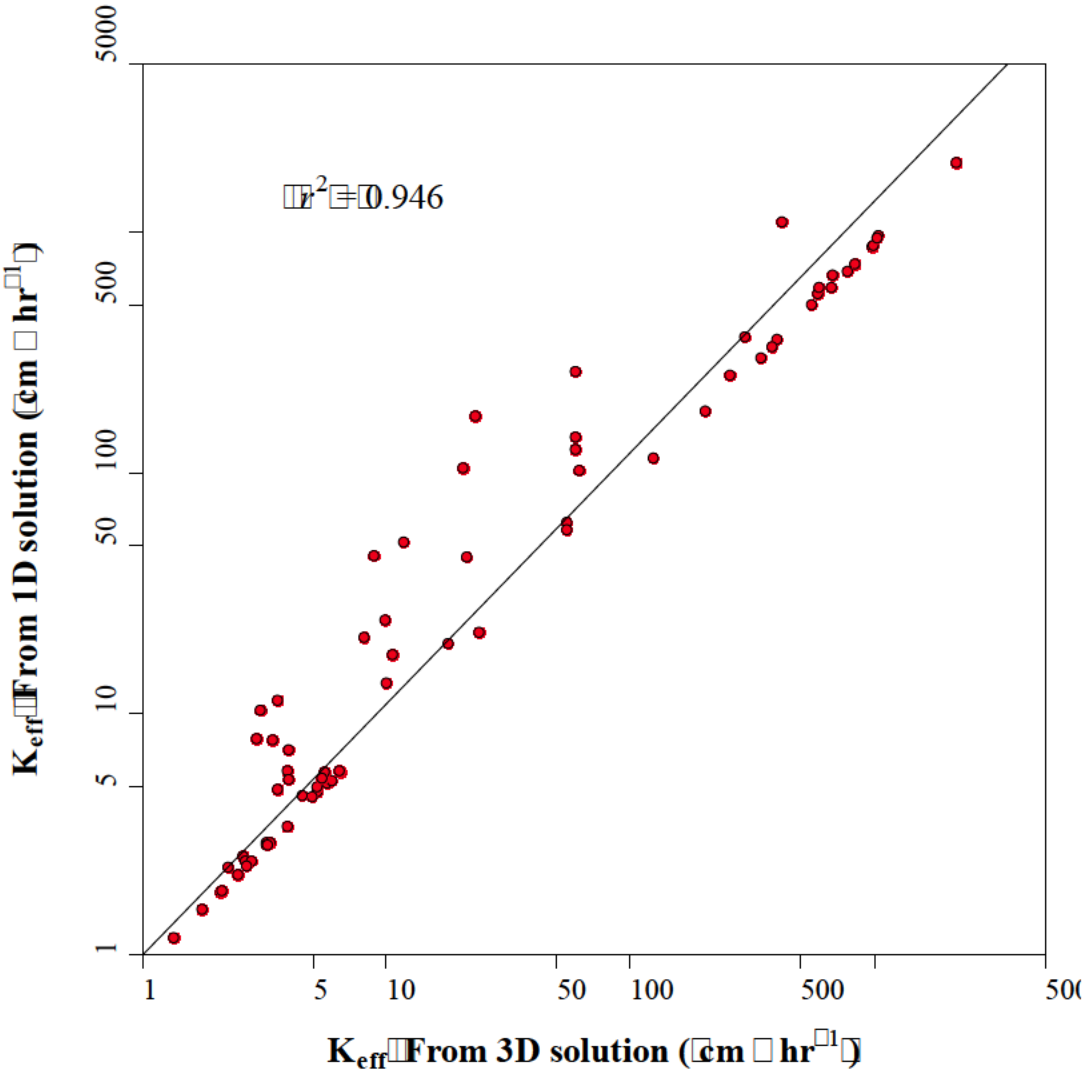

Figure C.2 - Comparison of one- and three-dimensional solutions for effective hydraulic conductivity (K_{eff}), taken from points which fell above the dashed line in Figure E.1. The three-dimensional solution was calculated using Equation (C.3) and assuming that $\beta = 0.55$, $\gamma = 0.7$, $(\theta_s - \theta_r) = 0.4$. The one-dimensional solution was calculated using Equation (C.2) and assuming that $P = 0.55$.

Appendix D – Supplemental material to the manuscript "Hillslope runoff thresholds with shrink-swell clay soils" (Chapter 4)

Visual assessment of irrigation uniformity

Irrigation uniformity was visually analyzed using images created with a krieging routine, where cumulative precipitation amounts were shown as contours, overlaid on the plot locations (Figure D.1). Each set of three plots were analyzed independently, due to the variation in experimental treatment between sets of plots. The contours for each set of plots were normalized relative to the each set's mean cumulative precipitation; therefore, contour values cannot be compared between sets of plots.

Crack image processing

Medium-to-large sized cracks from within five plots were marked by 0.5 x 0.5 m frames and then imaged from above at various times in the experiment. Images were collected from a height of 0.6 m using a Pentax K-x digital SLR and a 28mm lens. The surface area of cracks was quantified by converting the image to black and white and counting the number of black pixels. Figure D.2 shows an example of the converted images for a representative crack within Plot L4. The original photos can be seen in the main body of the text, in Figure 4.10.

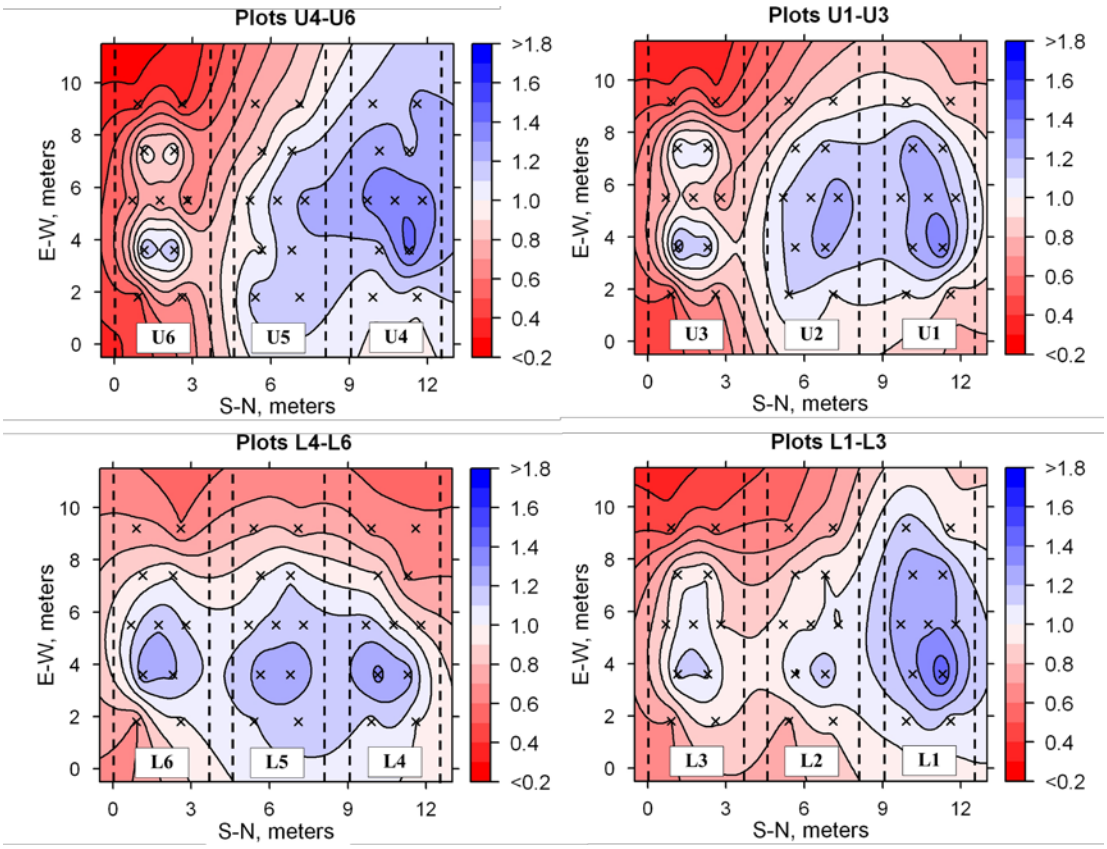

Figure D.1 – Overall uniformity for each set of three plots during the 2012 (Year 2) rainfall simulation experiment. Contours represent amount of precipitation relative to the mean value within each set, and can be used to assess intra-set uniformity only. Individual catchcan locations are indicated with the **x** symbol.

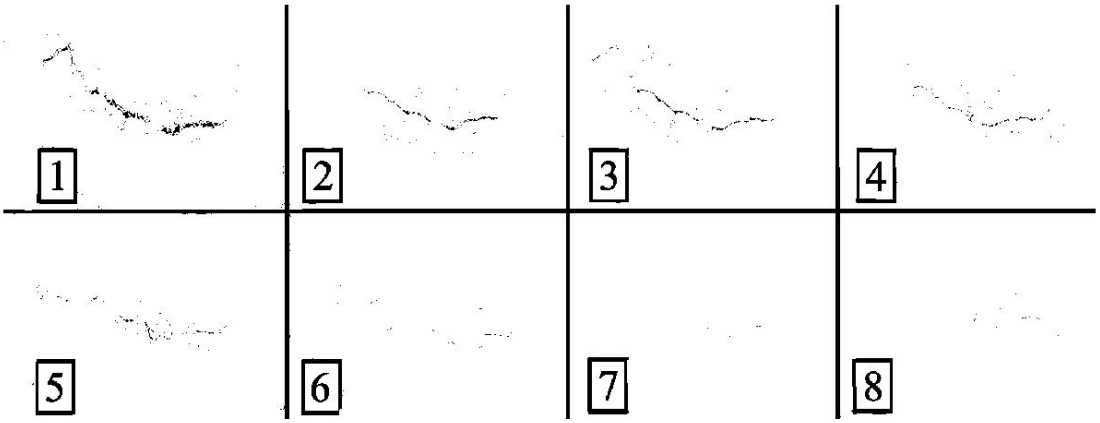

Figure D.2 – The crack photos presented in Chapter 4, Figure 10, converted to black and white so that the number of black pixels can be counted. Shadows, grasses and other artifacts can be seen as noise in the converted images.